

---

# **Characterization of IQ67-Domain Family Members and Their Interacting Kinesin Light Chain-Related Proteins**

---

**Dissertation**

zur Erlangung des

Doktorgrades der Naturwissenschaft (Dr. rer. nat.)

der

Naturwissenschaftlichen Fakultät I-Biowissenschaften-

der **Martin-Luther-Universität**

**Halle-Wittenberg,**

vorgelegt

von **Frau Dipannita Mitra**

geb. am 29.09.1987 in Burdwan (Indien)

---

## **Reviewers:**

### **I. Prof. Dr. Steffen Abel**

Leibniz institute of Plant Biochemistry, Martin Luther University,  
Halle-Wittenberg, Germany

### **II. Prof. Dr. Edgar Peiter**

Institute for Agricultural and Nutritional Sciences, Martin Luther University,  
Halle-Wittenberg, Germany

### **III. PD Dr. Axel Mithöfer**

Max Planck Institute for Chemical Ecology, Jena, Germany

Date of thesis defense-11.09.2020

(Datum der Verteidigung der Dissertation-11.09.2020)

## **Table of contents**

Table of contents.....	iii
1 List of abbreviations .....	v
2 Summary.....	viii
3 Zusammenfassung.....	ix
4 Introduction .....	1
4.1 Calcium signaling in plants.....	1
4.2 IQD proteins: Plant specific CaM targets.....	5
4.3 Kinesin light chain-related proteins: A class of IQD interacting proteins .....	6
4.4 MT cytoskeleton and cellulose deposition .....	8
4.5 Plant cell shapes .....	10
5 Outline.....	12
6 Results .....	13
6.1 Subcellular localization of IQD5 to IQD8, members of subclade IIIa.....	13
6.2 Phenotypes in <i>IQD</i> overexpression lines.....	19
6.3 Expression analysis of <i>IQD5</i> to <i>IQD8</i> .....	21
6.4 Phenotypic characterization of <i>iqd5</i> to <i>iqd8</i> knockout lines.....	26
6.5 Characterization of IQD5 functions during PC morphogenesis.....	31
6.6 Function of IQD5 in cellular signaling? .....	37
6.7 Subcellular localization of KLCR proteins and their interaction with IQD5 to IQD8 .	42
6.8 Expression analysis of <i>KLCR</i> .....	47
6.9 Phenotypic characterization of <i>klocr</i> loss-of-function lines.....	50
7 Discussion.....	53
8 Materials and methods .....	60
8.1 Materials .....	60
8.1.1 Chemicals.....	60
8.1.2 Media and buffers.....	60
8.2 Methods .....	63
8.2.1 Molecular biology techniques .....	63
8.2.2 Plants biology techniques .....	72
8.2.3 Cell biology assays.....	74
9 References.....	76
10 Supplementary data.....	82
10.1 Bacterial strains and constructs .....	82
10.2 DNA and protein markers.....	83

10.3	Instruments and kits .....	83
10.4	List of server/softwarees .....	84
10.5	List of primers .....	84
11	Supplementary figures .....	92
12	Appendix.....	96
12.1	Curriculum vitae .....	96
12.2	List of publications .....	97
12.3	Acknowledgments.....	98
13	Declaration .....	99
14	Ehrenwörtliche erklärung .....	100

---

## 1 List of abbreviations

Ammonium persulfate. ....	APS
Annealing temperature. ....	Ta
<i>Arabidopsis thaliana</i> salts. ....	ATS
Auxin response factor5. ....	ARF5
Base pair. ....	bp
Bovine serum albumin. ....	BSA
Ca <sup>2+</sup> binding proteins. ....	CaBPs
Calcium. ....	Ca <sup>2+</sup>
Calmodulin. ....	CaM
CaM binding proteins. ....	CaMBPs
Calcineurin B-like proteins. ....	CBL
Ca <sup>2+</sup> depenedent protein kinase. ....	CDPK
CBL-interacting protein kinases. ....	CIPK
CaM-like. ....	CML
Cellulose synthase complexes. ....	CSC
Cellulose synthase interacting. ....	CSI
Cellulose synthase uncoupling. ....	CMU
Cellulose synthases. ....	CESA
Coding sequence. ....	CDS
Complementary DNA. ....	cDNA
Confocal laser scanning microscopy. ....	CLSM
Cyclic ADP-ribose. ....	cADPR
Cyclic nucleotide-gated ion channel. ....	CNGC
Cytochrome P450. ....	CYP
Cytosolic Ca <sup>2+</sup> concentration. ....	[CytCa <sup>2+</sup> ]
Depolarization activated Ca <sup>2+</sup> channel. ....	DCC
Dimethyl sulfoxide. ....	DMSO
Forward primer. ....	F.P
Gram. ....	g
Green fluorescent protein. ....	GFP

Guanine-cytosine. ....	<i>G-C</i>
Helix-loop-helix. ....	<i>HLH</i>
Hyperpolarization activated Ca <sup>2+</sup> channel. ....	<i>HCC</i>
Inositol1, 4, 3-triphosphate. ....	<i>IP3</i>
IQ67-domain. ....	<i>IQD</i>
IQ Ras GTPase activating proteins. ....	<i>IQGAPs</i>
Kinesin heavy chain. ....	<i>KHC</i>
Kinesin light chain-related. ....	<i>KLCR</i>
Kinesin-like calmodulin-binding protein. ....	<i>KCBP</i>
Liter. ....	<i>l</i>
Luria bertani. ....	<i>LB</i>
Mechanosensitive Ca <sup>2+</sup> channel. ....	<i>MCC</i>
Melting temperature. ....	<i>T<sub>m</sub></i>
Microfilaments. ....	<i>MF</i>
Microtubules. ....	<i>MT</i>
Millimolar. ....	<i>mM</i>
Milliliter. ....	<i>ml</i>
Millimeter. ....	<i>mm</i>
Molecular weight. ....	<i>MW</i>
Monopteros. ....	<i>MP</i>
MT-associated proteins. ....	<i>MAP</i>
Naphtalic acetic acid. ....	<i>NAA</i>
Nuclear localization sequence. ....	<i>NLS</i>
Pavement cell. ....	<i>PC</i>
Phragmoplast orienting kinesin. ....	<i>POK</i>
Plasma membrane. ....	<i>PM</i>
Pleckstrin homology GTPase activating protein. ....	<i>PhGAP</i>
Polymerase chain reaction. ....	<i>PCR</i>
Propidium iodide. ....	<i>PI</i>
Reverse primer. ....	<i>R.P</i>
Reverse transcription polymerase chain reaction. ....	<i>RT-PCR</i>
RFP-tubulin alpha-5. ....	<i>RFP-TUA5</i>
Rho family GTPase. ....	<i>ROP</i>
Ribonucleic acid. ....	<i>RNA</i>
ROP interactive CRIB family protein. ....	<i>RIC</i>

Site-directed mutagenesis. ....	<i>SDM</i>
Slow-activating vacuolar. ....	<i>SV</i>
Super optimal broth. ....	<i>SOC</i>
Tetratrico peptide repeat. ....	<i>TPR</i>
Tomato bushy stunt virus. ....	<i>TBSV</i>
Tris/Borate/EDTA buffer. ....	<i>TBE</i>
Tris-buffered saline. ....	<i>TBS</i>
Ubiquitin10. ....	<i>UBQ10</i>
Vacuolar voltage-gated Ca <sup>2+</sup> . ....	<i>VVCa</i>
Volts. ....	<i>V</i>
Wild type. ....	<i>WT</i>

## 2 Summary

Calcium ( $\text{Ca}^{2+}$ ) serves as a versatile messenger in many adaptation responses and developmental processes in plants. Calmodulin (CaMs) and CaM-like (CMLs) proteins are universal  $\text{Ca}^{2+}$  sensors in eukaryotes that perceive local perturbations in  $\text{Ca}^{2+}$  levels by binding to  $\text{Ca}^{2+}$  ions via EF-hand motifs. Binding of  $\text{Ca}^{2+}$  induces conformational changes in CaM/CMLs, which lead to changes in their affinity to target proteins. The information encrypted in the  $\text{Ca}^{2+}$  signals is transduced via binding of CaM/CMLs to target proteins, which alters the biochemical properties of the targets, eventually resulting in downstream cellular responses.  $\text{Ca}^{2+}$  free apoCaM/CMLs and  $\text{Ca}^{2+}$ -bound holoCaM/CMLs differentially bind targets, depending on their  $\text{Ca}^{2+}$  occupancy, and interact with largely different sets of target proteins via a different set of motifs, thereby regulating the activity of these target proteins. IQ67-Domain (IQD) proteins are one of the largest family of CaM binding proteins in plants, with 33 members in *Arabidopsis thaliana*. Despite the large family size, functions of IQDs are largely elusive. A phylogenetic analysis revealed the presence of four subclades within the IQD protein families of *Arabidopsis thaliana* and rice (*Oryza sativa*) that mainly differ in the presence and distribution of additional conserved motifs of unknown function. Most IQDs are associated with microtubules (MT) and membranes, and several family members are localized to the nucleus. With few exceptions from other clades, subclade III *Arabidopsis* IQDs preferentially interact with the three *Arabidopsis* Kinesin light chain-related (KLCR) proteins, which have similarity with light chain-subunits of mammalian type 1-kinesin motor proteins. To elucidate biological roles of IQD-KLCR modules, our study focused on the functional characterization of group III *Arabidopsis* IQDs and their interacting KLCRs using a combination of reverse genetics, cell biology, molecular biology, and biochemistry. Our research work has shown that IQD5-KLCR1 modules have an important role in cell shape regulation. IQD5 also shows an effect on cellulose deposition. Together we assume that IQDs play an important role in linking  $\text{Ca}^{2+}$ -CaM signaling to cell shape regulation.



### 3 Zusammenfassung

Kalzium ( $\text{Ca}^{2+}$ ) dient als vielseitiger Bote in vielen Anpassungen und Entwicklungsprozessen in Pflanzen. Calmodulin (CaM) und CaM-ähnliche (CMLs) Proteine sind universelle  $\text{Ca}^{2+}$  Sensoren in Eukaryoten, die lokale  $\text{Ca}^{2+}$  -Signale durch Bindung an  $\text{Ca}^{2+}$ -Ionen über EF-Handmotive detektieren. Die Bindung von  $\text{Ca}^{2+}$  induziert Konformationsänderungen in CaM/CML, was zu Veränderungen in ihrer Affinität zu Zielproteinen führt. Die im  $\text{Ca}^{2+}$ -Signal verschlüsselte Information wird über die Bindung von CaM/CML an Zielproteine transduziert, welche die biochemischen Eigenschaften der Ziele ändern, was schließlich zu zellulären Antworten stromabwärts führt.  $\text{Ca}^{2+}$ -freie ApoCaM/CMLs und  $\text{Ca}^{2+}$ -gebundene HoloCaM/CML binden abhängig von ihrer  $\text{Ca}^{2+}$ -Bindung differenziell an Zielmoleküle und interagieren mit verschiedenen Zielprotein-Sets über verschiedene Gruppen von Motiven und regulieren die Aktivität der Zielproteine. Proteine der IQ67-Domäne (IQD) sind eine der größten Familien von CaM-Bindungsproteinen in Pflanzen, mit 33 Mitgliedern in *Arabidopsis thaliana*. Trotz der Größe der Familie sind Funktionen von IQDs weitestgehend unbekannt. Eine phylogenetische Analyse ergab, dass sich innerhalb der IQD-Proteinfamilien von *Arabidopsis thaliana* und Reis (*Oryza sativa*) vier phylogenetische Gruppen befinden, die sich hauptsächlich in der Präsenz und Verteilung zusätzlicher konservierter Motive unbekannter Funktion unterscheiden. Die meisten IQDs sind mit Mikrotubuli (MT) und Membranen assoziiert, und einige sind im Zellkern lokalisiert. *Arabidopsis* IQDs interagieren vorzugsweise mit den drei *Arabidopsis* Kinesin light chain-related (KLCR)-Proteinen, die Ähnlichkeit mit Leichtketten-Untereinheiten von Säuger-Typ 1-Kinesin-Motorproteinen haben. Um die biologischen Rollen von IQD-KLCR-Modulen aufzuklären, konzentrierten sich meine Studien auf die funktionale Charakterisierung von *Arabidopsis* IQDs der Gruppe III *Arabidopsis* und ihren interagierenden KLCRs unter Verwendung einer Kombination von reverser Genetik, Zellbiologie, Molekularbiologie und Biochemie. Meine Forschungsarbeit hat gezeigt, dass IQD5-KLCR1-Module eine wichtige Rolle bei der Zellformregulation spielen. IQD5 zeigt auch einen Effekt auf die Celluloseablagerung. Zusammengenommen nehmen wir an, dass IQDs eine wichtige Rolle bei der Förderung der  $\text{Ca}^{2+}$ -CaM-Signalübertragung zur Zellformregulation spielen.

## 4 Introduction

### 4.1 Calcium signaling in plants

Ca<sup>2+</sup> ions play a fundamental role as second messengers in cellular signaling and mediate the regulation of plant growth. Many extracellular signals and environmental cues, including biotic and abiotic stimuli, elicit changes in intracellular Ca<sup>2+</sup> levels. Stimulus-specific Ca<sup>2+</sup> signals, in terms of spatial and temporal dynamics of the changes in cytosolic Ca<sup>2+</sup> concentration [CytCa<sup>2+</sup>], nuclear, plastidal and mitochondrial Ca<sup>2+</sup> concentration, are referred to as Ca<sup>2+</sup> signatures. *In vivo* measurements in plants cells have shown that the patterns of Ca<sup>2+</sup> signatures can differ in amplitude, duration, localization, and frequency of Ca<sup>2+</sup> oscillations. These signatures are generated by a coordinated function of the influx and efflux of Ca<sup>2+</sup> (McAinsh and Pittman 2009). Regarding Ca<sup>2+</sup> influx channels many plant Ca<sup>2+</sup>-permeable channels have been characterized, but only a few have been thoroughly studied. Examples of Ca<sup>2+</sup> influx channels are the plasma membrane (PM) influx channels which comprise three groups, the mechanosensitive Ca<sup>2+</sup> channels (MCC) (Ryu et al. 2010), depolarization activated Ca<sup>2+</sup> channels (DCC) and hyperpolarization activated Ca<sup>2+</sup> channels (HCC). Cyclic nucleotide-gated ion channels (CNGCs) are ion channel homologous genes acting as PM localized Ca<sup>2+</sup> permeable channels (Ma et al. 2009). Apart from the PM channels there are also endomembrane Ca<sup>2+</sup> permeable channels including Inositol1, 4, 3-triphosphate (IP<sub>3</sub>) ( Zhang et al. 2007) and cyclic ADP-ribose (cADPR)-gated channels, the vacuolar voltage-gated Ca<sup>2+</sup> (VVCa) and slow-activating vacuolar (SV) channels. Ca<sup>2+</sup> is an essential nutrient, yet in all organisms, Ca<sup>2+</sup> is extremely toxic when present at high concentrations in the cytosol. There are two main pathways for [CytCa<sup>2+</sup>] removal: high-affinity Ca<sup>2+</sup>- ATPases and low-affinity Ca<sup>2+</sup> exchangers. Both Ca<sup>2+</sup> influx and efflux channels act as modulators of Ca<sup>2+</sup> signatures and recent studies provide important insights into the roles of these channel types in the generation of specific Ca<sup>2+</sup> signatures (McAinsh and Pittman 2009).

For Ca<sup>2+</sup> to act as a ubiquitous second messenger after encoding, as described above, the second step is the decoding where the Ca<sup>2+</sup> signatures are decoded by Ca<sup>2+</sup> binding proteins (CaBPs). Several CaBPs or Ca<sup>2+</sup> sensors have been identified in plants, which contain a helix-loop-helix (HLH) EF-hand. About 250 EF-hand motif-containing proteins, which carry one or more EF hands have been identified in *Arabidopsis thaliana* (Day et al. 2002) that differ significantly in sequence and number of EF-hand motifs. Some EF hand

containing proteins are regulatory proteins like CaM, some are also structural proteins like Calbindin, Parvalbumin as shown in mice (Caillard et al. 2000; Schmidt et al. 2012).

In  $\text{Ca}^{2+}$  signaling, CaBPs function as  $\text{Ca}^{2+}$  sensors or  $\text{Ca}^{2+}$  responders, the latter of which contain an additional kinase domain.  $\text{Ca}^{2+}$  sensors relays have no kinase activity and they must interact with other protein kinases to regulate their molecular activity after binding  $\text{Ca}^{2+}$ , for e.g. in plants, there are two types of sensor relays, one is plant-specific calcineurin B-like protein (CBL), which interacts to CBL-interacting protein kinases (CIPK) for downstream signaling (Liu et al. 1998) and the other  $\text{Ca}^{2+}$  sensor, CaM is present in most eukaryotes. The  $\text{Ca}^{2+}$  responder which contains a kinase domain is the  $\text{Ca}^{2+}$ -dependent protein kinase (CDPK) (Harmon et al. 2000). In our study we focus on  $\text{Ca}^{2+}$ -CaM mediated signaling pathway.

In *Arabidopsis thaliana*, seven genes encode for CaM isoforms and the CaM proteins contain four EF hands (Kudla et al. 2018). CML proteins closely relate to CaMs and are encoded by 50 genes in *Arabidopsis thaliana*, contain two to six EF hands, and, like CaMs, are universal  $\text{Ca}^{2+}$  sensors in plants that perceive local perturbations in  $\text{Ca}^{2+}$  levels by binding  $\text{Ca}^{2+}$  ions via their EF-hands. CaMs are encoded by a single gene in yeast but are encoded by multiple genes or gene families in vertebrates and in plants, which suggests that CaMs are evolutionary conserved and that family expansion may correlate with increased functions of  $\text{Ca}^{2+}$  signaling in multicellular organisms. The general function of CaM is to bind  $\text{Ca}^{2+}$  ions and then bind a target protein, affecting its activity. The binding of  $\text{Ca}^{2+}$  is achieved by the 4 EF-hand domains. An EF hand comprises of two perpendicular alpha helices with a 12-residue loop region between them, each of these residues contributes to  $\text{Ca}^{2+}$  binding. One of the residues, i.e. residue 12 is usually a Glu or Asp, and it contributes both oxygen from its side chain carboxylic acid group. Since Glu and Asp are negatively charged, they make a charge-interaction with the positively charged  $\text{Ca}^{2+}$  ion (Prebil et al. 2016).  $\text{Ca}^{2+}$  binding leads to a conformational change in CaM, allowing  $\text{Ca}^{2+}$ -CaM to bind to its target and elicit the downstream responses. The binding of CaMs to  $\text{Ca}^{2+}$  molecules exposes the globular domains i.e. CaM/CML's hydrophobic regions, so that these are localized on the surface and not on the interior side of the protein. This alters their affinity to target proteins and allows its interaction with the target protein, the hydrophobic surfaces interact with the hydrophobic regions of CaM's target proteins (Nelson and Chazin 1998 a and b; O'Neil and DeGrado 1990). The information encrypted in the  $\text{Ca}^{2+}$  signals is transduced via binding of CaM/CMLs to target proteins, which alters the biochemical properties of the targets, eventually resulting in downstream cellular responses.  $\text{Ca}^{2+}$ -CaM

binds many kinases, phosphatases, signaling proteins, and structural proteins affecting a wide variety of processes including neurotransmitter release, muscle contraction, metabolism, apoptosis, inflammation, membrane protein organization, and cytoskeleton movement. Apo-CaM can bind (via a different motif than Ca<sup>2+</sup>-CaM) neuroproteins, structural proteins, and signaling proteins involved in neurotransmitter production and release, nerve growth, muscle relaxation, and intracellular movement of organelles along actin filaments in animals.

CaM target proteins in plants include metabolic enzymes, cytoskeleton-associated proteins, ion transporters, chaperonins, transcription factors, protein kinases/phosphatases and also proteins of unknown function (Ranty et al. 2006). So far, many CaM-binding proteins (CaMBPs) have been identified. Expression analysis and subcellular localization studies have shown that CaM/CMLs are expressed and localized in diverse tissues or subcellular location, respectively. CaMs are mostly present in the cytosol, nucleus, and peroxisome and in the extracellular matrix and might play an important role in these compartments (Ranty et al. 2006). In CaMBPs, CaM is known to bind a small region of protein-stretch comprised of basic and hydrophobic residues which forms an amphiphilic helix that forms the CaM binding site. CaMBPs often contain 1-10 and 1-14 motifs which are defined based on the distribution of the hydrophobic residues. Other CaMBPs contain IQ motifs which bind CaM either in the absence (Apo-CaM) or presence of Ca<sup>2+</sup> (holo/Ca<sup>2+</sup>-CaM) (The Calmodulin Target Database; <http://calcium.uhnres.utoronto.ca/ctdb>).

Defects in Ca<sup>2+</sup> signaling causes various developmental disorders and several diseases, for example, Alzheimer's disease (Berridge 2011) and Parkinson's disease (Zaichick et al. 2017) in humans. In plants, defects lead to loss of ability to resist drought or pathogen attacks (Zhang et al. 2014). In muscle contraction, when Ca<sup>2+</sup> binds to Troponin C, it stimulates the contraction (Boyle 2008). The binding of Ca<sup>2+</sup> to CaM in Kinesin-Like Calcium-Binding Protein (KCBP) negatively impacts the motor protein and makes it inactive. KCBP is an MT localized protein, which plays a role in cell division, root growth and in trichome development in plants (Deavours et al. 1998; Narasimhulu and Reddy 1998).

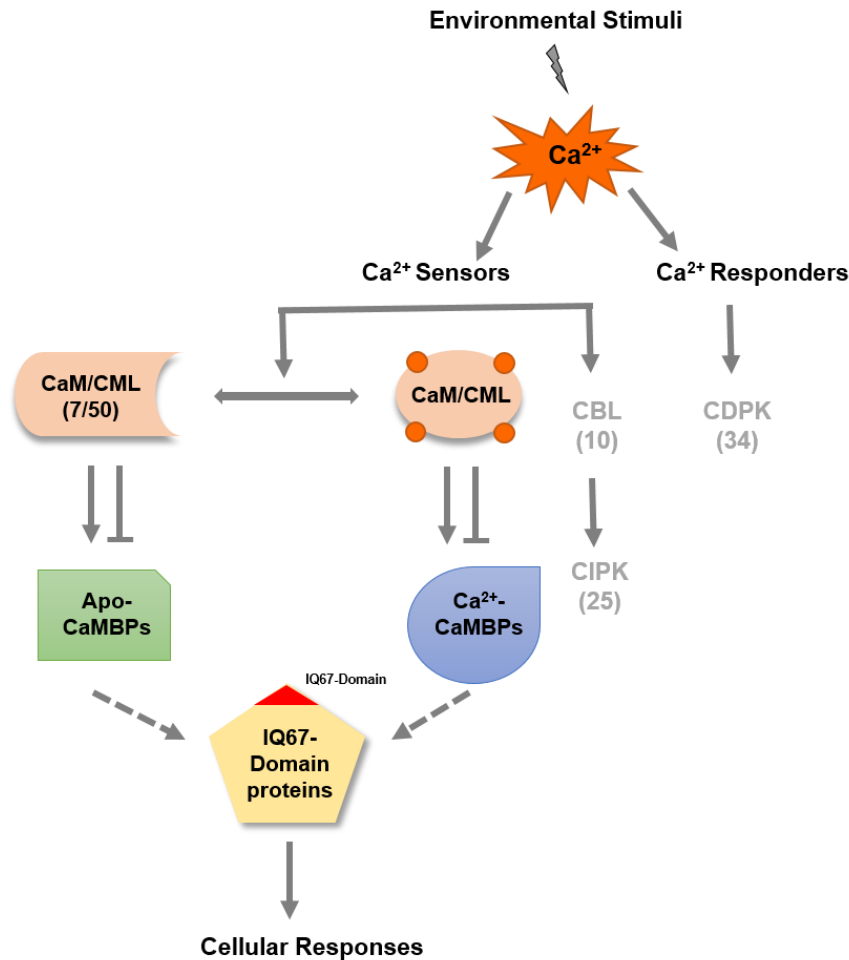


**Fig 1: Schematic overview of plant Ca<sup>2+</sup> signaling** CaBPs possess Ca<sup>2+</sup> sensors, CBLs and CaM/CMLs, which constitute the largest family of Ca<sup>2+</sup> sensors in *Arabidopsis*, the other class of CaBPs are the Ca<sup>2+</sup> responders e.g. CDPK which possess a kinase domain. CaM can bind to targets either in the Ca<sup>2+</sup>-free (apo) or Ca<sup>2+</sup>-bound (holo) state) and interact with the target proteins to elicit downstream cellular response. IQD family with the name giving IQ67 motif (shown in red) represents the largest family of CaM target proteins in *Arabidopsis*.

Expression data for CaM multigene family in plants indicate that CaM and CML genes are actively and differentially expressed over developmental stages and in various organs. CaM/CML target proteins play a role in plant growth regulation, plant-microbe interactions and abiotic stress responses. Thus, identification of CaM/CML target proteins and understanding their cellular function and modes of CaM-mediated regulation is key to elucidate the molecular mechanisms of Ca<sup>2+</sup> signaling. One such class of plant-specific

CaMBPs are IQ67-Domain (IQD) proteins. Our research focuses on the characterization of one of the largest group of CaMBP proteins, the IQD family (Fig.1).

#### 4.2 IQD Proteins: Plant specific CaM targets

IQD proteins constitute a novel and one of the largest family of putative CaM targets in *Arabidopsis*. IQD proteins were identified in a screening of *Arabidopsis* mutants for plants with altered glucosinolate content and composition. Glucosinolates are a class of secondary metabolites in plants (Levy et al., 2005). In this screening, it was found that overexpression of *Arabidopsis IQD1* in *iqd1-1D* lines stimulates accumulation of glucosinolates and plants are less susceptible against herbivores. Other than *IQD1*, *IQD12* in tomato has been reported to show a leaf shape and fruit shape alteration (Xiao et al., 2008). Genetic studies showed that overexpression of *IQD12* leads to elongated fruits and this is caused by retrotransposon-mediated *IQD12* duplication (Wu et al. 2011). Besides *Arabidopsis* and tomato, IQD families have been annotated in the genomes of rice and maize. IQDs in these plants are encoded by multigene families with members spanning from 23 to 67. Recently, studies have shown that rice *IQD21/ Grain size on Chromosome 5 (GSE5)* plays a role in alteration of rice grain size respectively (Duan et al., 2017).

The *Arabidopsis* IQD family consists of 33 members. The common feature of this family is the presence of a plant-specific central domain of 67 conserved amino acid residues, which is defined by a unique and repetitive arrangement of three different CaM-binding motifs: The IQ67 domain contains 1-3 copies each of the IQ motif (IQxxxRGxxxR or of its more relaxed version [ILV]QxxxRxxxx [R, K]), the 1-5-10 motif [FILVW]xxx[FILV]xxxx[FILVW], and the 1-8-14 motif [FILVW]xxxxxx[FAILVW]xxxxx[FILVW], which mediate Ca<sup>2+</sup>-independent and Ca<sup>2+</sup>-dependent CaM binding, as already studied for recombinant IQD1 and IQD20, which only consists of the IQ67-Domain and short N-terminal extension *in vitro* and in yeast (Levy et al. 2005; Bürstenbinder et al. 2013). In addition, several conserved basic and hydrophobic amino acid residues are flanking these motifs, and the IQ67 domain is predicted to fold into a basic amphiphilic helix. Based on the *in silico* data from Genevestigator, *IQDs* are known to be expressed in low levels in *Arabidopsis*.

IQDs are structurally diverse but are uniform at the physicochemical level, e.g., high isoelectric point and high content of basic residues (Abel et al. 2005). The IQD family also contains a high frequency of homologous gene pairs similar to protein families which are part of regulatory multiprotein complexes. Preferential retaining of sister genes is a typical

feature of gene families with regulatory roles in signaling (Remington et al. 2004; Reyes et al. 2004; Tian et al. 2004).

Cell biological assays of all 33 IQDs by transiently expressing them with reporter gene green fluorescent protein (GFP) fusion constructs under the control of the *CaMV 35S* promoter in *Nicotiana benthamiana* leaves showed that most of the *Arabidopsis* IQD proteins co-localize with MTs and some additionally localize to the PM. In addition, several IQDs are localized to the nucleus (Bürstenbinder et al. 2017a). Previous studies showed that IQD1 can recruit CaM2 to MTs, this would suggest that IQDs might function as MT-associated proteins (MAPs) that link CaM to the cytoskeleton.

Since MT localization is a hallmark of IQDs, our group was interested in quantitatively analyzing the MT patterns of all 33 IQDs. A tool was developed to monitor GFP-IQD decorated MT arrays in epidermis cells in *Nicotiana benthamiana*. The analysis showed that several clades of IQDs showed similar MT patterns and clustered together. Among the MT patterns of IQDs, IQD5, IQD11, IQD16, and IQD17 showed different patterns compared to all others. Overexpression of *IQD11* and *IQD16* showed similar phenotypes like elongated cells, leaves and twisted growth of aerial organs. First data of overexpression of *IQD5* and *IQD17* didn't show any major macroscopic alterations. To compare with a member with different MT pattern, a comparison study was performed with the overexpression line of *IQD14*, which showed a twisted phenotype. Since the expression domain of *IQD11*, *IQD16*, and *IQD14* partially overlaps in young developing tissues the observations suggested that IQDs play distinct roles in plant growth and development (Bürstenbinder 2017a). But in order to know exact molecular mechanism of IQD functions, it is important to know the interacting partners.

### **4.3 Kinesin light chain-related proteins: A class of IQD interacting proteins**

Previous analyses conducted in our group revealed that IQD1-GFP fusion proteins localize mainly to the nucleus and are associated with MTs. Interestingly, a Y2H screen identified KLCR1 protein as the strongest IQD1 interacting protein (Bürstenbinder et al. 2013). Binding of IQD1 to KLCR1 was confirmed by independent yeast transformation and Y2H assays. KLCR1 belongs to a 3-membered family of tetratricopeptide repeat (TPR) domain-containing proteins that mediate binding of kinesins to cargo. Physical interaction of IQD2 and IQD23 with KLCR2 was also noticed in plant immune networks which identified KLCR2 as a conserved hub in plant defense that was targeted by six independent effector proteins

from both, the gram-negative bacteria *Pseudomonas syringe*, and the obligate biotroph oomycete *Hyaloperonospora arabidopsis* (Mukhtar et al., 2011). In addition, analysis of *klocr2* loss-of-function lines revealed increased susceptibility of these lines to *H. arabidopsis* infection pointing to a role of KLCR2 in plant defense.

KLCRs share similarities with mammalian subunits of kinesin motor proteins. As dyneins are absent in plants, it is assumed that kinesins facilitate cargo-transport in both directions of the MTs. The cargo is either directly attached to the C-terminal tails of the Kinesin heavy chain (KHC) dimer, or indirectly via its associated KLCs or by adaptor proteins that bind to KLCs and form a scaffold for additional protein-protein interactions. Mounting evidence in animals on kinesin-cargo interactions suggests that entire pre-assembled signaling modules (e.g., MAP kinase cascades associated with vesicle-bound transmembrane receptors) are loaded onto KHC/KLC-interacting scaffolds, which subsequently trigger and inform transport along MTs to their final destination. Furthermore, the assembly of cargo complexes can be controlled by multiple mechanisms such as phosphorylation,  $Ca^{2+}$  signaling, and proteolysis (Akhmanova and Hammer 2010; Schnapp 2003). Evidence from studies conducted in animals states that KLC interacting scaffold proteins regulate cargo recruitment and kinesin motor activation by relieving autoinhibition. The assembly, loading and unloading of scaffold-associated cargo complexes are tightly controlled by phosphorylation, GTPase activity, and  $Ca^{2+}$  signaling and thus integrate multiple pathways to coordinate diverse cellular activities (Brown and Sacks 2009). Interaction between IQD and KLCR proteins may provide a molecular link between  $Ca^{2+}$  signaling and the regulation of kinesin activity. This hypothesis is supported by the conserved structure of the TPR12 domain in *Arabidopsis* KLCR1 and human KLC1, also by the subcellular localization of IQD1 and KLCR1 to MTs in both the cases. Thus, the hypothesis arises that the IQD family provides a broad array of scaffold proteins for diverse kinesin-dependent intracellular transport processes. The functions of the majority of the *Arabidopsis* kinesins (65%) remain unexplored, and virtually nothing is known about their associated light chains (Zhu and Dixit, 2011). KLC sequences have been predicted in the *Arabidopsis* genome but their experimental studies are still in the earlier stage. Alternatively, plant KLCRs may have functions independent of Kinesins. This is supported by a recent study that showed direct MT binding of KLCR1/ Cellulose MT Uncoupling1 (CMU1) protein and roles of KLCR1/CMU1 in MT organization and cellulose deposition (Lin et al. 2016).



#### 4.4 MT cytoskeleton and cellulose deposition

The plant cytoskeleton is comprised of microfilaments (MF) and MTs, which form an intracellular network that serves as tracks for cellular transport of various cargoes, including organelles, proteins, and other macromolecular complexes. MTs are tubular structures that consist of heterodimers of alpha and beta tubulins, which interact in a head to tail fashion thereby forming directional protofilaments, in which beta and alpha tubulins are exposed at the plus and minus end (Nogales 2001). MTs undergo constant turn over. Rapid depolymerization is followed by periods of polymerization which mostly occurs at the plus ends. MTs are bundled, cross-linked and tethered to the PM. The distribution and arrangement of the MFs and MTs are crucial for cell morphogenesis. Well-ordered transverse cortical MTs promote cell elongation and restricts cell expansion in the direction of their dominant orientation (Wasteneys and Galway 2003). For the cell shape in plants coordinated cell wall biogenesis is crucial. Mostly the cell shapes are formed by the constant breakage and re-formation of bonds between the cell wall components and the formation and deposition of new materials. In this regard, the cytoskeleton also plays a critical role in shaping the cell mainly because it influences the pattern of the deposition of the new cell wall materials (Smith 2003a). Cells can have various kinds of growth. Most of the cells grow diffusely where the new cell wall materials are distributed horizontally and equally. It is an anisotropic growth and is oriented in one direction. Here the cytoskeleton plays the major role since the arrangement of the cellulose microfibril serves as the structural component for the expanding cell walls. In the past few years, studies have identified a large number of proteins that play major roles in determining the orientation of diffuse cell expansion by regulating MT dynamics and arrangement. For e.g., the *Arabidopsis* TONNEAU2 (TON2) is required for normal spatial organization of cortical MTs in expanding and dividing cells, and encodes a protein predicted to function as a regulatory subunit for a type-2A protein phosphatase (Camilleri et al. 2002). Another example is *Arabidopsis* KATANIN1 (AtKTN1) which is subunit of the Katanin complex and is encoded by the mutational defined FRAGILE FIBER 2 (FRA2), BOTERO1 (BOT1) and ECTOPIC ROOT HAIR3 (ERH3) genes as identified in independent screens. *Arabidopsis* KTN binds MTs using a multimeric MT-binding domain and it functions in severing MTs (Burk et al. 2001; Bichet et al. 2001; Webb et al. 2002; Zhang et al. 2013).

Microtubule Organizing1 (MOR1) can be induced to grow with an effect on the morphogenesis at restrictive temperatures (Whittington et al. 2001). As *mor1-1* mutation

does not change the cellulose content of the walls (Sugimoto et al. 2003; Kawamura et al. 2005; Kawamura, Wasteneys 2008), the use of this mutant effect changes in cell wall organization on biomechanics. The regulation of the cell wall properties also involves the cortical cytoskeleton. Intracellular trafficking and targeted delivery of non-cellulosic wall material occur by an actin-myosin-dependent system (Wasteneys, Galway 2003; Wasteneys, Yang 2004; Bannigan, Baskin 2005; Smith, Oppenheimer 2005). Cell wall anisotropy is determined by the structure of the cell wall and the arrangement of cellulose within it. Cellulose consists of high molecular weight glucan chains arranged in partially crystalline bundles held together by numerous hydrogen bonds (Ivakov, Persson 2013). The strong cellulose fibrils are embedded in a pliant gel-like matrix consisting of hemicellulose and pectin polysaccharides. The cellulose fibrils within the cell wall is, therefore, an important determinant of the behavior of the wall during growth as well as in mature tissues (Burgert, Fratzl 2009).

MFs resist expansion most strongly parallel to their orientation and less strongly in other directions and thus form the basis for anisotropy. Cellulose is produced by cellulose synthases (CESA) complexes which are mobile in the PM and extrude glucan chains into the cell wall. Cellulose MFs have long been observed to co-align with MTs in the cell cortex (Green 1962). Plant MTs are mobile and highly dynamic structures which exhibit a treadmilling movement generated by a fast rate of net polymerization at the plus end and a slower rate of depolymerization at the minus end (Shaw et al. 2003). MT arrays have the ability to rapidly re-organize to new orientations. Such re-organization control Cesa trajectories and MF arrangements, which in turn influence cell shape. Cellulose synthase interacting1 (POM2/CSI1) is a large MT-associated protein which also interacts with the Cesa complex and was shown to be essential for the attachment of Cesa complexes to MTs.

MTs have been observed to aggregate into parallel bundles arranged transversely across future indentation regions (Fu et al. 2005b; Zhang et al. 2011) restricting local growth through their control of the ordered deposition of cellulose microfibrils. Cortical MTs also serve as tracks for cellulose synthase complexes (CSC) which aids in the synthesis of cellulose. Cellulose is the principal component of the plant cell wall and deposition of cellulose restricts growth and expansion, thus determines the direction of growth. Cellulose fibres are synthesized by CESAs at the PM. CSCs track along the cortical MTs guided by protein CSI1/POM2 (Somerville et al. 2004; McFarlane et al. 2014; Gu et al. 2010; Bringmann et al. 2012; Li et al. 2012; Liu et al. 2016). Interestingly in an unrelated study, it

was identified that this MT based guidance of CSC is affected by KLCR proteins, which are also called CMUs, mainly maintain the MT stability to direct cellulose synthase movement (Liu et al. 2016; Bürstenbinder et al. 2017a; Bürstenbinder et al. 2017b). MT needs to be tethered to the PM to withstand the force generated by CSC. CMU proteins were identified as crucial for maintaining MT stability at the PM. KLCR/CMUs are located as static puncta along cortical MTs. Knock down mutants *cmu1* and *cmu2* caused lateral MT displacement and compromised MT-based guidance of CSC movement. CSCs interacts with the MTs via CSI1/POM2, which prompts the lateral MT displacement. Interestingly some IQDs (i.e. IQD12, IQD22) were localized to MTs and punctate structures in the PM which is reminiscent of membrane subdomains which are thought to serve as a platform for signal transduction. A hallmark of IQDs is a high pI value which might contribute to the subcellular localization at MTs via electrostatic interactions with acidic tubulin motifs and PM via the acidic phospholipid surface.

It was hypothesized that due to MT displacement, *klcr1,klcr2/cmu1,cmu2* mutants were significantly shorter and wider compared with wild-type seedlings. They showed left-handed twisting of epidermal cell files in etiolated hypocotyls and also showed changes in the leaf pavement cell (PC) shape (Liu et al. 2016). Thus suggesting the function of IQD:KLCR modules at PM-MT nexus and possibly regulating cellulose deposition and ultimately cell shape.

#### **4.5 Plant cell shapes**

Plant cells exhibit a wide variety of shapes, for example, elongated shapes of root hairs, pollen tubes, trichomes, and vascular elements are all functionally significant. The shapes of these tissues provide a great impact on their function.

Among other cell shapes, PC morphogenesis is a great model system to study the cell polarity and growth in plants. Polarity formation is initiated by a polarizing signal which regulates the polar distribution of signaling molecules and leads to polarity establishment and maintenance through the cytoskeleton and vesicular trafficking (Yang 2008). Cytoskeleton plays an important role in both as an essential cellular linkage to molecular pathways by responding to the initial polarity signal and providing spatial information for feedback regulation of the polarity signaling pathways. Cytoskeleton which includes the MTs and actin MFs plays a major role in cell polarity. MT act to induce cell polarity formation by targeting and or locally activating signaling molecules at the polar site in yeast and animal cells (Yang 2008; Siegrist, Doe 2007). Till date it is known that signaling molecule regulated

by MT in these systems is a Rho family GTPase, with actin-based polarity formation and also feedback regulation of MT stabilization.

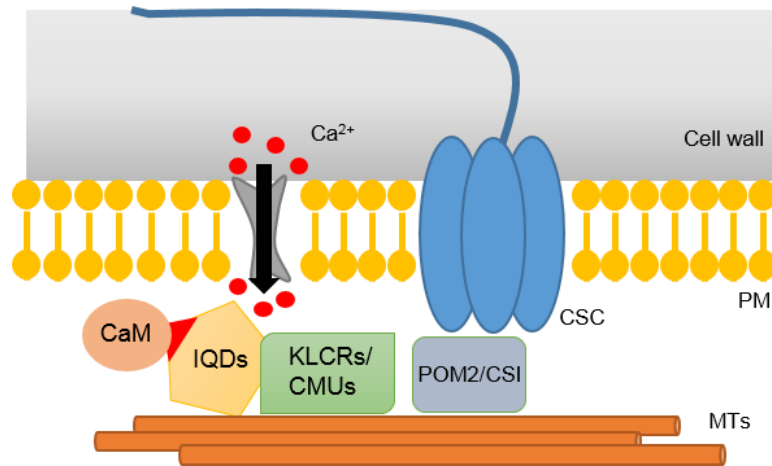


**Fig 2: Proposed model of IQD:KLCR interaction** IQD proteins localize to the PM and MTs, where they recruit CaM as well as KLCR/CMUs. IQD proteins share hallmarks of scaffold proteins, and interact with apo-CaM and Ca<sup>2+</sup>-CaM *in vitro*. We hypothesize that (i) IQD proteins sequester CaM sensors at distinct subcellular sites and thus helps in Ca<sup>2+</sup> signaling and (ii) they are part of the scaffolding complex along with KLCRs/CMUs, which links MTs to the PMs and thus helps in cellulose synthase movement.

Since KLCRs/CMUs shows the cell shape alteration phenotypes by affecting the MT stability and CSC movement and are the interacting partners of IQD proteins in yeast and *in planta* and they both localize to MTs and PMs, a hypothesis can be made that IQDs might play a role as a scaffolding protein and either directly or indirectly help in linking KLCRs/CMUs to the MTs and PM (Mukhtar et al. 2011; Bürstenbinder et al. 2017b) (Fig 2). Loss-of-function *cmu/kclr* mutants shows defects in MT dynamics and MT-related phenotypes for e.g. cell file rotation, cell shape change, altered CSC movement along the MTs etc. Interestingly, enhancement of MT recruitment of KLCR/CMUs upon co-expression of IQD1 was observed in our previous studies, suggesting a role of IQDs in targeting and stabilizing KLCR/CMUs at PM (Bürstenbinder et al. 2017b). Together it suggests that IQD-KLCR/CMU complexes might regulate plant growth in meristematic tissues at PM-MT nexus and might also indirectly affect the cellulose deposition. Taken this together IQDs might be good candidates for tethering MT to the PM and function together with KLCR/CMUs in the cell shape formation. To elucidate the molecular mechanism of IQDs *in planta*, most of the work in our group is thus based on the functional characterization of *Arabidopsis* IQDs and KLCRs.

## 5 Outline

To elucidate the molecular function of IQD-KLCR modules, the focus of this work is the functional characterization of four phylogenetically related IQD proteins of subclade IIIa (IQD5, IQD6, IQD7, and IQD8) and KLCR1, KLCR2 and KLCR3 from *Arabidopsis thaliana* by reverse genetic approaches. This include establishment of transgenic lines, generation of expression maps by analysis of transgenic *Promoter:GFP-GUS* reporter lines to identify spatiotemporal expression domains, generation and analysis of *IQD* and *KLCR* overexpression lines and characterization of T-DNA insertion lines and phenotypically investigating these lines.

Major aims of the project are to study:

1. Subcellular localization of IQD subclade IIIa and KLCR proteins
2. Expression domain of *IQD IIIa* and *KLCR* family
3. Phenotypic analysis of the *iqd* and *kacr* misexpression lines
4. Identification of novel interacting partners

## 6 Results

### 6.1 Subcellular localization of IQD5 to IQD8, members of subclade IIIa

Subclade IIIa comprises IQD5, IQD6, IQD7, IQD8, IQD9, and IQD10 (Fig 3A). Within this work, IQD7 and IQD8, which are encoded by a pair of sister genes, and the most closely

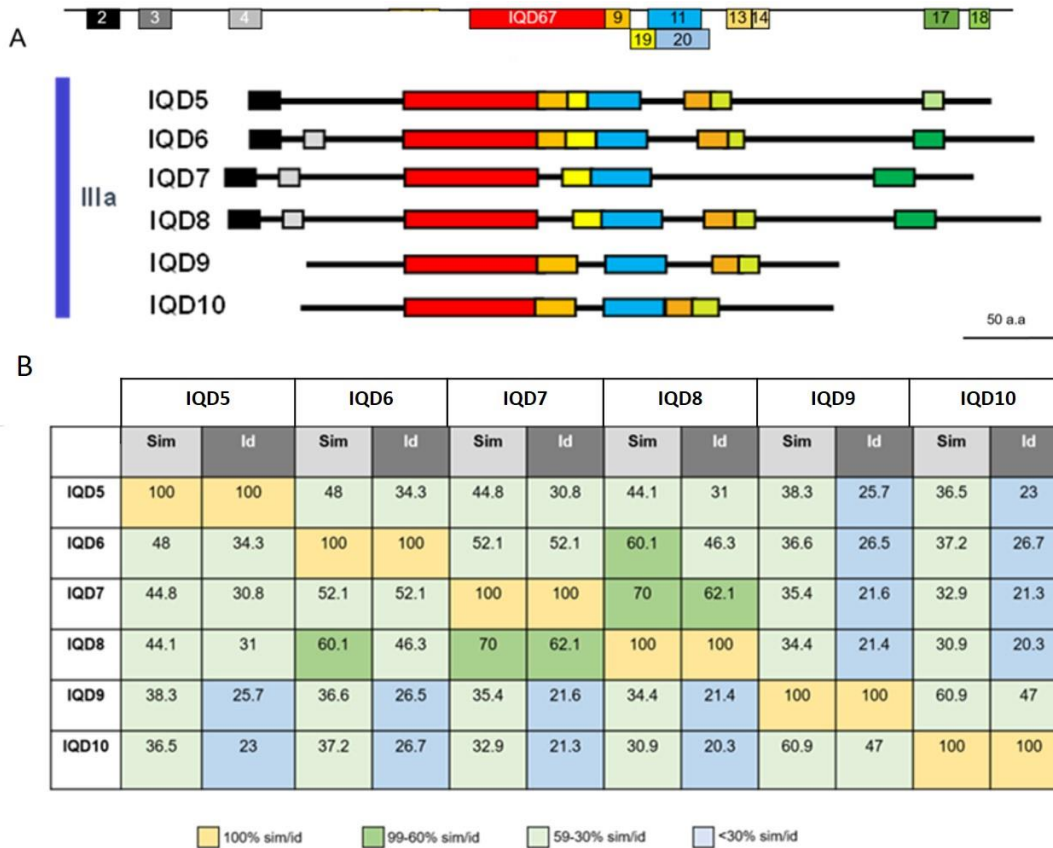


**Fig 3: Sequence similarity comparison among IQD subclade IIIa proteins** (A) Motif distribution of subclade IIIa IQD members modified from Abel et al. (2005), all motifs are related family members IQD5 and IQD6 were analyzed. A sequence similarity and sequence identity analysis was done using Basic local alignment search tool (<https://blast.ncbi.nlm.nih.gov>), to compare the IQD subclade IIIa proteins based on their amino acid sequences. The analysis showed that IQD9 and IQD10 are least similar to the other members of the subclade (Fig 3B), which can be further explained based on their sequence structure. This weak similarity most likely is due to the reduced length i.e. IQD9 and IQD10 lack the N- and C- terminal motifs which are commonly found in the other IQDs

of the same subclade (Fig 3A). Furthermore, the subcellular localization of IQD9 and IQD10 showed weak MT localization compared to the other members. Thus in this project, we mainly focused on IQD5 to IQD8 and excluded IQD9 and IQD10 from our analyses.

Previous work demonstrated localization of N-terminal GFP fused IQD5-IQD8 variants to MTs and also partial PM association of IQD6-IQD8 (Bürstenbinder et al. 2017). To test the influence of the GFP tag on the subcellular localization, the analyses with both N- and C-

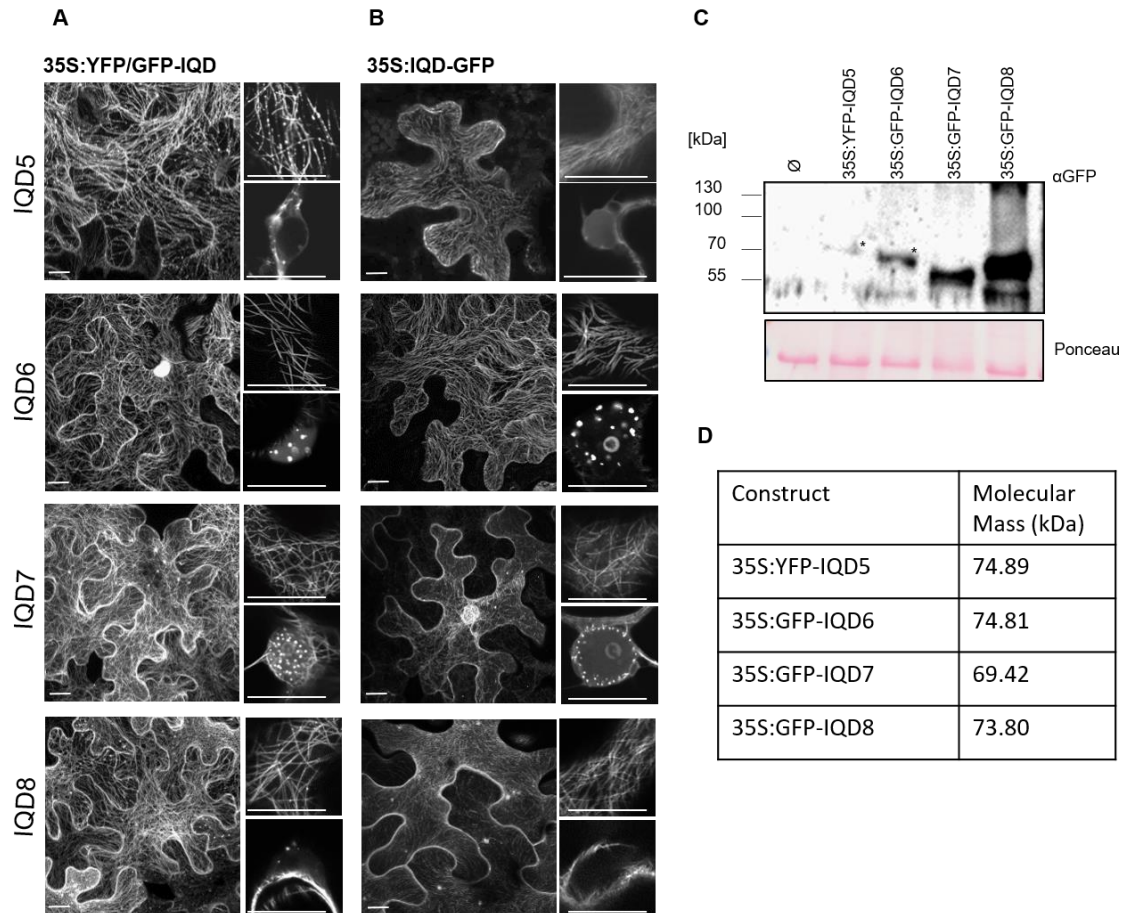


**Fig 4: Subcellular localization of Arabidopsis GFP-IQD fusion proteins in *N.benthamiana***

(A) Transiently expressed N-terminal GFP-IQD (IQD5-IQD8) fusion proteins expressed under the *CaM35S* promoter tagged with GFP. (B) Localization of C-terminal IQD (IQD5-IQD8) fusion proteins expressed under the *CaM35S* promoter tagged with GFP. Micrographs of cells are projections of Z-stack; insets are single layer images. Scale bars represent 20  $\mu$ m and 10  $\mu$ m (insets; top-MT localization; bottom-nucleolar localization). (C) Immunoblot analysis to show the expression of full-length GFP-IQD fusion proteins using an anti-GFP antibody. Asterisks (\*) represent full proteins. (D) Molecular sizes of the full length 35S:GFP-IQD fusion proteins. Immunoblot assays were not performed for C-terminal fusions.



terminal GFP reporter gene tagged IQD constructs were studied to test if the MT localization is the native localization of the IQD subclade IIIa proteins and it is independent of the fact that to which terminal GFP is tagged. Fig 4A and 4B shows similarities and differences between N- and C- terminal tagged variants, where mainly the difference can be seen for IQD7 and IQD8. The N-terminal GFP tagged IQD7 and IQD8 show more MT localization and for C- terminal tagged variants, they show more PM localization. For IQD6 the MTs for

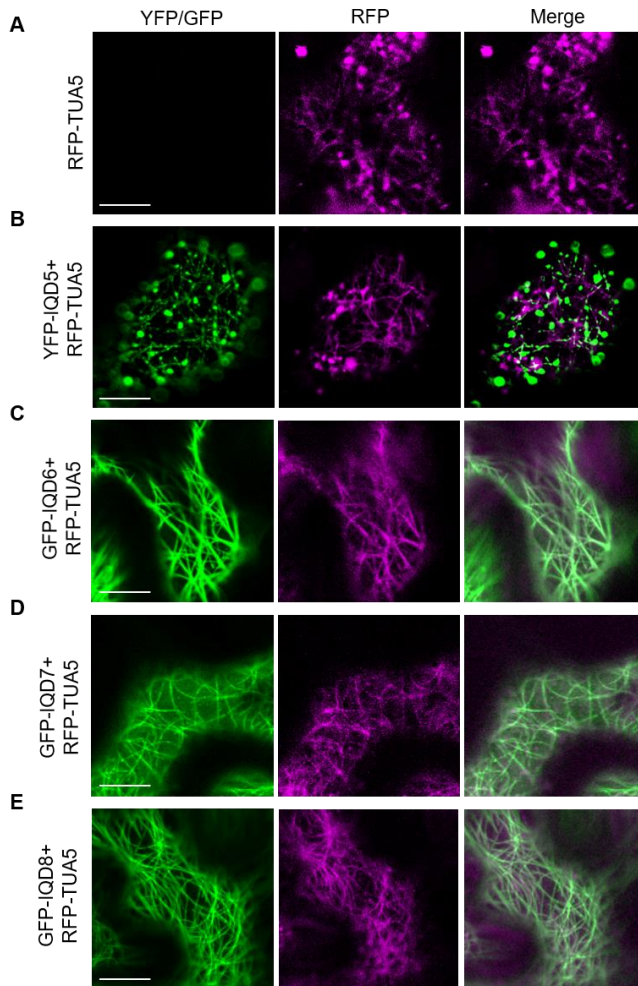


**Fig 5: Validation of MT localization of GFP-IQD fusion proteins in *N.benthamiana*** Co-expression of *35S::RFP-TUA5* with *35S::YFP/GFP-IQD* (IQD5-IQD8) (B-E) in *N.benthamiana* (A) Expression of RFP-TUA5 alone. The left column shows the GFP channel, middle RFP, right merged channels. Micrographs of cells are projections of single layer images. Scale bars represent 20  $\mu$ m.

C-terminal GFP variant looks thicker than the N-terminal variant. Also for IQD5, it is prominent that N-terminal GFP tagged variant shows punctured structures whereas it is not visible for the C-terminal variant. Apart from the MT localization, IQD6 and IQD7 show nucle(o)ar localization as well. IQD6 and IQD7 show punctured structures of unknown function, in the nucleus for both N- and C-terminal GFP tagged variants (Fig 4A insets). In IQD8, localization is visible on the nuclear envelope. Thus it suggests that IQDs might be actively be imported in nucleus since diffusion is not possible, as the nuclear pore can only support proteins with sizes upto 40 kDa (Kabachinski et al. 2015). The integrity of full-length fusion proteins was confirmed by western blot analysis using an anti-GFP antibody and it could successfully detect the full proteins of interest (Fig 4C). MT localization of IQD subclade IIIa proteins was confirmed by co-expression with



the MT marker RFP-TUBULIN ALPHA-5 (RFP-TUA5) (Gutierrez et al. 2009). RFP-TUA5 labels MTs and GFP/YFP fusions of all four analysed IQD proteins co-localized with RFP-TUA5 labelled MTs (Fig 5).

To validate the localization patterns, and to study functions of IQDs in *Arabidopsis*, we generated transgenic plants, overexpressing the respective *IQDs*. We generated most of the stably transformed IQD lines and successfully could also establish the homozygous  $T_3$  lines. All  $T_2$  lines were analyzed for a 3:1 segregation ratio on selective media to verify the presence of a single insertion, and subsequently  $T_3$  homozygous were established. To confirm the localization of subclade IIIa IQDs in stably transformed *Arabidopsis thaliana* lines, we analyzed homozygous  $T_3$  lines expressing N-terminal and C-terminal GFP fusions of the four IQDs (IQD5-IQD8) expressed under the *CaMV35S* promoter. *35S:IQD5-GFP* could not be included in this study as there were no homozygous lines available. MT localization of IQD5, IQD6, IQD7, and IQD8 in *Arabidopsis thaliana* suggests that the localization observed in *N.benthamiana* is not an artifact of expression but it is also detectable in *Arabidopsis* (Fig 6 and Fig 7).

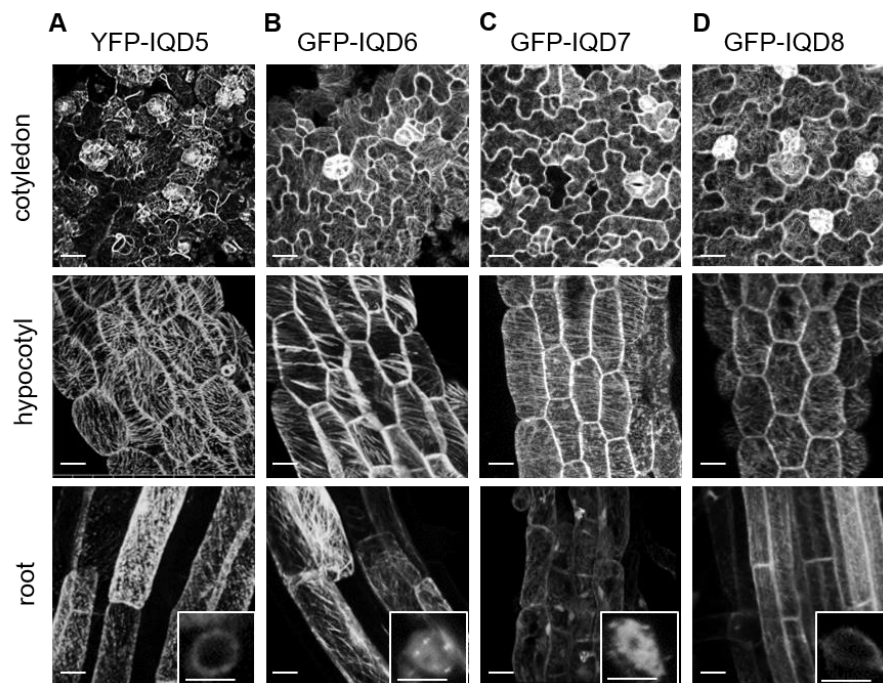


**Fig 6: Subcellular localization of IQD5 to IQD8 in transgenic *35S:YFP/GFP-IQD*** Subcellular localization of (A) YFP-IQD5, (B) GFP-IQD6, (C) GFP-IQD7, and (D) GFP-IQD8 in cotyledons (top), hypocotyl (middle) and root cells (bottom) of transgenic *Arabidopsis* plants. Images are maximum projections of z-stacks, scale bars, 20  $\mu\text{m}$ . Insets show single optical sections of nuclei; scale bar, 10  $\mu\text{m}$ .

Similar to the effects observed in tobacco, overexpression of *IQDs* altered MT organization in transgenic *Arabidopsis* plants with *IQD* overexpression. The patterns of N- and C-terminal fusions MTs differed between lines as for *IQD7* and *IQD8*, the localization for the C-terminal GFP tagged variant were more on the membrane side rather than on the MT side as in the N terminal tagged variants (Fig 6 and 7).

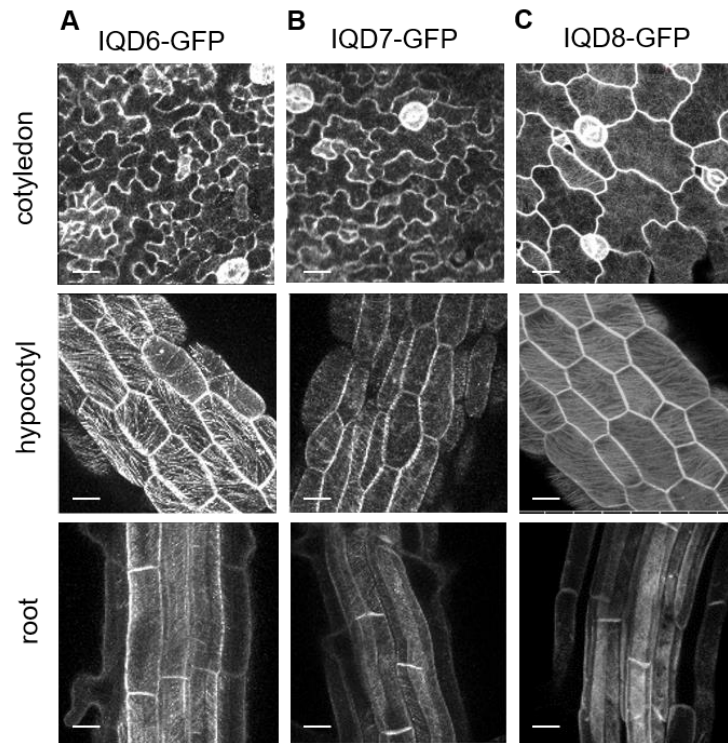


**Fig 7: Subcellular localization of IQD5 to IQD8 in transgenic *35S:IQD-GFP*** Subcellular localization of (A) *IQD6-GFP*, (B) *IQD7-GFP*, (C) *IQD8-GFP*, in cotyledons (top), hypocotyl (middle) and root cells (bottom) of transgenic *Arabidopsis* plants. Images are maximum projections of z-stacks, scale bars, 20  $\mu$ m.

Apart from the localization, there were also cell shape changes visible, for e.g; *35S:YFP-IQD5* and *35S:GFP-IQD8* had altered cell shape in the cotyledon and hypocotyl. The PCs in the cotyledon of *IQD5* and *IQD8* lines were more circular in shape than in other overexpressed *IQDs* and the hypocotyls were much shorter with more circular cells than the wild type (WT). The overall phenotype was also different as the seedlings for overexpressed *IQD5* and *IQD8* were shorter and thicker than WT or *IQD6* and *IQD7* overexpression lines.

Overall from the above experiment, we hypothesize that IQDs function in MT organization and patterning. Treatment of the *35S:GFP-IQD* plants with the MT-depolymerizing drug oryzalin was performed to confirm the MT localization of IQD IIIa proteins. Oryzalin is a dinitroaniline herbicide that shows a strong binding affinity for plant tubulins and it inhibits MT polymerization (Bogyo et al. 2014). For positive control, the MT marker plants GFP-

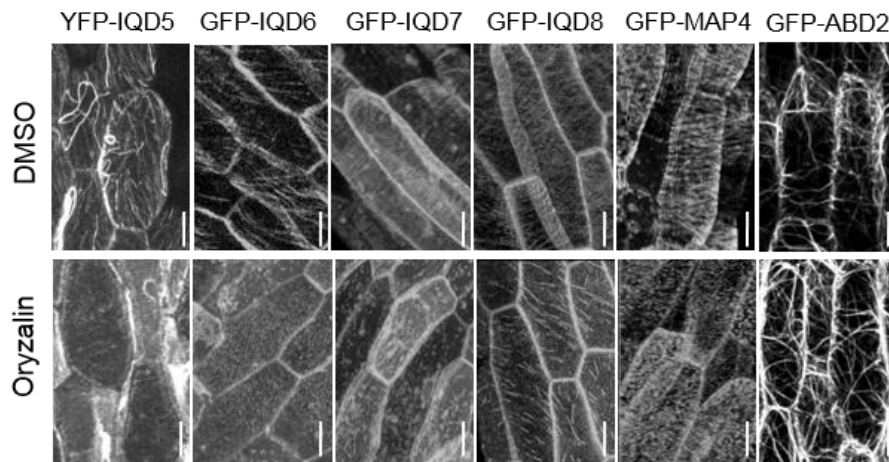


**Fig 8: Validation of MT localization by oryzalin drug treatment in transgenic Arabidopsis lines** Subcellular localization of GFP-IQD (IQD5-IQD8), GFP-MAP4 and GFP-ABD2 fusion proteins in hypocotyls of GFP-IQD (5-8) treated with DMSO or with MT-depolymerizing drug oryzalin. Micrographs of cells are projections of Z-stack images. Scale bars represent 20  $\mu\text{m}$ .

MAP4 were also treated with oryzalin, which showed depolymerization of MTs upon treatment. For negative control, actin-binding protein GFP-ABD2 upon treatment with oryzalin showed no effects (Fig 8), demonstrating efficiency of oryzalin mediated MT disruption and specificity towards MTs. Thus the experiment validated the fact that IQDs are localized to the MTs. The sensitivity to oryzalin, however, was different for the IQDs (IQD5-IQD8), as in GFP tagged IQD5-IQD7, the MTs were depolymerized within 20 minutes of the treatment, the MTs of GFP-IQD8 were only partially depolymerized within this time, suggesting that IQD8 might play a role in stabilizing the MTs.

During our analysis of the *IQD5-IQD8* overexpression transgenic lines, we observed some unknown bundle like patterns in the *IQD5* overexpression lines, both in the cotyledon and in hypocotyl (Fig 9). The exact functions of these pattern are not known but we hypothesize that IQD5 could lead to bundling of MTs resulting in these patterns. To know the exact

functions, mcherry-TUA5, a MT marker is incorporated into untagged *IQD5* overexpression lines and the homozygous lines will be established and analyzed in future experiments.

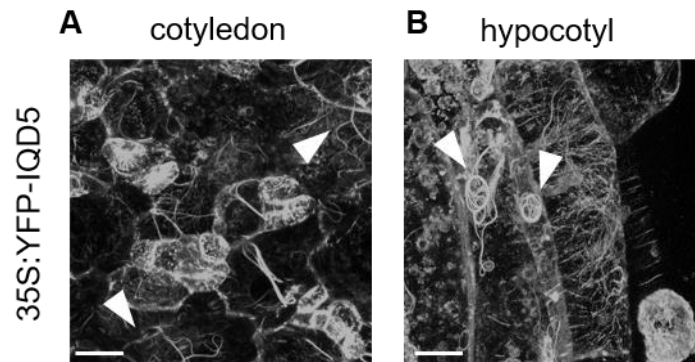


**Fig. 9: MT organization of oxYFP-IQD5 lines** Subcellular localization of *35S:YFP-IQD5* in (A) cotyledon and (B) hypocotyl of transgenic *Arabidopsis* plants. Images are maximum projections of z-stacks, scale bars, 20  $\mu$ m.

## 6.2 Phenotypes in *IQD* overexpression lines

Phenotypic analysis conducted in our group with overexpression lines previously revealed, that plants overexpressing *IQD8* display a phenotypic alteration in the cellular and morphological level when compared to WT (Bürstenbinder et al. 2017) also shown in Fig.10, which was not the case with *IQD6* and *IQD7* overexpression lines.

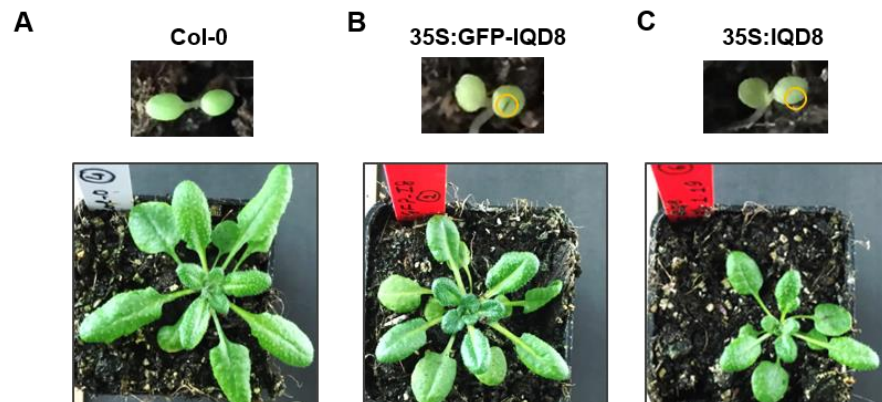


**Fig 10: Phenotypic analysis of *IQD8* overexpression lines:** Analysis of (top) 5-day old seedling and (bottom) 2-weeks old plants of (A) WT, (B) *35S:GFP-IQD8* and (C) *35S:IQD8*.

We repeated the analysis with N-term, C-term and untagged *IQD8* overexpression lines and a similar phenotype in *35S:GFP-IQD8*, *35S:IQD8-GFP* and *35S:IQD8* untagged overexpression lines confirmed the functionality of GFP fusions. Overexpression of *IQD8*

led to leaf PC alteration with large circular cells (Fig 11), there was an increase in the circularity of the cells and number of lobes were decreased. Quantification using the Fiji (ImageJ) plugin showed decrease in margin roughness, in this case possibly caused by the decrease in number of lobes thus suggesting more circular cells when compared to WT. The effect was similar in all the three lines, the untagged overexpression lines and the GFP tagged variants in this initial experiment. Thus the PC shape observed in the overexpressing lines of *IQD8* indicates possible role of *IQD8* in leaf cell shape pathway. To understand better if overexpression of *IQD8* in these lines affect the MTs and thus cause this alteration in cell shape, we have incorporated *35S:mcherry-TUA* into the untagged *35S:IQD8* and the homozygous lines will be analyzed in future experiments.

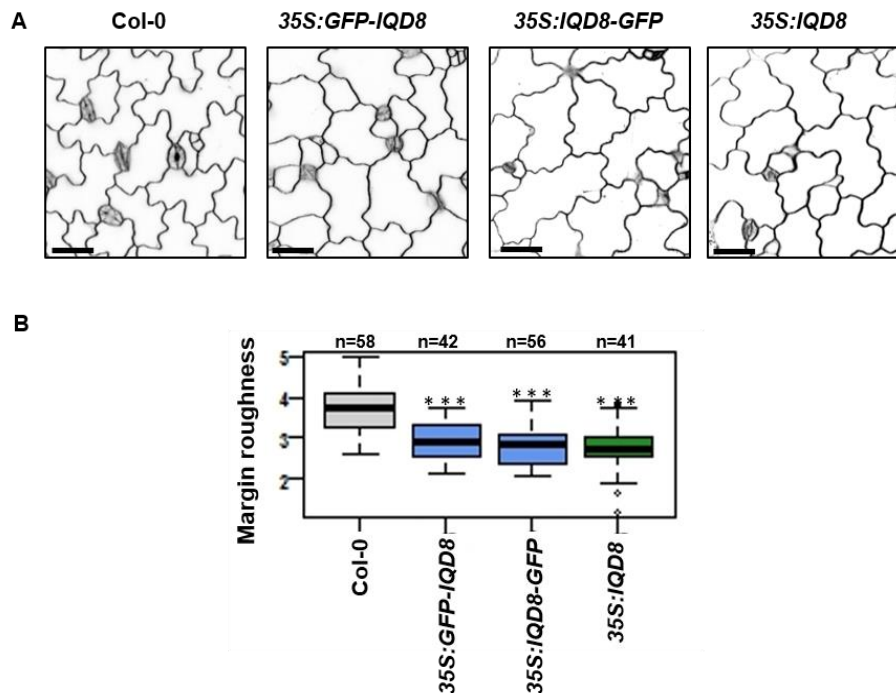


**Fig 11: Alteration of leaf PC in *IQD8* overexpression lines** (A) Overexpression of *IQD8* alters the leaf PC shape when compared to WT. PM was stained with FM4-64. Scale bar represents 50  $\mu$ m. (B) Quantification based on margin roughness shows a significant difference in *IQD8* gain-of-function lines compared to WT. P value calculated by one way ANOVA, Tukey test. Micrographs of cells single optical images of the adaxial (upper) side of the cotyledons. Results are median of  $n > 40$  cells,  $p < 0.001$  one-way ANOVA. Asterisks (\*\*\*) represents high significance.

Next we additionally checked with the newly established homozygous overexpression lines of *IQD5* if they have any similar effects on PC cell shape like *IQD8*. Indeed, the initial experiments showed that overexpression of *IQD5* had a similar effect on PC (Fig 12). For

the preliminary analysis, two homozygous  $T_3$  lines and two  $T_2$  lines with 3:1 segregation ratio were used. Since, all the lines for overexpression of *IQD5* including N- and C-terminal and untagged homozygous lines are not available, an analysis with the full set with quantification will be done after we establish all the missing lines.

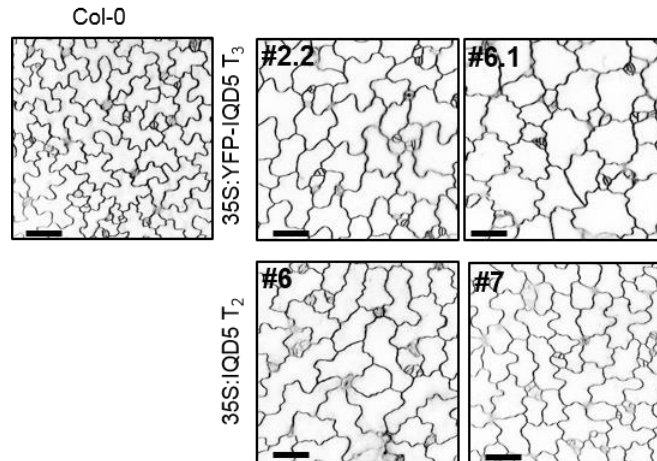


**Fig 12: PC phenotypes in *IQD5* overexpression lines** Epidermal PC shape analysis in 5-day old *IQD5* overexpression lines and in WT, #number represents the  $T_2$  and  $T_3$  lines. Cell PM was stained using FM4-64 stain. Scale bars represent 50  $\mu$ m.

One possibility could be that phenotypes in these overexpression lines, could be artifact of ectopic overexpression or dosage dependent effects of individual IQDs on MT organization. Thus to know the true phenotypes of *IQD5* and *IQD8* which localize to MTs, with overexpression lines altering the MT stability (as shown in Fig. 8), we studied the expression patterns of these *IQDs* and analyzed their knock-out lines.

### 6.3 Expression analysis of *IQD5* to *IQD8*

To gain insights into the biological functions of IQD proteins, tissue-specific and developmental expression patterns of *IQDs* were studied. To study the spatio-temporal expression patterns of *IQDs*, promoter GFP-GUS reporter constructs were studied. For the *Promoter:GFP-GUS* reporter expression analysis, we cloned two different promoter length starting from upstream of ATG sequence of the gene, one spanning 1.5 kb and the long fragment spanning around 2.2 kb upstream of the translational start site of the *IQD* gene (Fig 13 left panel), which were fused to the reporter to generate short and long promoter variants respectively. Two different lengths were chosen since the position of the regulatory



cis-elements are not known. The  $T_2$  stably transformed lines were first segregated based on their representative staining pattern and then based on their 3:1 segregation ratio. The presence of the correct constructs was confirmed by polymerase chain reaction (PCR) in three independent  $T_3$  homozygous lines by amplifying the construct using the forward primer (F.P) of the promoter and the GFP promoter (Figure 13 right panel).

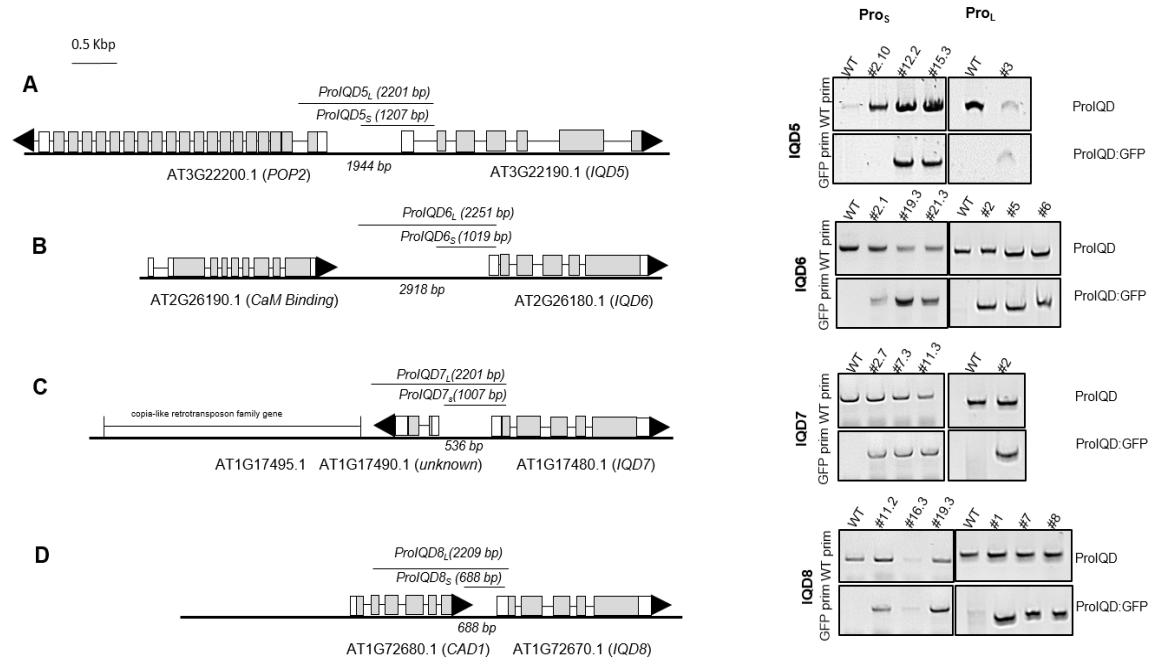


**Fig 13: Generation of transgenic *PromoterIQD:GFP-GUS* reporter lines** (Left) Gene model showing the region of long and short promoter amplification selected for generating the *Promoter:GFP-GUS* construct. Boxes indicate the 5'UTR and 3'UTR, and exons. Introns are represented by the black line. Scale represents 500 bp. (Right) PCR confirmation of promoter-reporter constructs of (A) *IQD5*, (B) *IQD6*, (C) *IQD7* and (D) *IQD8*. In the PCR gels, upper band: obtained from the amplification of the whole gene; lower band: obtained from the amplification of gene specific forward primer and GFP specific reverse primer (R.P).

To study expression patterns, we compared the GUS and GFP localization in the two promoter variants to identify the native expression domain of the *IQD5-IQD8*. Unique patterns were observed in the roots, where *IQD5* was mostly expressed in the root cap, *IQD6* activities were observed in the stele, *IQD7* in the columella and *IQD8* throughout the entire root meristem. Histochemical GUS analysis of *ProIQD:GFP-GUS* lines throughout development revealed strong promoter activity in cotyledons and leaves, in the vasculature of leaves and the hypocotyl, as well as in the shoot apical meristem (Fig. 14). Similar expression patterns were observed in *ProIQD<sub>L</sub>:GFP-GUS* lines (Fig 14A, B and C right

panel), suggesting that the short promoter fragment was sufficient to show native *IQD* expression patterns.

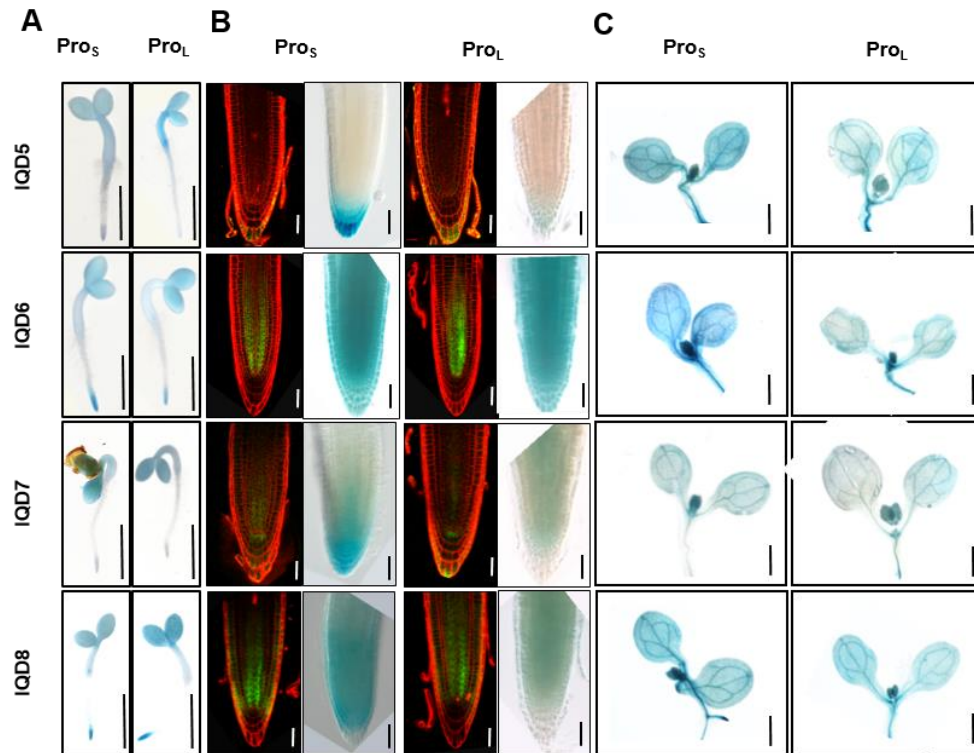


**Fig 14: Promoter activity of *IQD5* to *IQD8* in 4-day-old seedlings** Histochemical GUS and GFP fluorescence analysis and comparison of transgenic lines of *ProIQD: GFP-GUS (IQD5-IQD8)* for short ( $Pro_S$ ) and long promoter ( $Pro_L$ ) fragments in 4-day old seedlings of *Arabidopsis* plants (A) whole seedling (B) roots and (C) cotyledons. Scale bars represent 1 mm in GUS stained images and scale bars in Fig B represent 20  $\mu$ m.

GUS activity was largely absent from reproductive organs, such as flower buds, flowers, siliques and seeds (Fig 15 and Fig 16). Our analysis thus reveals preferential expression of *IQD5* in vegetative tissues of shoots and roots. *IQD6-IQD8* are expressed stronger in meristematic tissues. For a higher resolution cell-specific analysis of promoter activities, we took advantage of the GFP reporter fused to GUS and analyzed the GFP signal under a confocal laser scanning microscope (CLSM), which showed expression of *IQDs* in specific cells in roots (Fig 14B). Since, now we had a hint of where and when the individual *IQDs* are expressed, we screened mutants for a phenotype to know what biological role these complexes might play. Based on the available data, phenotypic characterization studies were initiated with loss-of-function lines as analysis of gain-and loss-of-function lines will allow the identification of biological functions of individual IQD members.



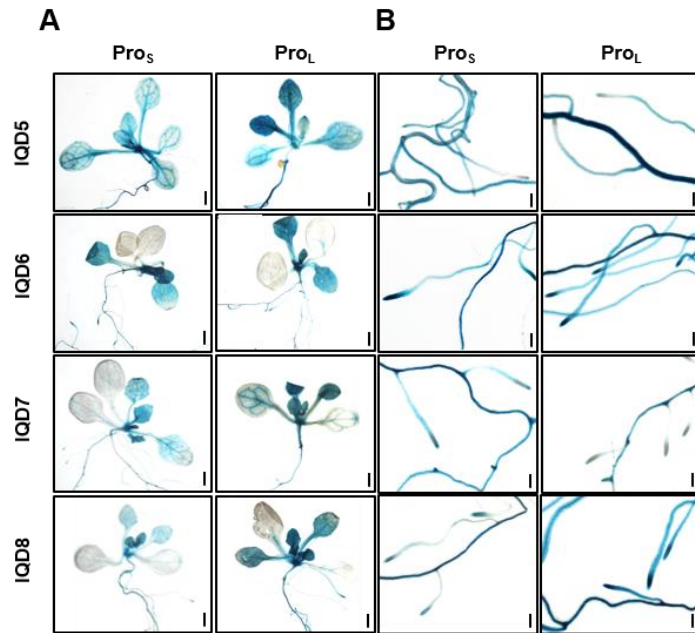


**Fig 15: Expression of *IQD* subclade IIIa genes in 10-day old seedlings** Histochemical GUS and GFP fluorescence analysis and comparison of transgenic lines of *ProIQD:GFP-GUS* (*IQD5-IQD8*) for short ( $Pro_s$ ) and long promoter ( $Pro_L$ ) fragments in 10-day old seedlings of *Arabidopsis* plants (A) shoot and (B) lateral roots. Scale bars represent 1mm in GUS stained images.

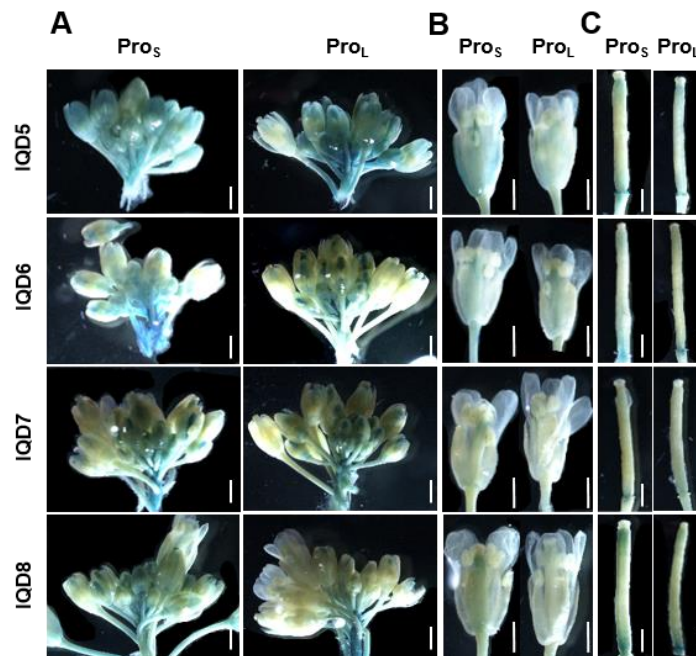


**Fig 16: Expression of *IQD* subclade IIIa genes in flowers and siliques** Histochemical GUS and GFP fluorescence analysis and comparison of transgenic lines of *ProIQD: GFP-GUS* (*IQD5-IQD8*) for short ( $Pro_s$ ) and long promoter ( $Pro_L$ ) fragments in (A) floral bud, (B) flower and (C) siliques of 6-week old plants. Scale bars represent 1mm in GUS stained images.

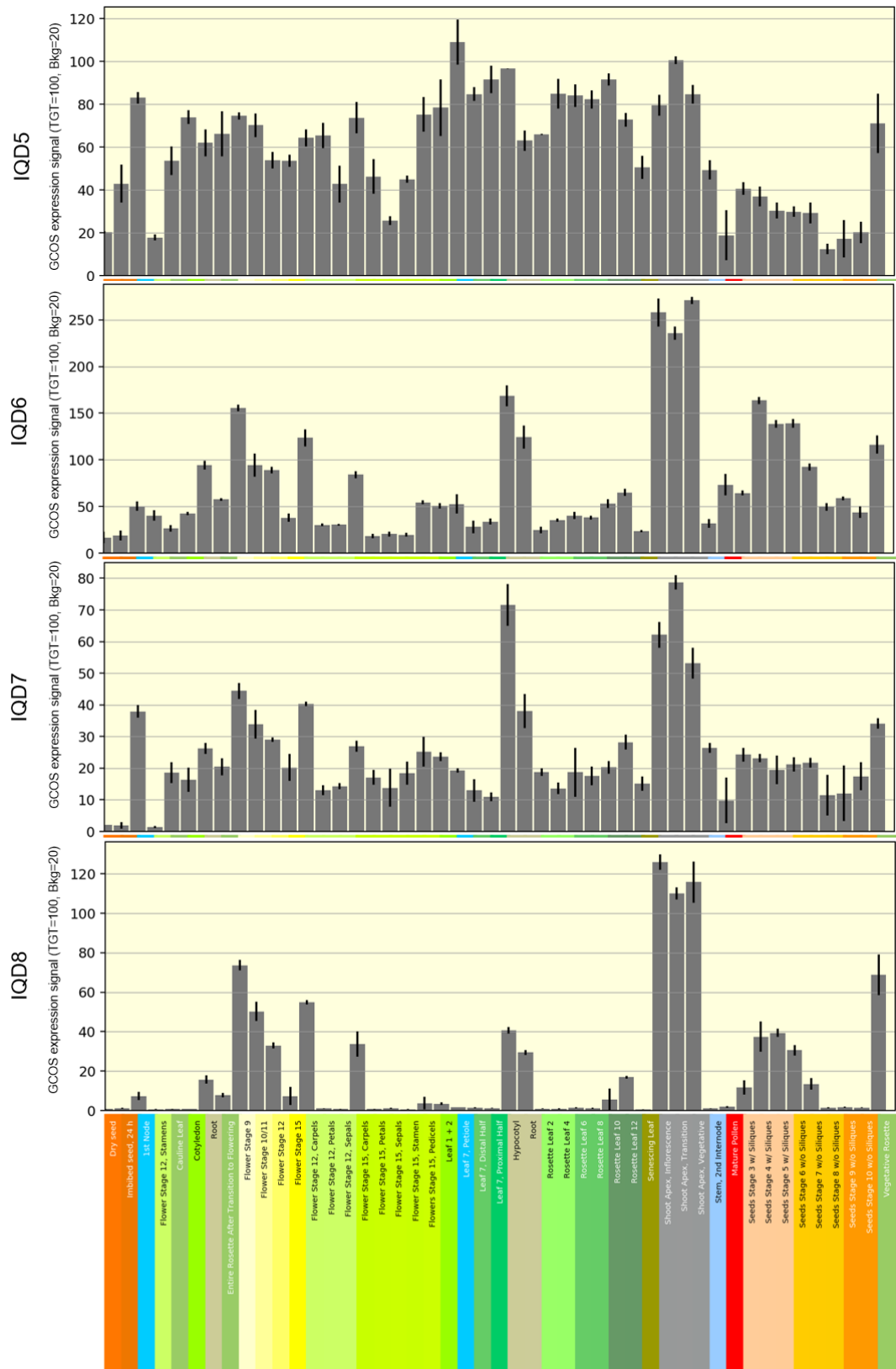


**Fig 17: *In silico* expression analysis of IQD subclade IIIa genes** *In silico* expression analysis values of IQD5-IQD8 obtained from eFP browser.

The GUS patterns are consistent with developmental *IQD5-IQD8* expression data obtained from publicly available microarray datasets (Fig 17 and Supplementary Fig S1 and S2) indicating that *IQDs* might play a role in the growth and development in plants.

Thus the result obtained for this section, *IQD5-IQD8* show unique and overlapping expression domains. *IQD8* strongest in root a shoot meristem, partially overlapping with *IQD6* and *IQD7*. *IQD5* mostly absent from dividing tissues, more present in expanding vegetative tissues. Expression domains partially overlap with tissues, in which overexpression caused phenotypic differences and thus most likely are a consequence of dosage-dependent effects than artefacts of ectopic overexpression. Thus to test if these phenotypic differences also can be observed in the absence of these genes, we next studied the knock out lines.

#### **6.4 Phenotypic characterization of *iqd5* to *iqd8* knockout lines**

For the identification of loss-of-function by knockdown and knockout alleles, we took advantage of publicly available selected T-DNA insertion lines, if possible multiple T-DNA alleles, preferentially in early exons. Homozygous T-DNA insertion lines were already available in the group. For *IQD6* and *IQD8*, only single lines were available, for *IQD7*, in other lines T-DNA cassette was not detectable.

All lines were back-crossed to reduce risk of second site insertions. Fig. 18A shows the gene model with the position of insertions in *IQD5-IQD8*. To test whether the T-DNA cassettes cause loss of the respective genes, RT-PCR analyses were conducted. For *iqd5-2*, *iqd5-3*, *iqd6-1*, *iqd7-3* and *iqd8-1*, RNA was extracted from the whole seedlings and gene expression was analyzed by RT-PCR (Fig.18B). For RT-PCR the amplifications were made from the full transcript. Genomic DNA was also included to check the possibility of genomic DNA contamination in RNA extraction and milliQ water was included to check contamination if any in the PCR buffer.

*Actin2* is a house keeping gene that expresses in all tissues and it was used in the above RT-PCR as a control (González-Aguilera et al. 2016). Amplification of *Actin2* in this case shows the integrity of RNA and efficiency of cDNA synthesis.

For IQD5, there are two publicly available T-DNA insertions lines, among which *iqd5-2* shows no transcript but *iqd5-3* shows a faint transcript indicating the possibility of *iqd5-3* to be a knock down mutant, but further q-PCR studies were performed in our group which confirmed this line also to be a knock-out line (Mitra et al. 2019).

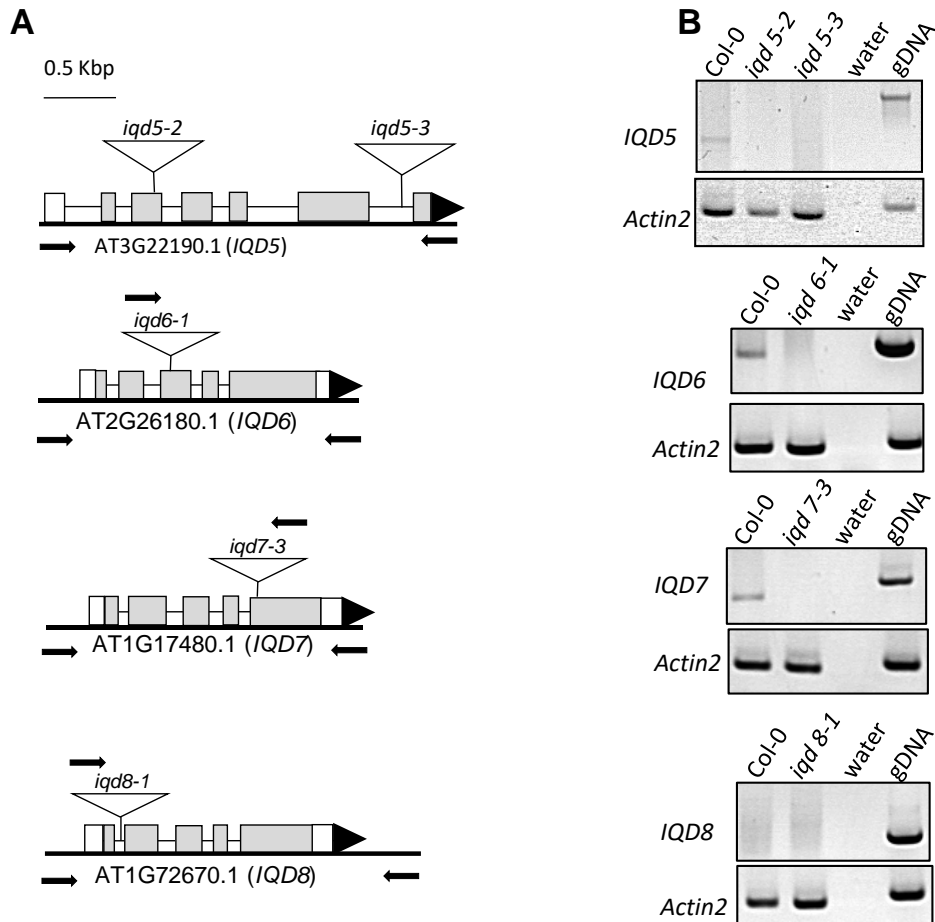


**Fig 18: Establishment of *IQD* subclade IIIa knock out lines** (A) Gene model and position of T-DNA insertions in *IQD5*, *IQD6*, *IQD7*, and *IQD8*. Boxes indicate the 5'UTR and 3'UTR, and exons. Introns are represented by the black line. The black arrows represents the region amplified in RT-PCR. (B) Upper band: RT-PCR analysis of *IQD* (5-8) transcript levels in Col-0 and knock out lines. Lower band: RT PCR analysis of reference gene *ACTIN2*.

For *iqd6-1*, *iqd7-3*, amplification made from the full transcript shows no band thus confirming that these are complete knock out mutants. For, *iqd8-1*, amplification using the primers for the full transcript was not successful at first attempt (Fig 18B), though using high quantity

of RNA could amplify the WT band and gave no transcript for *iqd8-1* for the region amplified, thus confirming the line as a knock out mutant (Mitra et al 2019).

From previous studies, the exact biological functions of IQDs were not known. Given the large size of the family, they should have an important function, but until now as shown in the previous section, we only had hints about their role from the available overexpression lines of *IQD5-IQD8*. We compared the growth phenotype of the T-DNA lines with WT Col-0 lines. To elucidate the biological role of IQDs, we initially did a macroscopic analysis of

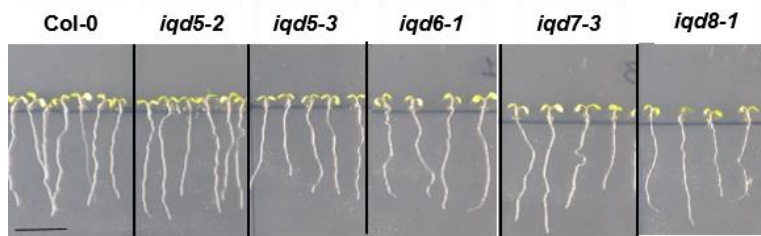


**Fig 19: Growth analysis of *iqd* loss-of-function lines** 5-day-old plants grown vertically on ATS plates were analyzed macroscopically. Scale bar represents 1 cm.

the seedlings.

The experiment was repeated with proper biological and technical replicates, but the single knock-out lines didn't show any alteration in growth (Fig 19). Since IQDs

are MT localized, and MT is the backbone of many features of the plants, we started comprehensively analyzing the plants at the macroscopic level on soil and on ATS plates for alterations if any, but we didn't find any visible macroscopic phenotypic changes. Thus next we started analyzing seedlings at the microscopic level.

To extend our study, *IQD5*, *IQD6*, *IQD7* and *IQD8* which also shows expression in leaves and shoot apical meristems, we conducted PC shape analysis in all the single knock out mutants of *iqd5-iqd8*. PCs are the most abundant cell type in the leaf epidermis and provide mechanical strength to protect the underlying mesophyll layers and the photosynthetic machinery against damage, e.g. from the invasion of pathogens or from physical stress. The cells form jigsaw puzzle-like patterns, and the degree of interdigitation directly affects the physical properties of the leaf. The formation of lobes and indentation is mediated by the actin and MT cytoskeleton, respectively.

First phenotypic analyses suggest that the *iqd5* single knock shows a significant alteration in the PC shape with more circular PC cell shape and less lobular when compared to the WT Col-0 (Fig 20A). Though the expansion in general is not affected as indicated by similar

area of PCs in WT and *iqd5*.

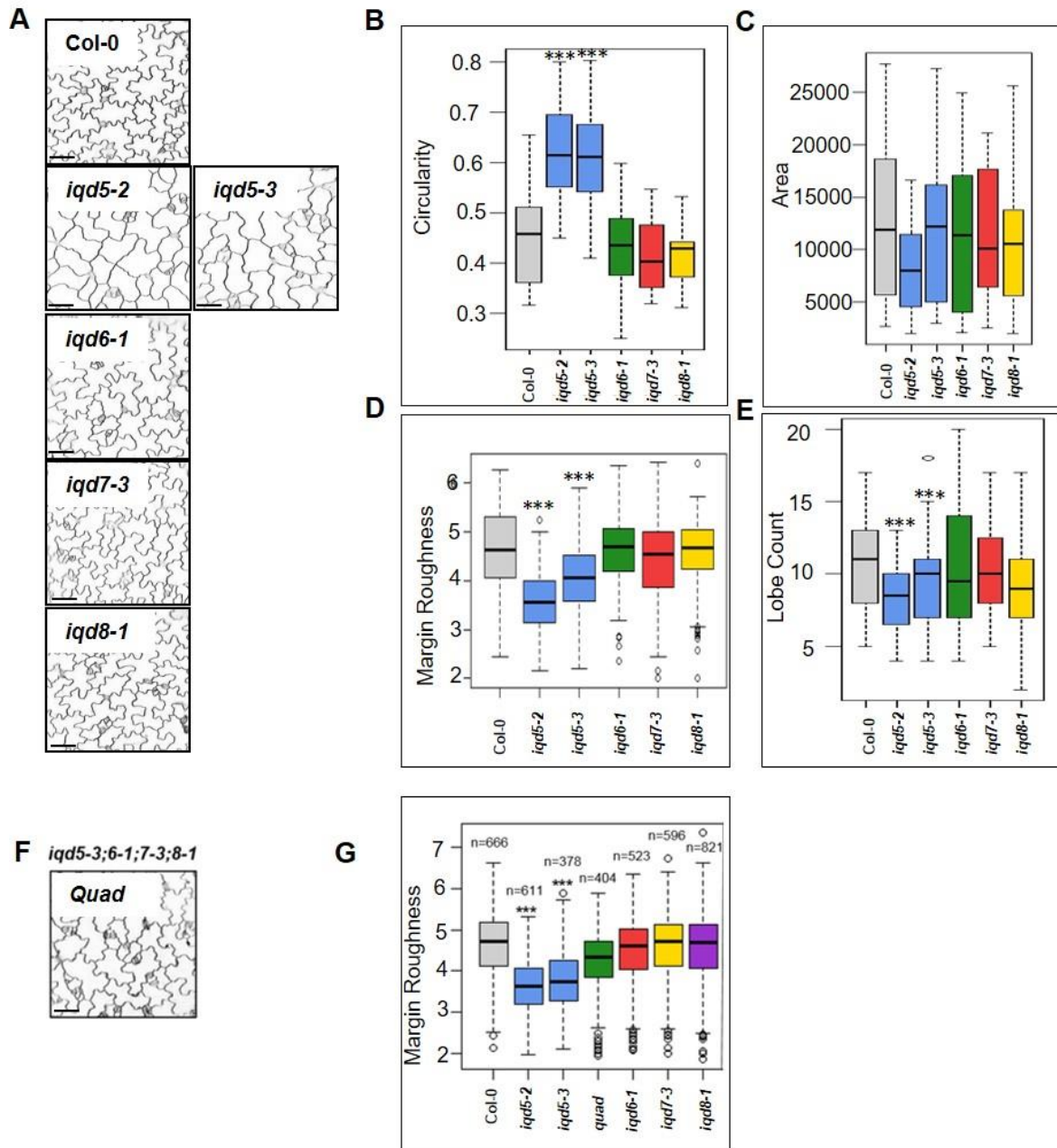


**Fig 20: PC phenotypes in *IQD* subclade IIIa knock out lines** (A) Epidermal PC shape analysis in *iqd* *ko* lines and in WT. 5-day old seedlings were used for analysis. PM was stained using FM4-64 stain. Scale bar represents 50  $\mu$ m. (B,C,D,E,) Quantification shows significant alteration in circularity and margin roughness in *iqd5* PCs. (F) shows cell shape in the quadruplet mutant (G) quantification based on margin roughness. Results are median of  $n > 100$  cells,  $p < 0.001$  one way ANOVA. Asterisks (\*\*\*) represents high significance.

Whereas *iqd6*, *iqd7*, and *iqd8* single loss-of-function lines had no obvious phenotypes when compared to WT, either due to functional redundancy or unrelated functions. To study if *IQD6*, *IQD7* and *IQD8* act functionally redundant, we established the quadruple mutant of *iqd5-3*, *iqd6-1*, *iqd7-3* and *iqd8-1* (*Quad*). Interestingly, the *iqd5,6,7,8* quadruple mutant showed PC shape similar to WT that differed from defects observed in the *iqd5* single mutants (Fig 20F).

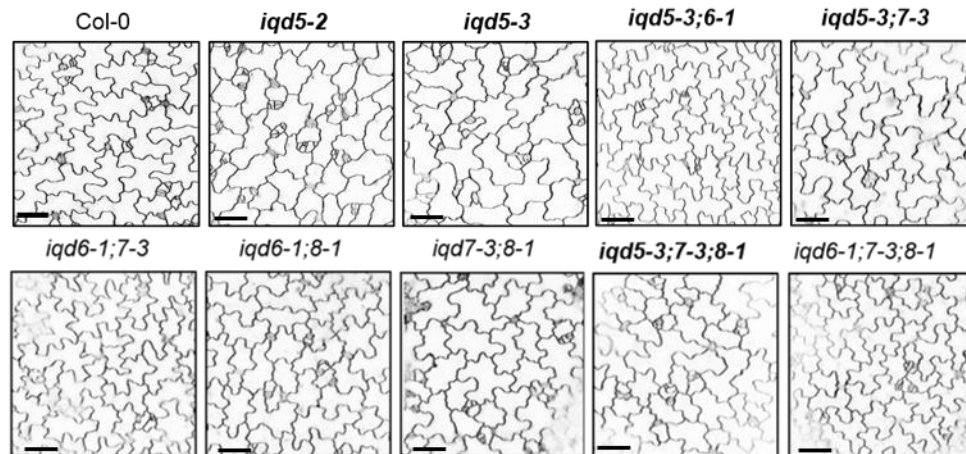


**Fig 21: PC phenotypes in higher order *IQD* subclade III knock out lines** Epidermal PC shape analysis in higher order lines and in WT 5-day old seedlings were used for analysis. PM was stained using FM4-64 stain. Scale bars represent 50  $\mu$ m.

To test potential antagonistic functions, we aimed at analysis of PC shape in double and triple mutant combinations between *iqd5*, *iqd6*, *iqd7* and *iqd8*. Double mutant *iqd5-3*, *iqd8-1*, triple mutant *iqd5-3*, *iqd6-1*, *iqd7-3* and *iqd5-3*, *iqd6-1*, *iqd8-1* are the missing lines of the set. Establishment of the missing lines are in progress and a complete quantification analysis will be done with the whole set together in future. But from the initial experiments, PC analysis showed that the available higher order mutants do not cause any major alteration in cell shape (Fig 21) unlike *iqd5* single knock out mutant. This suggests the possibility of antagonistic functions of *IQD6*, *IQD7* and *IQD8* to that of *IQD5* since *IQD6*, *IQD7* and *IQD8* might neutralize the effect of *IQD5* on the PC shape, as indicated by partial rescue of *iqd5* mutant phenotype in double, triple and quadruple mutant combinations. The distinct punctured MT pattern of *IQD5* and the similarity at protein level between *IQD5* and other *IQDs* (*IQD6-8*) of the same clade could be one of the explanations for their antagonistic behavior (Bürstenbinder 2017a). Taken together, the result shows identification of phenotypes in two independent *iqd5* mutant alleles together with MT

localization of IQD5 which links IQD5 to regulation of cell expansion. It suggests a possible distinct role of IQD5 in MT function and hence in cell differentiation and in cell shape establishment.

Moreover, since from our experiments, we observed overexpression of *IQD5* had a similar effect on PC as that of loss-of-function of *IQD5*, this could be because of the fact that both have an impact on the MTs, and alteration of the protein abundance might cause disorientation of the MT which could result in a similar cell shape alteration. It further supports scaffolding functions of IQDs because both, loss and over accumulation of a scaffold result in defects in the stoichiometry of assembled complexes.

## **6.5 Characterization of IQD5 functions during PC morphogenesis**

To understand the effect of *IQD5* expression in PC morphogenesis, we also performed a time-course analysis of the PC in four different developmental stages. Three phases of *Arabidopsis* PC development have been proposed which lead to the complex jigsaw puzzle like structure with alternate lobes and indentations (Lin et al. 2015). At stage I, small cells expand to form elongated polygons, cells enter stage II where the lobe initiation starts forming (1-2 days after cotyledon unfurling) and stage III where reiterative lobe formation generates highly complex shapes. Changes in *iqd5* mutant cell shape were visible throughout all analyzed stages, which suggests that IQD5 functions from the initial stage of lobe formation to the fully differentiated stage (Fig 22).

We quantified the data obtained based on different parameters, circularity, area, lobe depth, lobe count and margin roughness and observed a significant alteration in the cell shape for both the two independent *iqd5* mutant alleles (Fig 22A and B). We confirmed expression of *IQD5* in cotyledons throughout all stages of PC establishment by analysis of *ProIQD5<sub>s</sub>:GFP-GUS* (Fig 22A bottom panel).



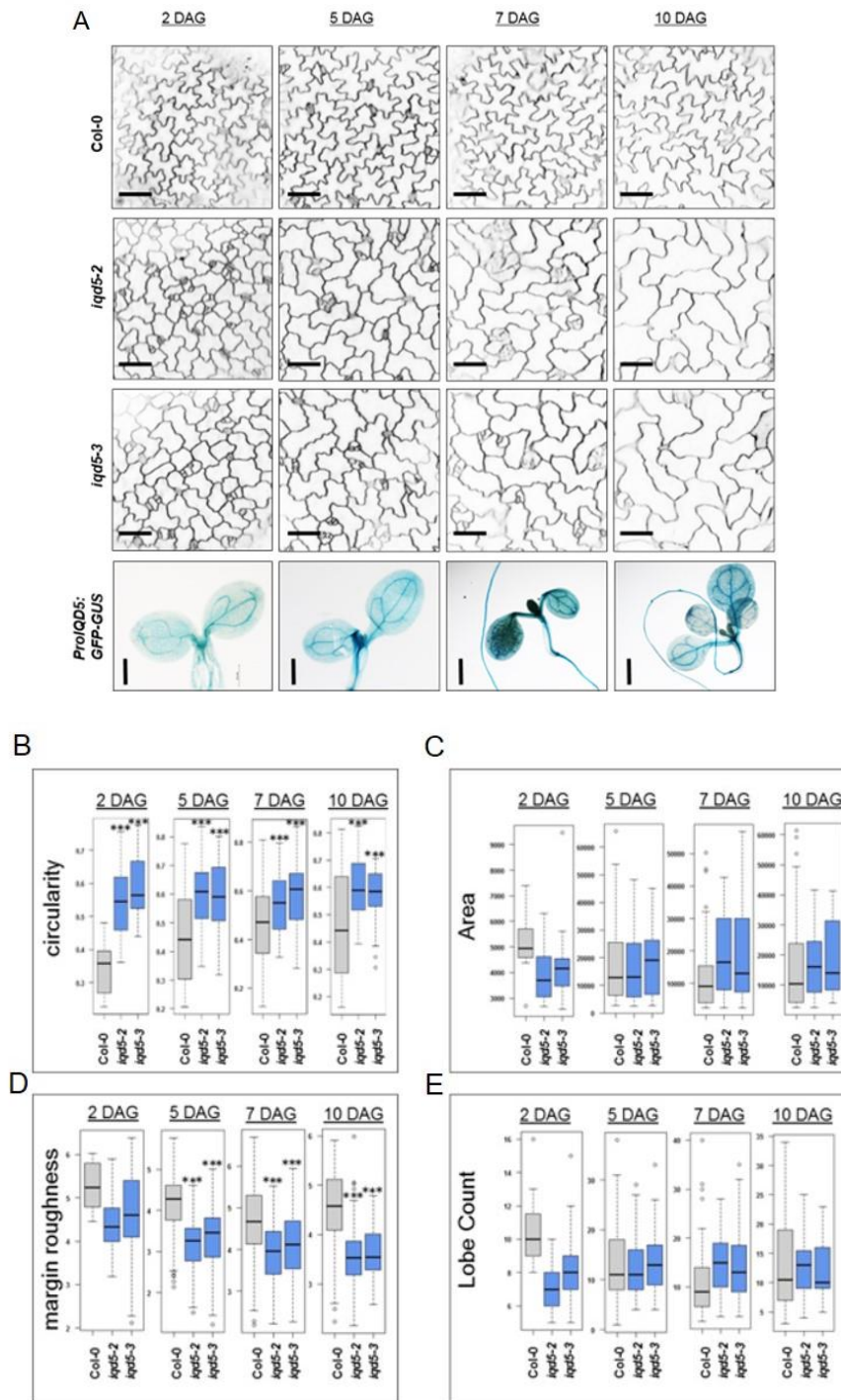
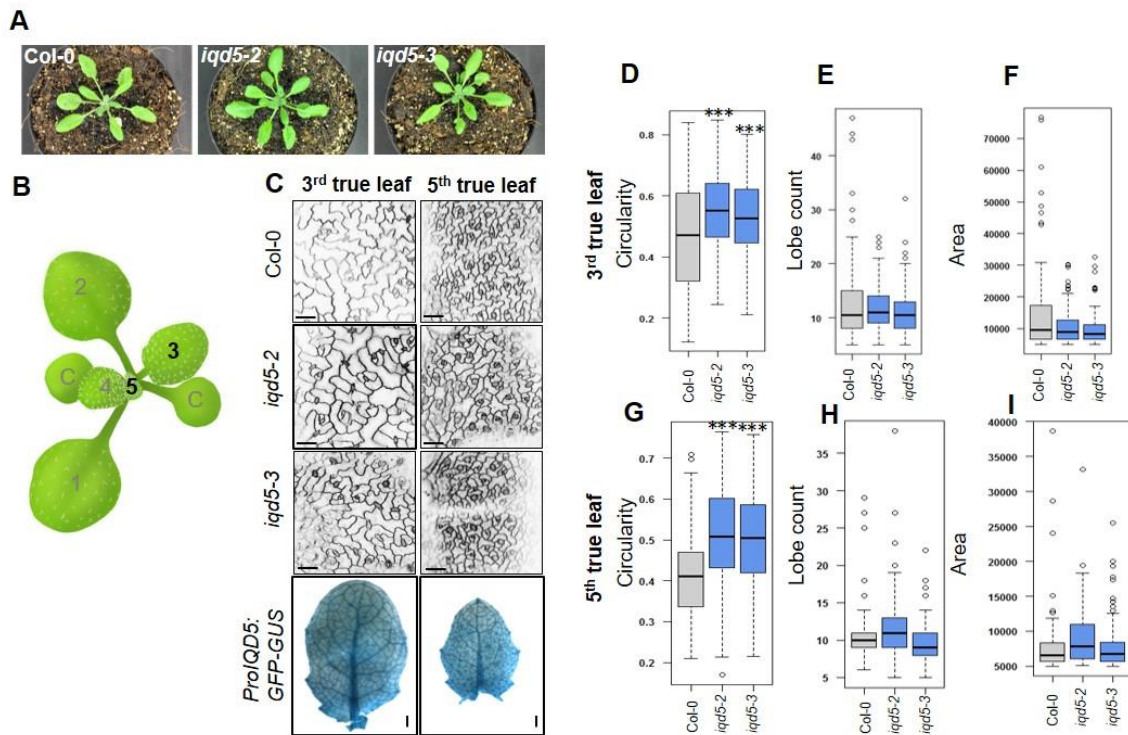


**Fig 22: Time course analysis of epidermal PC shape in *iqd5* mutant** (A) Cell shape analysis in 2-day, 4-day, 7-day and 10-day old seedlings in WT and *iqd5* ko lines. PM stained using FM4-64 stain. Histochemical analysis of *ProIQD5: GFP-GUS* lines revealed promoter activity in all these developmental stages. Scale bars represent 50  $\mu$ m. (B) Quantification shows significant differences in *iqd5* ko lines compared to WT. Results are median of  $n > 100$  cells,  $p < 0.001$  one-way ANOVA. Asterisks (\*\*\*) represents high significance.

The above experiments showed that IQD5 functions in the PC shape of cotyledons. The cotyledons also called seed leaves, come directly from the seed and are the food reserve for the seedling. Upon germination, the cotyledon may become the embryonic first leaves of a seedling. Whereas the true leaves resemble more of what the adult plant looks like and, true leaves and cotyledons are developmentally distinct.



**.Fig 23: IQD5 plays a role in cell shape in true leaves** (A) Macroscopic analysis of true leaves of *iqd5* knock out lines compared to WT Col-0, (B) Picture showing the 3<sup>rd</sup> and 5<sup>th</sup> leaves which were analyzed (C) Cell shape analysis in third and 5<sup>th</sup> true leaves in WT and *iqd5* ko lines. PM staining was done by FM4-64. Promoter GUS analysis shows IQD5 promoter activity in third and fifth true leaves. Scale bars represent 50  $\mu$ m. (D) Quantification based on circularity, (E) lobe count and (F) Area and shows a significant difference between WT and *iqd5*. Fig (G), (H) and (I) shows the quantification for the same parameters in the 5<sup>th</sup> true leaves. \*\*\* represents high significance. Results are median of n>100 cells, p<0.001 one-way ANOVA.

Cotyledons are formed during embryogenesis, along with the root and shoot meristems, and are therefore present in the seed prior to germination. True leaves, however, are formed post-embryonically (i.e. after germination) from the shoot apical meristem, which is responsible for generating subsequent aerial portions of the plant (Zheng et al. 2011).

To analyze whether IQD5 plays a role in the PC in true leaves, PC shape was analyzed in rosette leaves of 3-week-old plants (Fig. 23A and B). Morphologically, the first two true leaves in *Arabidopsis* are similar to cotyledons. So to reflect characteristics of true leaves, we focused on the third and fifth rosette leaves. Quantification of PC shape features revealed similar cell shape changes in the *iqd5* knock-out lines as seen in cotyledons, which suggests that IQD5 plays a role in PC cell shape growth during embryogenesis as well as in post-embryogenesis.

In order to confirm that the alteration in PC shape is caused by *IQD5* loss-of-function, complementation analyses were performed. For which, a construct with the genomic

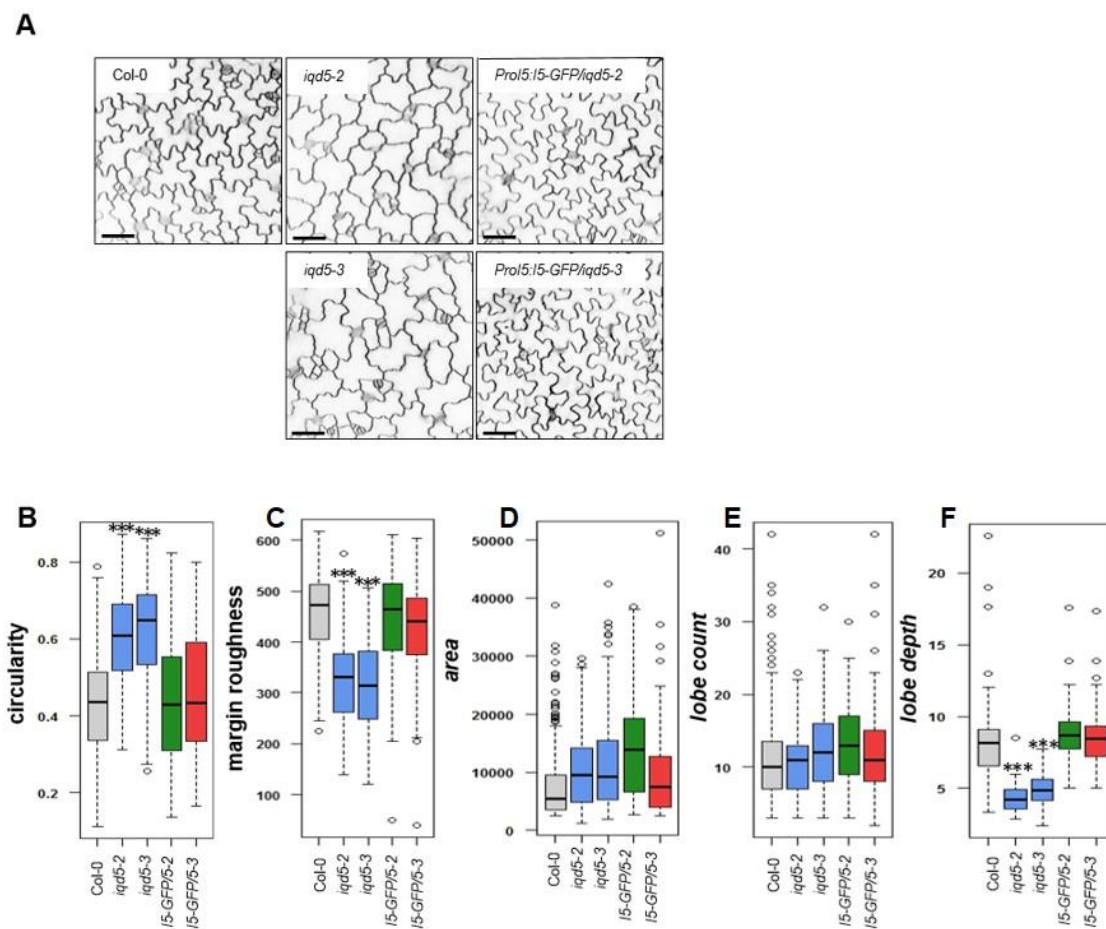


**Fig 24: Complementation analysis of *iqd5* mutants** (A) Cell shape analysis in 5-day old seedlings in wild-type and *iqd5* ko and complementation lines. PM stained using FM4-64 stain. Scale bars represent 50  $\mu$ m. Quantification based (B) circularity, (C) margin roughness, (D) area, (E) lobe count and (F) lobe depth shows significant differences in *iqd5* ko lines compared to WT. \*\*\* represents high significance. Results are median of  $n > 100$  cells,  $p < 0.001$  one-way ANOVA.

fragment of *IQD5* fused to a C-terminal GFP tag was generated, which we could express under the endogenous promoter. *Agrobacterium*-mediated transformation of the construct was performed in the *iqd5* mutant background and genotyping of the  $T_2$  generation plants was done. The  $T_2$  seeds were analyzed for their segregation ratio and plants with a 3:1 ratio, which indicates the presence of a single insertion, were propagated to establish homozygous  $T_3$  plants. From the homozygous lines, two independent lines were chosen for each construct for *iqd5-2* and *iqd5-3*, genotyped and also the insertion of the whole cassette was checked by PCR analysis. The  $T_3$  lines analyzed showed that the altered cell shape phenotype was rescued in the complemented line (Fig 24A and B).

In addition to analyzing these lines for their complementation ability, the native subcellular

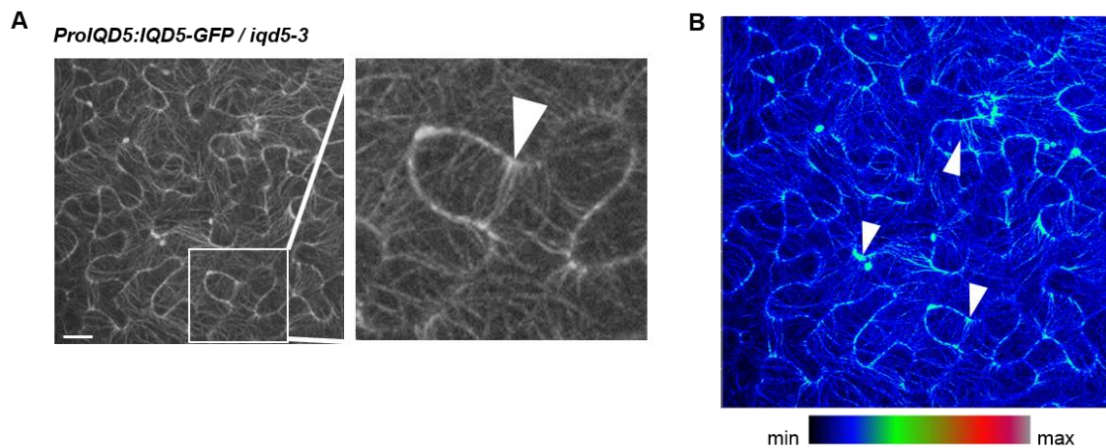


**Fig 25: Subcellular localization of IQD5-GFP in neck regions** (A) GFP fluorescence images were taken at images of 5-day old seedlings. (B) Fluorescence intensity map showing the maximum intensity at ring-like structure at the neck region. Scale bar represents 50  $\mu\text{m}$ .

localization of IQD5-GFP was also analyzed, which will enable us to study the dynamics of IQD5 localization at MTs and the MT organization during PC development. Localization studies in these lines revealed a ring-like structure around the indentation of the PCs (Fig 25A and B), which further points to a role of IQD5 at MTs, and possibly in the organization of MT ring structures or in MT bundling. Previous work on PCs has shown these type of ring-like structure in many MT localized proteins which plays a major role in bundling (Wang et al. 2007).



As stated previously, MTs serve as tracks for CSCs and MT bundling around the indentation in PCs causes local deposition of cellulose MFs to parallel to the underlying MTs, which restricts growth at these sites resulting in the indentations (Panteris et al. 2005, Gutierrez

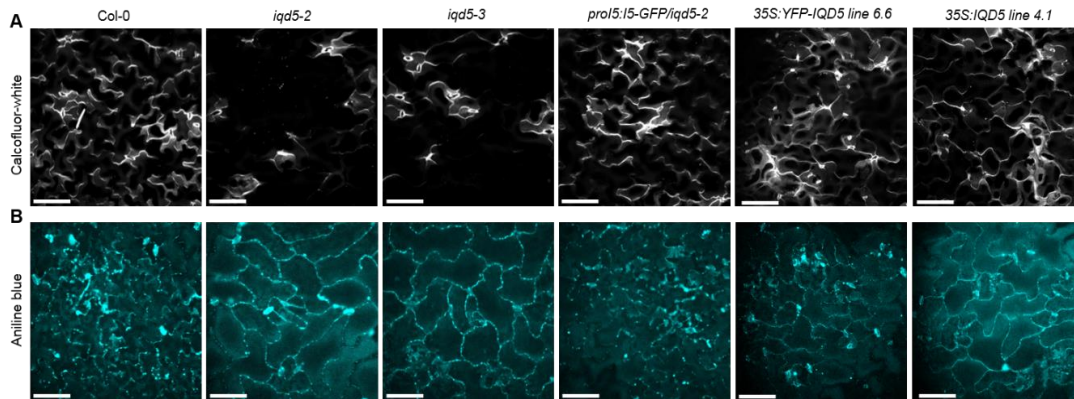


**Fig 26: IQD5 alters cellulose deposition** (A) Calcofluor white staining in *iqd5* knock out lines, complementation line and overexpression lines and WT Col-0 to show the cellulose deposition (B) Aniline blue staining analysis in IQD5 mutant lines to stain callose. Scale bars represent 20  $\mu$ m.

et al. 2009). Since *IQD5* under the native promoter shows preferential accumulation in neck regions as ring formation and mutants defective in *iqd5* display PC shape defects reminiscent of decreased growth restriction at necks, to visualize cellulose in the neck regions of the PCs of *iqd5*, calcofluor white staining was performed, where calcofluor stains the glucan chains present in the cell membrane. The data indicated reduced deposition of cellulose in *iqd5* mutants compared to WT seedlings (Fig 26A). To verify the data by an independent approach, the quantification of the cellulose content in WT and in the mutant background will be done using quantitative methods in another project. Since calcofluor white does not discriminate between  $\beta$ -1,3 and  $\beta$ -1,4-glucan chains which are the building blocks of callose and cellulose respectively (Harris et al. 2009), we included aniline blue staining to visualize callose. Data obtained showed no difference between callose deposition in *iqd5* mutant lines when compared to WT (Fig 26B). Thus the data from this experiment suggested that *IQD5* specifically alters the cellulose deposition.

CESA typically track along the cortical MTs in growing *Arabidopsis* cells (Paradez et al. 2006). Since we assume that the MT organization is altered in the *iqd5* mutants, it will be interesting to study if the CESA trajectories are also affected in *iqd5* mutants. For our analysis, we have introduced the CESA marker lines in *iqd5* mutant lines and currently, our

group is establishing them for tracking CESA localization in *iqd5* mutants, which will be used for a collaborative project in future. A similar experiment was conducted in Liu et.al. 2017 in KLCRs/CMUs, which showed that KLCR/CMUs have an impact on CESA trajectories.

Thus together, we observed that loss of *IQD5* affects PC shape in cotyledons and true leaves and consistent with promoter activity and *IQD5* protein abundance *IQD5* accumulates at neck regions of PCs. Also cellulose deposition is altered in *iqd5* knock out lines. Now, the next open question for us was to know the whether  $Ca^{2+}$  signaling or other pathways known to elicit  $Ca^{2+}$  signals?

## 6.6 Function of *IQD5* in cellular signaling?

Another interesting and novel aspect will be to link  $Ca^{2+}$  signaling to MT organization. The prospect arises that IQD proteins might sequester CaM signaling modules at distinct subcellular sites to orchestrate  $Ca^{2+}$  CaM signaling from membranes via the MT cytoskeleton to the nucleus. Interestingly, in yeast and animals, IQ Ras GTPase activating like proteins (IQGAPs) also functions as key regulators of intracellular  $Ca^{2+}$ -CaM signaling (Pathmanathan et al. 2011). IQGAP is an evolutionary multidomain protein and the three IQGAP isoforms have been identified in mammals (Wang et al. 2007; Brill et al. 1996; Weissbach et al. 1994). The three isoforms in vertebrates IQGAP1, IQGAP2, and IQGAP3 have diverse roles in vertebrate physiology, operating in the kidney, nervous system, cardiovascular system, pancreas, and lung (Hedman et al. 2015; Brown, Sacks 2006). Several studies report an effect of  $Ca^{2+}$ -CaM on cytoskeletal structures in animals and plants. With few examples, the mechanisms of  $Ca^{2+}$  mediated control over the cytoskeleton are unknown.

Our data suggest that *IQD5* is a novel player that potentially links  $Ca^{2+}$ -CaM mediated signaling to the regulation of MT and eventually cell shape establishment. From the experiments conducted in our group previously, we know that IQDs interact with CaMs (Bürstenbinder *et al.* 2012) and that *IQD5* recruits CaM2 to MTs (Fig 27B). To further strengthen this fact, *in vitro*, CaM binding assays conducted in our group revealed binding of *IQD5* to apoCaM ( $Ca^{2+}$  free) and to  $Ca^{2+}$  CaM (Fig 27C). GST-tagged *IQD5* and the GST alone were expressed as a control in *E.coli* to investigate interaction with immobilized bovine CaM in the presence ( $Ca^{2+}$ ) and absence (EGTA) of  $Ca^{2+}$ . GST-*IQD5*, but not GST, cosedimented with apo-CaM, and CaM binding of GST-*IQD5* was enhanced in the

presence of  $\text{Ca}^{2+}$ . Thus the predicted CaM-binding motifs are functional in mediating interaction with both states of CaM, the  $\text{Ca}^{2+}$ -free apo-CaM and  $\text{Ca}^{2+}$ -bound holo-CaM.

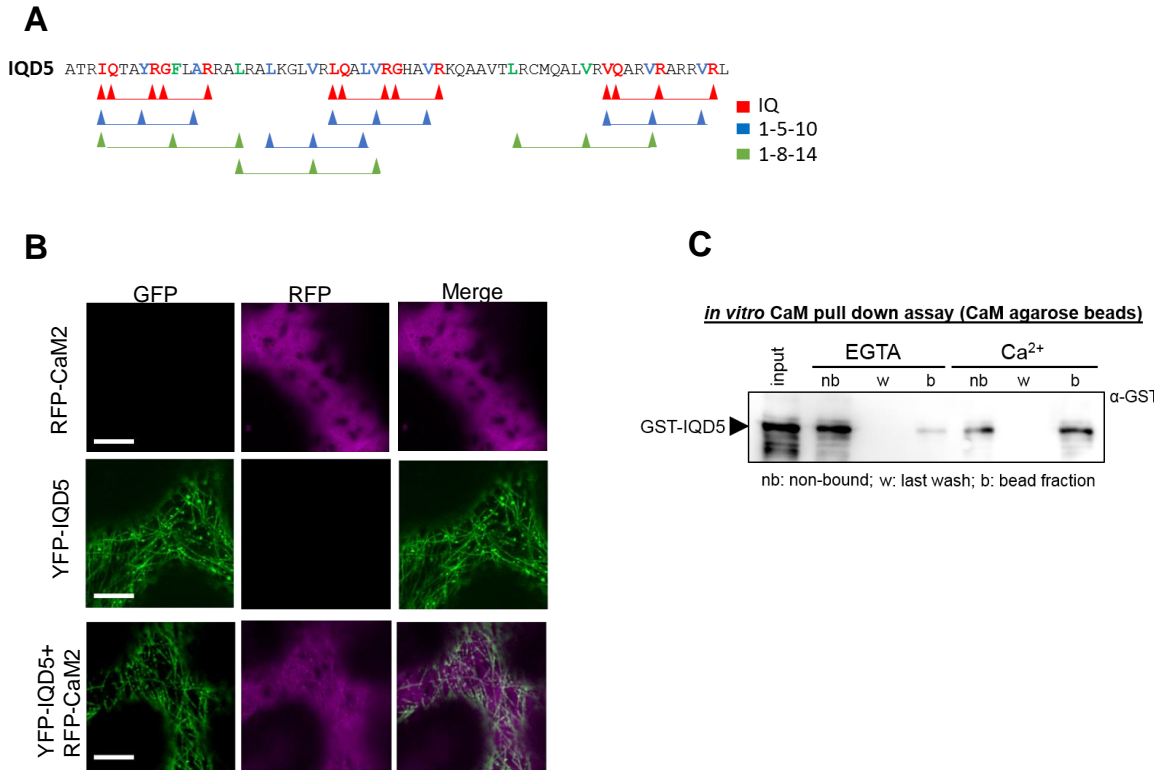


**Fig 27: IQD5 interacts with CaM2.** (A) Predicted CaM binding motifs show in protein sequence of the IQ67 domain of IQD5. (B) Co-expression of *35S::RFP-CaM2* and *35S::YFP-IQD5*. (C) *in vitro* pull-down assay by a colleague (Paul Pflug) to further show IQD5- bovine CaM interaction.

To study the role of CaM interaction in IQD5 biological functions, a mutagenesis study was initiated to generate apo- and holo-CaM binding deleted variants of IQD5. The generation of site directed mutagenesis (SDM) modified variants of IQD5 are currently in progress. The construct IQD5 with mutated IQ motif resulting in a deleted  $\text{Ca}^{2+}$  binding IQD5 variant was generated and generation of deleted apo-binding region is in progress. For the mutation, the strategy used is similar to that of the CaM mutation for IQGAP1 to elucidate the molecular mechanism by which apoCaM and  $\text{Ca}^{2+}$ /CaM differentially regulate IQGAP1 (Li et al. 2003). Using the CaM database, the predicted CaM binding regions were identified in IQD5, which consisted of the IQ-motifs, 1-5-10 and 1-8-14 motifs (Fig 27A). The IQ motif comprises 20–25 amino acids, with the core fitting the consensus IQxxxRGxxxR (where x is any amino acid), 1-5-10 comprises of the sequence [FILVW]xxx[FAILVW]xxxx[FILVW] and 1-8-14 comprises of [FILVW]xxxxxx[FAILVW]xxxxx[FILVW] (Supplementary Fig S4). Using the similar approach from IQGAP1 experiments, same mutations were done in IQD5.

The basic charged arginine residues were mutated to Glycine in the IQ motif to abrogate the binding of IQD5 to apo-CaM, and it is presumed that there will be no effect on the interaction with Ca<sup>2+</sup>/CaM. A second mutant is planned where hydrophobic residues in the IQ, 1-5-10 and 1-8-14 motifs were mutated to Aspartic Acid (acidic charge) to prevent the binding of IQD5 with both apo-CaM and Ca<sup>2+</sup>/CaM.

The coexpression analysis and *in vitro* pull-down will be done in our group to check if these constructs could still align and interact with CaM2. Once both the mutated variants impaired in CaM binding will be ready, we plan to introduce into the *iqd5* mutant background and analyze their (dis)ability to complement the mutant phenotype.

Another known regulator of PC shape are phytohormones. Phytohormones like auxin and cytokinin control and coordinate lobe formation via downstream ROP-GTPases, which are central regulators of cell polarity (Fu et al. 2005, Li et al. 2013). Auxin induces Ca<sup>2+</sup> spikes but how auxin action is linked to Ca<sup>2+</sup> signaling is still elusive (Shishova et al. 2004). Moreover, several studies implicated functions Ca<sup>2+</sup> signaling in cytoskeleton reorganization and cell shape regulation, the molecular mechanisms, however, are largely unknown. As mentioned above, auxin and cytokinin are key players that regulate PC shape formation.



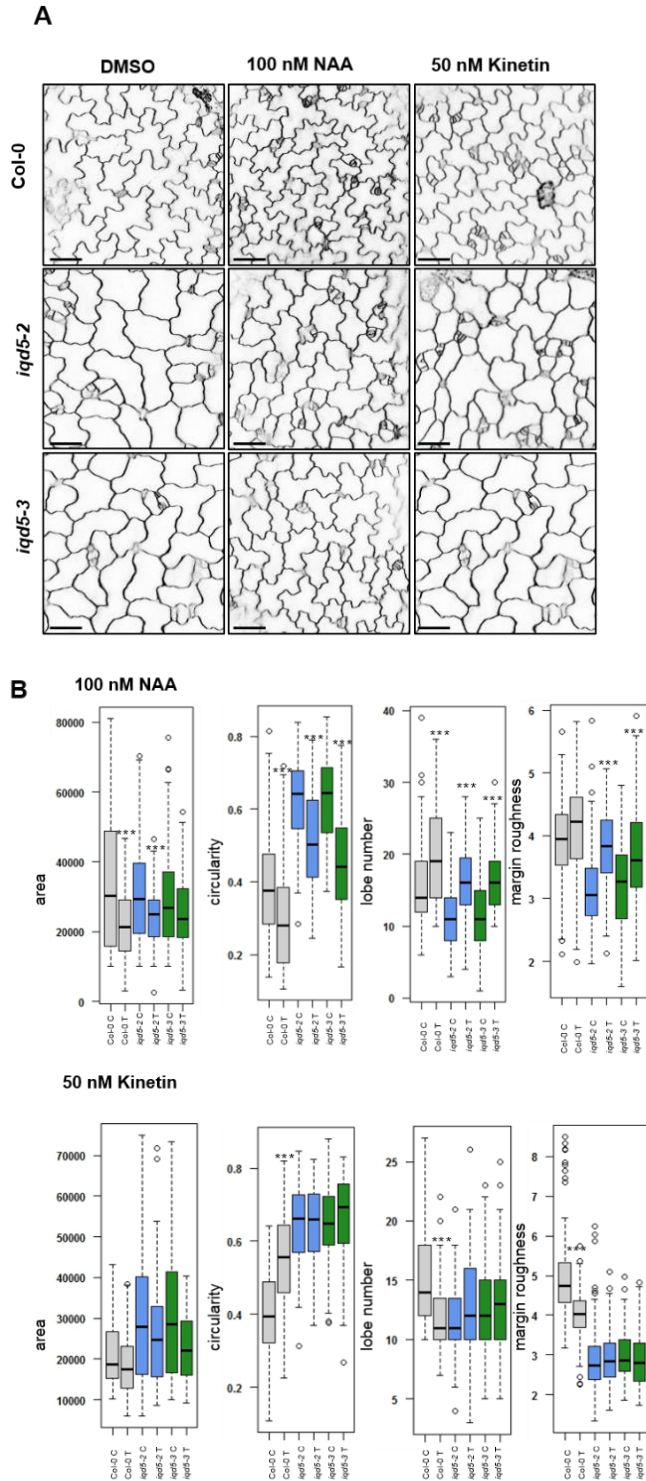


**Fig 28: Auxin and cytokinin treatment to *iqd5* knock out plants** (A) NAA and kinetin treatment on PC shape of *iqd5* compared to WT Col-0 in 5-day-old seedlings. PM was stained with FM4-64. Scale bars represent 50  $\mu$ m. (B) Quantitative analysis of data obtained from Fiji PC shape analysis. C and T represent Control and treated seedlings respectively. Results are median of  $n > 100$  cells,  $p < 0.001$  one-way ANOVA. \*\*\* represents high significance.

We are interested to elucidate if IQD5 may function within any of the two signaling pathways. Promoter analysis showed Auxin binding cis-elements present in the promoter region of *IQD5* (Supplementary Fig S3). Thus, hormone treatment experiments were established and performed with exogenous auxin and cytokinin to study whether *iqd5* mutants are altered in their sensitivity towards hormone treatment. Data obtained from treatment experiment could not conclude anything about the cross talk as treatment with synthetic auxin (NAA) introduced increased lobe formations to all the three genotypes consistent with already published data and kinetin showed an effect on size of the cell with a reduced number of lobes (Fig 29). It can be concluded that mutants are still sensitive to auxin but regarding kinetin it was not clear as no further reduction in lobe number or growth was observed.

But whether IQD5 plays a role in any of the signaling pathways could not be concluded from the above hormone treatment experiment. To further study the role of IQD5 in the known PC signaling pathway, crosses were made between the *iqd5* mutant and other known PC regulators like ROP6 (a Rho family GTPase), RIC1 (ROP interactive CRIB family protein) (Fu et al. 2005) and KTN1 (Burk et al. 2007), which are downstream regulators of auxin and cytokinin pathway respectively. We could establish the homozygous mutants for these downstream regulators by PCR genotyping. *Ktn1-5* has a strong phenotype with stunted growth with thick stem and leaves, *rop6-1* and *ric1-1* didn't show any definite phenotype on soil. The homozygous crosses of *iqd5* mutants and the downstream regulators will be studied in our group in future.

Thus, the PC phenotype in *iqd5* mutants in combination with the MT localization of IQD5 suggests that IQD5 plays a major role in MT organization during PC shape establishment. Notably, so far, all studies on IQD function were based on the analysis of overexpression lines in *Arabidopsis* and tomato. For the first time, our study has identified a phenotype in a loss-of-function line, which enables detailed studies on the molecular mechanisms of endogenous IQD function. Future interaction studies with known PC regulators will possibly elucidate the molecular mechanism of IQD5 function at the MT cytoskeleton to regulate PC shape.

## 6.7 Subcellular localization of KLCR proteins and their interaction with IQD5 to IQD8

Previous Y2H studies showed that IQD1 interacts with KLCR proteins (Bürstenbinder et al 2013). To delve deeper into the biological role of IQD:KLCR modules, in addition to the IQD proteins, we initiated the characterization of the IQD interacting KLCR protein family by reverse genetic approaches. There are three members of KLCRs in *Arabidopsis*

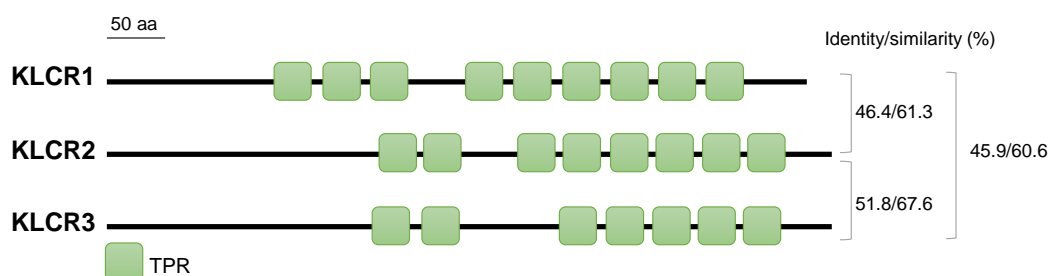


**Fig 29: Motif distribution and similarity among *Arabidopsis* KLCR proteins.** KLCR proteins containing multiple TPR in their central to C-terminal part. Similarities and identities are calculated from pairwise comparisons, as indicated on the right side. Scale represents 50 amino acids.

(Bürstenbinder et al 2013 and Lin et al. 2016). To compare the sequence similarity and identity, the amino acids sequences of all the three KLCRs were analyzed. The analysis showed that KLCR2 and KLCR3 are more similar compared to KLCR1 (Fig 30). To analyze the subcellular localization of KLCR proteins, transient expression assays of N- and C-terminal GFP tagged KLCR proteins were done in *N. benthamiana* leaves. The analysis showed that when expressed under the *CaMV35S* promoter, KLCRs mainly localize in the cytosol and nucleus but are excluded from the nucleolus. Localization in the nucleus is not seen in the N- terminal GFP-tagged KLCR3 whereas in C-terminal GFP tagged KLCR3 is localized to the nucleus as well and absent from the nucleolus (Fig 31A and B). The nuclear localization suggests a possibility of active import of KLCRs to the nucleus because the GFP-tagged KLCR fusions are larger than the exclusion size of the nuclear pores which is 40 kDa, and additionally there was no nuclear localization sequence (NLS) found in KLCRs. For mapping the NLS, we used the bioinformatics tool NLS mapper ([http://nls-mapper.iab.keio.ac.jp/cgi-bin/NLS\\_Mapper\\_form.cgi](http://nls-mapper.iab.keio.ac.jp/cgi-bin/NLS_Mapper_form.cgi)), and it did not predict any NLS in

KLCR1-KLCR3. The integrity of the whole protein was confirmed by immunoblot analysis (Fig 31C).

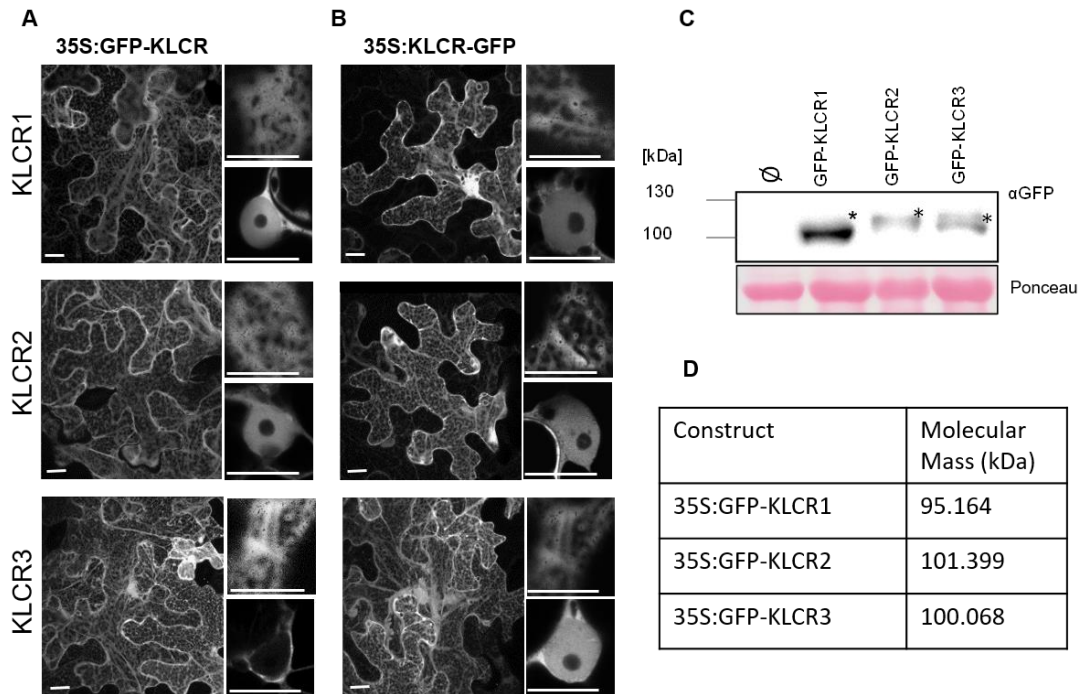


**Fig 30: Subcellular localization of Arabidopsis GFP-KLCR fusion proteins in *N.benthamiana*** (A) Transiently expressed N terminal GFP-KLCR (KLCR1-KLCR3) fusion proteins expressed under the *CaM35S* promoter. (B) Localization of C-terminal KLCR (KLCR1-KLCR3) fusion proteins. Insets show cytosolic (top) and nuclear (bottom) localization. Micrographs of cells are projections of Z-stack; insets are single layer images. Scale bars represent 20  $\mu\text{m}$  and 10  $\mu\text{m}$  (insets). (C) Expression of full-length GFP-KLCR fusion proteins was confirmed using immunoblot analysis using an anti-GFP antibody. Asterisks show the full length proteins. (D) Calculated molecular sizes of the full length proteins. Immunoblot assays were not performed for C-terminal fusion proteins.

Upon co-expression with IQD1, a redistribution of GFP-KLCRs to MTs was observed as has been reported previously (Bürstenbinder et al. 2013). We performed co-expression of all three KLCRs with IQD5-IQD8 to study if KLCRs get recruited to the MTs equally or differentially and whether co-expression has an impact on MT organization. Upon co-expression with IQD5-IQD8, all three KLCRs were recruited to the MTs (Fig 32).

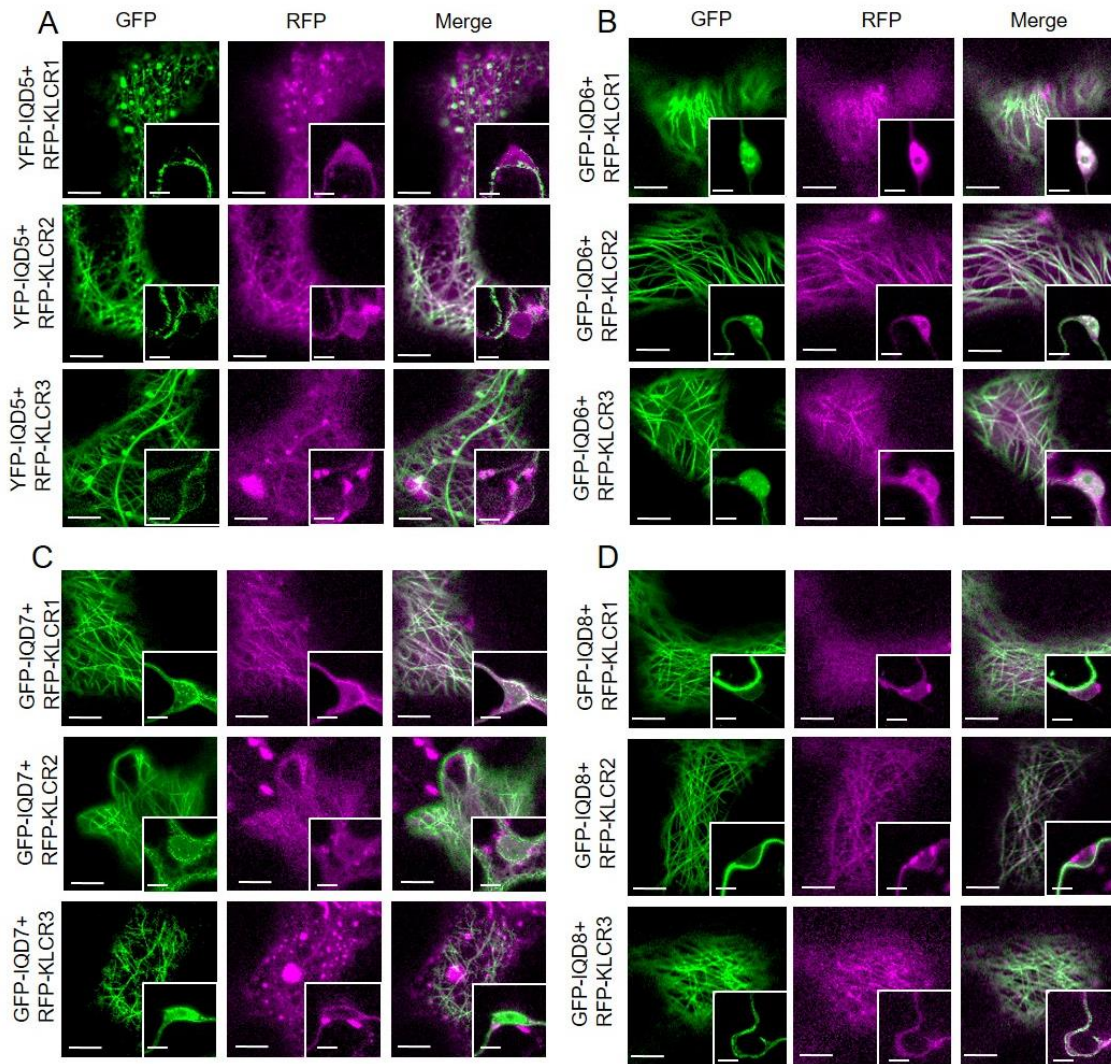


**Fig 31: KLCRs localize to MTs upon co-expression with IQD5-IQD8 in *N.benthamiana*** co-expression of *35S::RFP-KLCR1-3* with (A) *35S::YFP-IQD5*, (B) *35S::GFP-IQD6*, (C) *35S::GFP-IQD7* and (D) *35S::GFP-IQD8*. Micrographs of cells are projections of Z-stack; insets are single layer images. MTs localization (top) and nucle(o)ar localization (bottom). Scale bars represent 20  $\mu\text{m}$  and 10  $\mu\text{m}$  (insets).

From our earlier studies, we observed an alteration of MT patterns with the overexpression of the individual *IQDs* in *N.benthamiana* and *Arabidopsis* (Bürstenbinder et al. 2017). Similar to previous reports on *IQD11*, *IQD14* and *IQD16*, *IQD5* has a distinct MT pattern compared to others when studied in transgenic *Arabidopsis* lines and in *N.benthamiana*. Preliminary data from Fig 32 suggests that there was no alteration of MT patterns upon co-expression with KLCRs. Thus overall from the above experiment, we assume that *IQDs* function in recruiting KLCRs at the MTs and interaction with KLCRs however doesn't



change their MT pattern, indicating that the MT organizing function of IQD5 is independent of KLCR binding during the process. Also no visible alteration were observed in the nuclear patterns from the first studies.

From earlier experiments we observed that when expressed alone, *35S:RFP-KLCR* fusions accumulated in the cytosol but upon coexpression with IQDs, KLCRs were recruited to MTs. This intrigued the question about native localization of KLCRs. We speculate that, over accumulation of KLCR expressed under the *35S* promoter hinders the localization to MTs due to limited abundance of endogenous IQD proteins and thus reducing the expression by using a weaker promoter might eliminate the hindering effect and the native localization of KLCRs can be observed.

We thus reduced *KLCR* expression levels by use of the native promoter or the weaker *UBIQUITIN10* (*UBQ10*) promoter. This resulted in MT localization of KLCRs already in the absence of *IQD* overexpression (Fig 33A). We also observed MT localization in transgenic N-terminal tagged variant, GFP-KLCR1 plants and also in the C-terminal tagged variant, KLCR1-GFP expressed under the endogenous promoter (Fig. 33B and 33C) which suggests that KLCRs localize to MTs and nucleus *in planta*.

To confirm MT localization of KLCRs, co-expression of *UBQ10:GFP-KLCR1* was performed with the MT marker RFP-TUA5. The images obtained show GFP-KLCR1 overlaps with the RFP-TUA5 at the MT, thus validating MT localization of KLCRs (Fig. 33D).

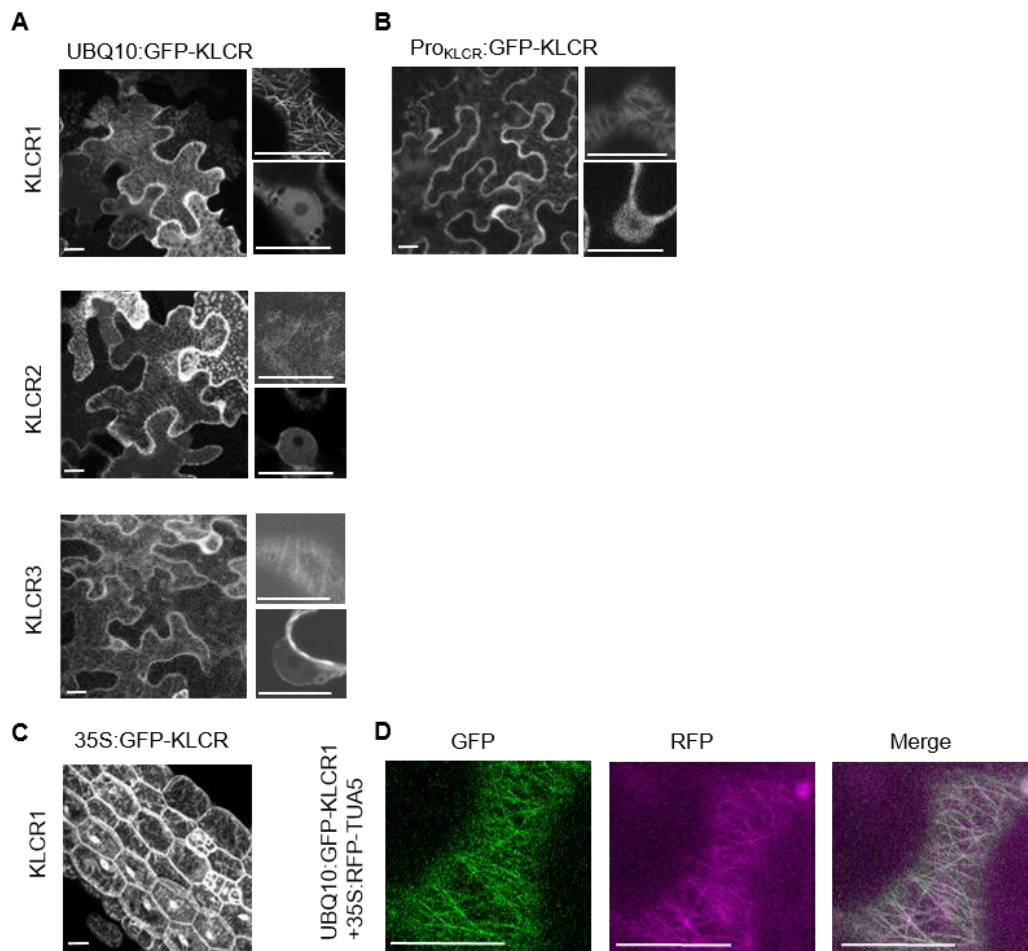


**Fig 32: Subcellular localization of Arabidopsis GFP-KLCR under UBQ10 promoter fusion proteins in *N. benthamiana*.** (A) Transiently expressed N terminal GFP-KLCR (KLCR1-KLCR3) fusion proteins under the *UBQ10* promoter. MT (top) and nuclear (bottom) localization. (B) KLCR1 under endogenous promoter fusion protein (C) Subcellular localization of *Arabidopsis* GFP-KLCR1 expressed under 35S promoter (D) Co-expression of 35S:*RFP-TUA5* with *UBQ10:GFP-KLCR1* *N.benthamiana*. Micrographs of cells are projections of Z-stack; insets are single layer images. Scale bars represent 20  $\mu\text{m}$  and 10  $\mu\text{m}$

We thus hypothesize that KLCRs typically co-localize with MTs in plant cells and that 35S promoter-driven over accumulation of KLCR proteins exceeds the capacities of the cell to properly localize KLCRs to MTs, possibly due to limited IQD abundance. We thus propose that the endogenous localization of both, IQDs and KLCRs are at MTs and that IQDs might act as scaffold proteins that recruit KLCRs to MTs.

## 6.8 Expression analysis of *KLCR*

Since *KLCRs* are the interacting partners of *IQD* proteins, we were interested to find out whether they have similar expression patterns as *IQD5-IQD8*. *GUS* expression analysis with  $T_3$  lines of the short promoter of *KLCRs* showed that *KLCRs* express in young and dividing cells, mainly in the shoot apical meristem, root meristem. Similar to *IQDs*, we cloned two different promoter length starting from upstream of *ATG* sequence of the gene, one spanning 1.5 kb and the long fragment spanning around 2.2 kb upstream of the translational start site of the *KLCR* gene (Fig 34A). The  $T_3$  lines of the short promoter were first analyzed for the presence of the entire cassette using PCR reaction (Fig.34B).

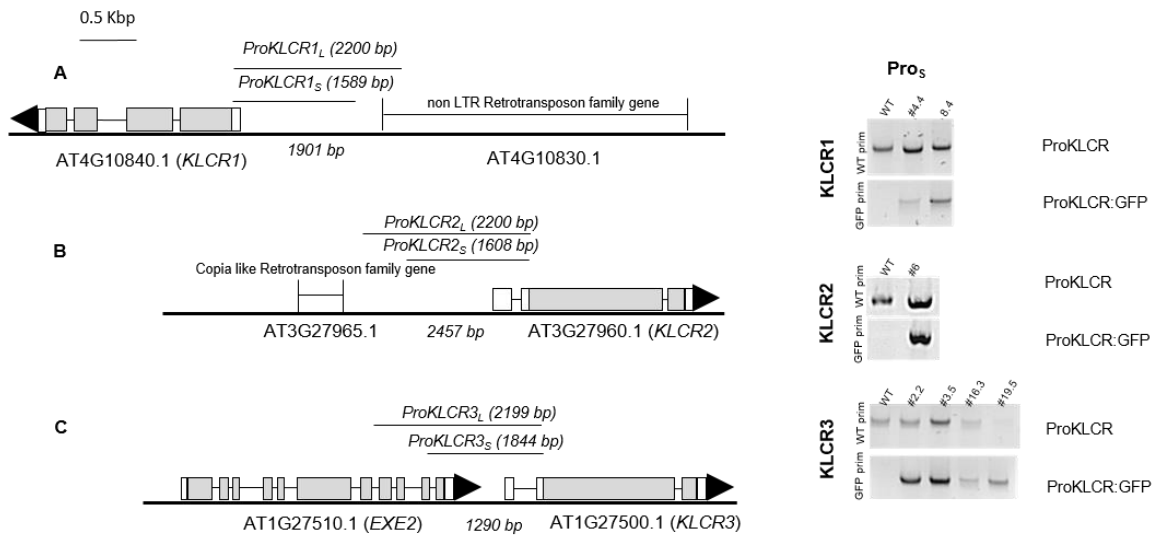


**Fig 33: Generation of transgenic *promoterKLCR:GFP-GUS* reporter lines** (Left) Gene model of *KLCR1-KLCR3* showing the promoter region selected for amplification for generating the *promoter:GFP-GUS* construct, Scale represents 500 bp. (Right) PCR confirmation of promoter-reporter constructs of *KLCR* for short promoter fragments of (A) *KLCR1*, (B) *KLCR2* and (C) *KLCR3*. In the gel images, upper band: obtained from the amplification of the whole gene; Lower band: obtained from the amplification of gene specific forward primer and GFP specific reverse primer (R.P).

To compare the true expression domain, long promoters of *KLCRs* were also generated and  $T_2$  lines were included for this experiment. Our first analyses suggest an overlapping expression pattern of the analyzed *IQD* subclade IIIa and *KLCR* genes (Fig 35). Promoter activity of all four analyzed *IQDs* and all three *KLCRs* was detectable in dividing and



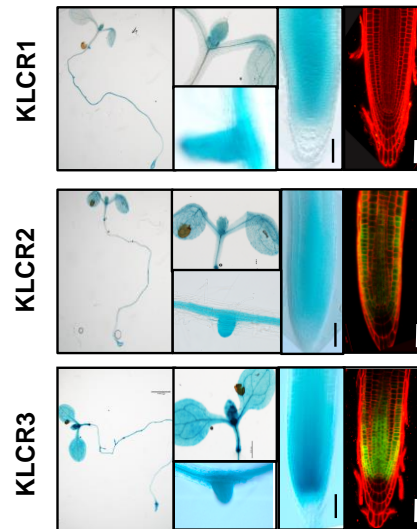


**Fig 34: Expression map of *KLCR1-KLC3* genes using promoter-reporter constructs** (A) PCR confirmation of promoter-reporter constructs of *KLCR1-KLCR3* for short promoter fragments. (B) Histochemical GUS and GFP fluorescence analysis and comparison of transgenic lines of *ProIQD:GFP-GUS (IQD5-IQD8)* for short promoter fragments in all 5 day-old seedlings of *Arabidopsis* plants.

differentiating cells (Fig.35). Fluorescence analysis of GFP-GUS lines revealed the expression of *KLCR2* and *KLCR3* not only in the stomata but also in the stomatal precursor cells (Fig 36) indicating KLCR in stomata lineage. Altogether, since *KLCRs* are expressed in dividing and differentiating cell and both are localized to the MTs, we predict that they might be involved in initial plant growth and development.

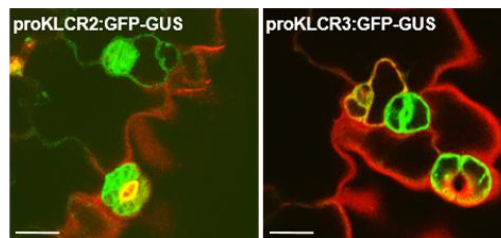


**Fig 35: Expression map of *KLCR2*, and *KLCR3* in stomatal precursor cells** GFP fluorescence analysis and comparison of transgenic GFP-GUS lines reveal the expression of *KLCR2* and *KLCR3* short promoter in meristemoid cells. To negate the possibility of autofluorescence, WT was taken as a control to set the GFP intensity. Micrographs are single layer images. Scale bar represents 20  $\mu$ m.

The preliminary expression analysis of *KLCR1-KLCR3* shows that endogenous expression domains are resembled by the *ProKLCR:GFP-GUS* constructs to that of the *in silico* data from genome-wide expression analyses (Fig 37 and Supplementary Fig S2).

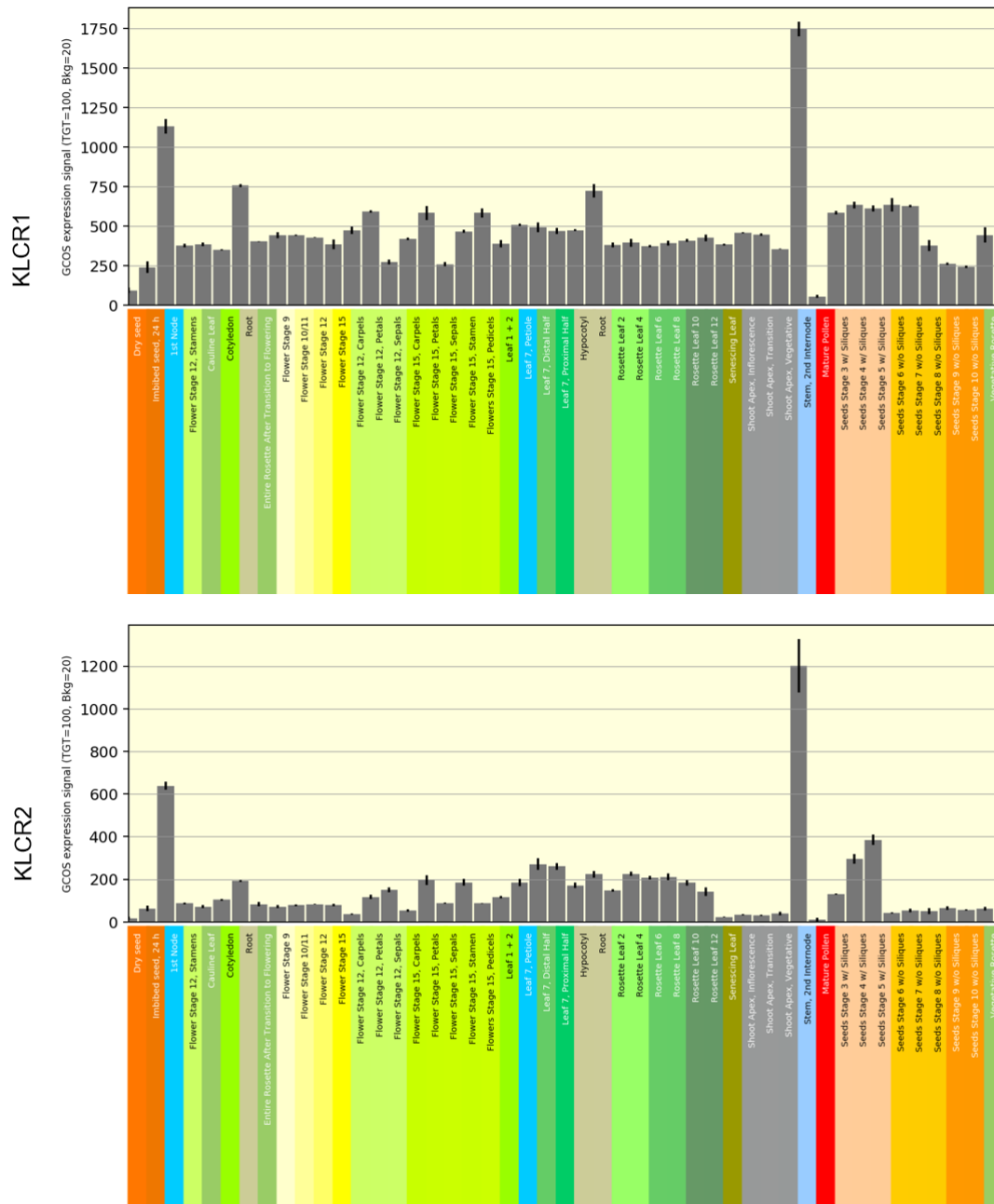


**Fig 36: *In silico* expression analysis of *KLCR* genes** *In silico* expression values of *KLCR1-KLCR2* as obtained from eFP browser.

## 6.9 Phenotypic characterization of *klcr* loss-of-function lines

To identify if *KLCRs* have a similar biological role in leaf epidermal cells as *IQD5*, cell shape analysis was studied in *klcr* loss-of-function lines, preliminary analysis with overexpression lines of *KLCRs* didn't show any obvious defects. T-DNA insertion lines for *KLCR1* and *KLCR2* except for *KLCR3* were already available in the laboratory. *KLCR1* loss-of-function line shows possibly an alteration in leaf PC shape when compared to WT (Fig 38A and B), which however was not statistically significant. However, work done in the Persson group, could show that *KLCR1/CMU1* has an impact on PC shape (Liu et al. 2016). This effect is not evident in *klcr2* loss-of-function line neither in *klcr1*, *klcr2* double knock-out line showing specifically the phenotype is caused by *KLCR1*. For *KLCR3*, there are no publicly available T-DNA insertion lines. To understand the functions of *KLCR2* and *KLCR3*, we aim to generate a *KLCR3* loss-of-function line. We also speculate that there might be functional redundancy in the *KLCR* family and to analyze this further we eventually plan to generate a triple mutant of *klcr1*, 2, and 3.

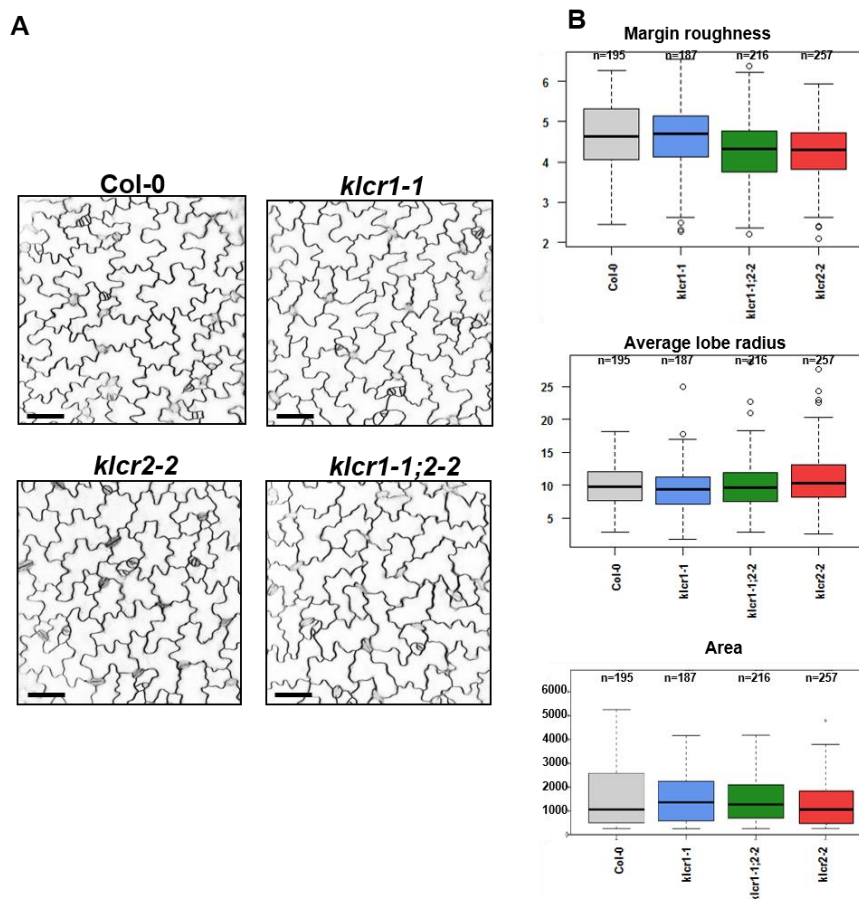


**Fig 37: PC phenotypes in the *klcr1-klcr2* knock out lines** (A) Epidermal PC shape analysis in *klcr* ko lines and in wild-type. 5-day old seedlings were used for analysis. PM was stained using FM4-64

stain. Scale bar represents 50  $\mu\text{m}$ . (C) Quantification based on margin roughness, average lobe radius and area. Results are median of  $n > 100$  cells,  $p < 0.001$  one-way ANOVA.

Our analysis of loss-of-function lines revealed altered PC shape in epidermis cells of cotyledons in two independent *iqd5* mutant alleles as shown before, and to a lesser degree in *klcr1* mutants. Compared to WT plants, epidermal PCs in *iqd5* mutants generate less pronounced lobes and indentations. A similar tendency for reduced lobe formation was visible in *klcr1* mutants (Fig 38). Since IQD5 had a significant impact on PC and also KLCR1 partially, we were intrigued to study if IQD5 and KLCR1 had an equal impact on the other major factors of leaf epidermis, stomata and trichome. Preliminary data on microscopic analysis of stomata didn't show any alteration in *iqd5* and *klcr1* knock out lines probably because of the fact that *IQD5* and *KLCR1* do not express in the stomatal cells.

One aspect of *de novo* pattern formation in plants is the patterning of trichome on *Arabidopsis* leaves, which involves genetic regulation and cell-to-cell communication. These processes are potentially variable due to, e.g., the abundance of cell components or environmental conditions. To elevate the understanding of regulatory processes underlying the pattern formation it is crucial to quantitatively analyze the variability in naturally occurring patterns. MTs and actin cytoskeleton also plays a major role in patterning and branching respectively. Since IQDs are localized at the MTs, we focused our analysis on trichome patterning in *iqd5-iqd8* and *klcr1-klcr2* lines. Preliminary study shows no major alteration in trichome patterning in *iqd5* and *klcr1* knock-out lines (Fig 39).

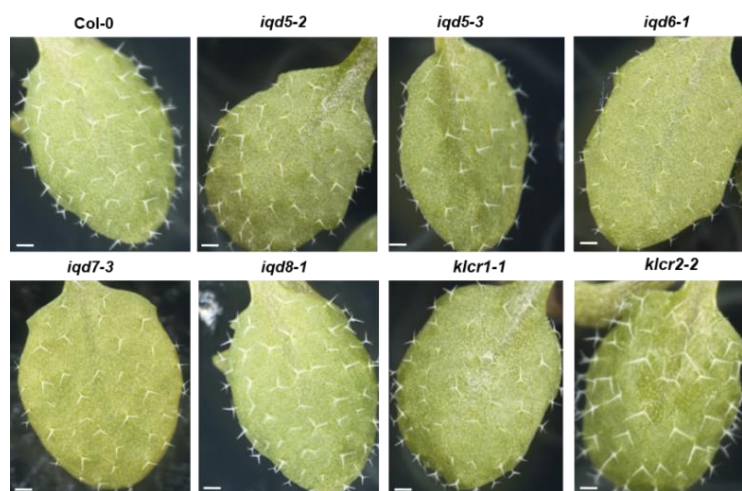


**Fig 38: Trichome patterning in IQDs and KLCRs** Trichome patterning analyzed in *iqd5-iqd8* and *klcr1-klcr2* knock out lines in comparison to WT Col-0. Scale bar represents 5  $\mu\text{m}$ .

Thus suggesting that IQD5 and possibly KLCR1 have specific function in PC shape establishment. Overall, our characterization and analysis of *IQD* and *KLCR* lines revealed that the promoter activity by histochemical GUS assays in *ProIQD<sub>s</sub>:GFP-GUS* and *ProKLCR<sub>s</sub>:GFP-GUS* lines revealed that expression throughout development in unique and overlapping domains within roots, hypocotyls, cotyledons, and leaves. Promoter activity was highest in dividing and elongation cells, and largely absent from differentiated tissues. Analysis of homozygous *T<sub>3</sub>* lines revealed altered growth and cell shape in lines overexpressing *IQD5* and *IQD8*. The phenotypes are comparable in *35S:IQD* and *35S:GFP-IQD* as well as *35S:IQD-GFP* lines, which indicates functionality of the GFP-fusion proteins. The phenotypes are reminiscent of mutants with defects in MT function. GFP-fused IQD and KLCR variants labeled MTs in *Arabidopsis*. IQD6 and IQD7 additionally localize to the sub-nuclear compartment, which suggests the roles of IQDs in orchestrating signaling from membranes to the nucleus.

## 7 Discussion

Previous studies identified CaM binding IQD protein family as one of the largest MAPs in plants (Bürstenbinder et al. 2017b). From our study, we know that promoter activities of *IQD5-IQD8* reveals the fact that expression of *IQDs* is highest in dividing and elongation cells, and largely absent from differentiated tissues (See Fig 14-16). Given a large MT-associated family, *IQDs* likely have a major conserved function. Consistently, *IQDs* have been proposed to play roles in plant growth and development, as first experimental data showed altered fruit shape and grain size with elevated expression of tomato *SUN/IQD12* and in rice *GSE5/IQD21* respectively (Xiao et al., 2008; Duan et al., 2017). But the precise molecular mechanism of is still elusive. Various functional roles of *IQDs* in MT organization is based on differential MT patterns with ectopic overexpression of individual *IQDs* in transient expression in *N.benthamiana* (Bürstenbinder et al. 2017b). For e.g., *IQD16* shows a differential MT pattern and has a distinct cell shape phenotype upon overexpression.

From functional characterization of clade IIIa, for the first time, we could show a true phenotype in the loss-of-function lines of *IQD5*, where *IQD5* has a role in PC shape morphogenesis (see Fig 20). The fact that the MT pattern analysis in overexpression line *35S:YFP-IQD5* in transient expression suggested unique MT organization and clustered separately from other *IQD* members of the same clade (see Fig 9) , it strengthens the hypothesis that *IQD5* plays a distinct function than other members of clade IIIa and may regulate PC morphogenesis by affecting the MT stability or dynamics. Spatio-temporal expression domains of *IQD5* also shows promoter activity in cotyledon and leaves (see Fig 20 and Fig 22), in vasculature and in the shoot apical meristem suggesting the involvement of *IQD5* in PC shape, growth, and development.

PCs are the most abundant cell type in the leaf epidermis in the model species *Arabidopsis* and in several other plant species (Ivakov and Persson 2013; Jacques et al. 2014). PCs are thought to provide mechanical strength, which is of extreme importance as the leaves should be sufficiently stiff to overcome gravitational forces and to orient its surface for optimal light capture to drive photosynthesis and to orient its surface for optimal light capture to drive photosynthesis. (Javelle et al. 2011). PCs also protect the underlying mesophyll layers, photosynthetic machinery and resists outside invasion (Gorton, Vogelmann 1996). As the leaf grows, the epidermal cell layer encounters different mechanical stresses, which include cell-generated forces (turgor pressure) (Somerville et al. 2004; Kutschera 2008; Segado et al. 2015). An enormous number of plant species appear with a wide diversity in

leaf shape and architecture. Even at the cellular level, many different shapes and sizes exist. It is also important that a leaf has to maintain its integrity despite the low number of cell layers and the large air cavities in the mesophyll cells (Glover 2000). Also, a leaf should be able to bend and bow during wind and rain without breaking (J 2002), thus it is suggested that interlocking anticlinal cell walls of PCs provide additional adhesive strength and stability by increasing the contact area between neighboring cells.

These interlocking, jigsaw puzzle shaped PCs are also common in ferns and especially well developed in the broad blades of many dicot cotyledons, true leaves, and found in monocots as well (Panteris et al. 1994). PCs form a protective layer for the underlying mesophyll cells that contain the photosynthesis machinery. In the leaf primordium, PCs are polyhedral. As the leaf gradually expands, these cells undergo massive changes in size and shape, producing undulations with neighboring cells resulting leaf surface pattern that resembles complex jigsaw puzzle-like structures with alternate interdigitation within each cell (Kotzer et al. 2004). The degree of interdigitation affects the physical properties of the leaf by increasing the surface area between adjacent cells and thus provides mechanical strength to the leaf and also helps in intercellular communication. PC morphogenesis also relies on lobe initiation and anisotropic expansion to generate the complex multi-lobed shapes of PCs (Zhang et al., 2011). PCs comprise alternate lobe and neck regions. The lobe regions are the sites of growth and exocytosis and neck regions are the sites where growth is prevented since anticlinal walls are shared by neighboring cells and the rate of expansion is always identical in lobes and necks. The establishment of PC shape before cells are fully expanded, which suggests that the neck regions undergo considerable growth, but grow minimal in the radial direction (Fu et al. 2005b; Xu et al. 2010).

IQD5 as a proposed novel regulator of PC morphogenesis, shows significantly reduced growth restriction at the neck region in the loss-of-function lines (see Fig. 24), which correlates with a reduced deposition of cellulose in anticlinal walls of PCs (see Fig. 26). Lobe initiation in *iqd5* was affected, but overall growth was same, which indicates that IQD5 specifically functions in control of anisotropic expansion of PCs. Also the findings from a time course study during various stages of PC development, shows that shape defects in *iqd5* mutants starts at the early phase but the overall growth of *iqd5* mutants is unaffected suggesting IQD5 only functions in controlling the anisotropic expansion of PCs (see Fig. 21-23). By analyzing the GFP fluorescence in transgenic *ProIQD5:IQD5-GFP/iqd5-2* lines, we demonstrate subcellular localization of IQD5-GFP to cortical MT arrays in leaf epidermal

PCs (see Fig 26). Functionality of the GFP-tagged IQD5 protein is indicated by efficient complementation of PC shape defects in *pIQD5:IQD5-GFP/iqd5-2* lines (see Fig. 24).

To understand the molecular mechanism behind the puzzle like the pattern of PC shape, years of research has been conducted. Various molecular and genetic players involved in cell shape establishment have been identified by mutant phenotyping and from these studies, important roles of the plant cytoskeleton during formation of PC interdigitation were revealed. The plant MT cytoskeleton plays an important role in the anisotropic expansion of PCs during PC shape establishment. Genetic and pharmacological studies have identified key signaling events during PC shape establishment that shows that altered MT stability or dynamics in certain MAPs like KTN, TRM1/2, ROPs, RICs etc. reduces the cellular complexity in the PCs (Akita et al. 2013, Lee et al. 2005). MOR1 mutant exhibit severely defective PC shapes, with near absence of lobes (Whittington et al. 2001; Wasteneys, Yang 2004). The cytoskeleton in general plays key role in determining plant cell shape, mainly by influencing the patterns in which wall materials are deposited in expanding cells. Studies employing cytoskeleton-disrupting drugs, together with studies of mutants with cytoskeletal defects, have demonstrated that both MTs and actin filaments are critical for all modes of cell expansion, although their precise roles remain poorly understood (Elliott, Shaw 2018). In recent years, however, significant progress has been made in understanding the contributions of a variety of proteins that influence cell shape by regulating the organization and polymerization of cytoskeletal filaments in expanding cells (Smith 2003b). MT disruptions also affect PC morphogenesis. MT localization was validated in IQD5 by oryzalin treatment in transgenic *Arabidopsis* plants (see Fig 8) and by co-localization of *35S:YFP-IQD5* with the MT marker *35S:RFP-TUA5* in transient expression assays in *N. benthamiana* (see Fig 5). Our work thus for the first time identifies a direct link between MTs and cell expansion in an *iqd5* knockout mutant.

Quantification of fluorescence intensities in the outer periclinal cell wall suggested the accumulation of IQD5-GFP at convex sides of indenting neck regions. Similar to IQD5, accumulation of MT bundles at neck regions has been reported for several other MAPs in several other studies and this pattern of MT accumulation correlates with reduced growth in the neck regions (Fu et al., 2005; Sampathkumar et al., 2014). In a recent study, live-cell imaging and biochemical analyses performed on IQD5 demonstrated that IQD5 binds to MTs and promotes MT assembly. MT-depolymerizing drug treatment and *in vivo* MT dynamics assays conducted suggested that IQD5 functions to stabilize MTs (Liang et al. 2018). Thus, we hypothesize that IQD5 stabilizes the MTs at the neck regions of PCs. To



understand this mechanism, we plan to use our construct *ProIQD5:IQD5-GFP/iqd5-2*, generated for complementation analysis and track the MT organization and dynamics in *iqd5* and *35S:IQD5* lines.

Since another known fact is that cortical MTs serve as tracks for PM-localized CSCs and here, in our study using histochemical staining, we could show that *iqd5* mutants accumulate reduced amounts of cellulose in their anticlinal walls while callose deposition was completely unaffected (see Fig 23). Thus we speculate that IQD5 may mediate coupling of CESA movement to MT tracks, possibly by direct interaction with KLCR/CMU family members.

KLCRs mediate PM tethering of MTs to stabilize cortical MTs against the pushing forces of CSCs (Liu et al., 2016). *Arabidopsis* IQD1, IQD2, and IQD23 interact with KLCR family members in yeast, and IQD1 recruits KLCR1 to MTs in transient expression assays in *N. benthamiana* (Mukhtar et al., 2011; Bürstenbinder et al., 2013). Our study suggests that IQD5 plays a major role for in PC morphogenesis, cellulose deposition possibly by controlling MT dynamics and organization. This was also confirmed by Liang et al. 2018 as their group could show that IQD5 functions in MT stability. Altogether, since IQD5 interacts with KLCR/CMUs which mediate PM tethering of MTs to stabilize cortical MTs against the pushing forces of CSCs (Liu et al., 2016), the prospect arises that IQD5:KLCR1 module could possibly co-ordinate MT organization and lateral stability of cortical MTs at the PM–MT nexus collectively. To better understand this phenomenon, we plan to study the localization of KLCR1 in *iqd5* mutant and understand whether IQDs are required for MT recruitment of KLCRs or perhaps there is reduction in MT binding of KLCR1 in *iqd5* mutant. For this purpose, we have incorporated *ProKLCR1:KLCR1-GFP* in *iqd5* mutants and the homozygous lines will be studied in future experiments.

*IQDs* at the transcriptional level has been shown to be regulated by phytohormone auxin. Transcriptomic datasets have identified subclade IIIa and II of IQ-domain proteins including *IQD6*, *IQD8*, *IQD15*, *IQD16*, *IQD17*, and *IQD18* acting downstream of *MONOPTEROS* (MP)/*AUXIN RESPONSE FACTOR5* (ARF5) (Wendrich et al. 2017). MP is known to play crucial roles in embryonic apical root initiation and disruption of MP function leads to defects in transcriptional responses and cellular processes in root development (Möller BK 2017). This points to a possible regulation of the gene expression of *IQDs* by auxin in an early stage of plant development and could indicate a role of *IQDs* in embryogenesis.

From literature we know that, RAC/ROP GTPase proteins (Fu et al. 2005a; Fu et al. 2009) functions at MTs and actin in an auxin dependent pathway. Rop2/4, when inactivated GTP bound form, act stimulate the aggregation of fine actin filaments by activating the ROP effector RIC4, while locally inhibiting the assembly of ordered MT arrays. ROP interacting MT binding RIC1 inhibits the local assembly of fine actin where MTs are abundant through inactivation of ROP2 and promotes MT assembly and thus making cortical fine actin and MTs mutually inhibiting and the MTs self-activating. ROP6-GTPase promote assembly of ordered MT arrays by activating the RIC1 protein (Fu et al. 2009). Another unrelated study revealed that IQD13 associates with cortical MTs and PM, to laterally restrict the localization of ROP GTPase domains, and thereby directing the formation of oval secondary cell-wall pits. Overexpression of *IQD13* increased the presence of parallel cortical MTs and confines the area of active ROP domains within the lattice of the cortical MTs, causing narrow ROP domains to form. Thus, it provides the first hints for role of IQDs, in this case IQD13 in spatial control of ROP signaling domains required for cell wall patterning (Sugiyama et al. 2017). A similar mechanism might apply to IQD5 during PC shape formation, thereby providing a potential link between auxin actions, Ca<sup>2+</sup> signaling, and ROP GTPase activation.

Evidences include antagonistic functions of auxin and cytokinin in the activation of distinct ROPs in lobes and necks (Fu et al. 2005a). ROP signaling regulates the actin and MT cytoskeleton via different effector proteins (Fu et al. 2002; Fu et al. 2009; Feiguelman et al. 2017), thereby affecting the composition and mechanical properties of the cell wall, eventually resulting in asymmetric expansion of PCs (Sampathkumar et al. 2014; Majda et al. 2017). Auxin is involved in nearly all aspects of plant development ranging from embryogenesis, root and shoot development, phototropism and fruit development. Evidence from the literature suggests a connection between Auxin and IQDs. IQD1, the founding member of IQD family, plays a role in transcript accumulation of cytochrome P450 (CYP) genes including *CYP79B3* and *CYP79B2*. The CYPs catalyze the conversion of tryptophan into indole-3-acetaldoxime (iaaM) in tryptophan-dependent auxin biosynthesis in *Arabidopsis*. In tomato overexpression of *IQD12* homolog SUN results into elongated and seedless fruit, reminiscent of parthenocarpic, elongated and pointed tomato fruit from the expression of auxin biosynthetic gene *iaaM* (Wu et al. 2011). Thus, *IQD12* may be causing this phenotype by affecting the auxin levels or distribution in the fruit. Altogether we can assume that IQDs could act in plant development via regulating auxin levels.

A hallmark of IQD protein family is their ability to bind Ca<sup>2+</sup> sensors (see Fig 1). CaMs as already mentioned above are the Ca<sup>2+</sup> sensors which transduce Ca<sup>2+</sup> signals into cellular

responses by the regulation of various target proteins.  $\text{Ca}^{2+}$  is one of the universal second messengers in plants as demonstrated by its involvement in a multitude of essential processes including cell division, transcriptional regulation, cellular polarity, responses to light, responses to biotic and abiotic stresses, plant immunity etc. (Hepler 2005, Kudla et al. 2010, Dodd et al. 2010). Interestingly, IQD5 interacts *in vitro* with both states of CaM, the  $\text{Ca}^{2+}$ -free and  $\text{Ca}^{2+}$ -bound apo- and holoCaM (See Fig 24), respectively similar to, IQD1 and IQD20 shown in previous studies (Abel et al., 2005; Bürstenbinder et al., 2013). This suggests possible roles for IQDs in linking CaM-mediated  $\text{Ca}^{2+}$  signaling to the regulation of the MT cytoskeleton via unknown mechanisms (Abel et al., 2005, Hepler, 2016; Bürstenbinder et al., 2017b). *iqd5* mutant phenotype and IQD5-dependent recruitment of CaM to cortical MTs, provide the first hints regarding the functions of  $\text{Ca}^{2+}$  signaling in PC morphogenesis. Until now, there is not much information about role of  $\text{Ca}^{2+}$  on PCs neither

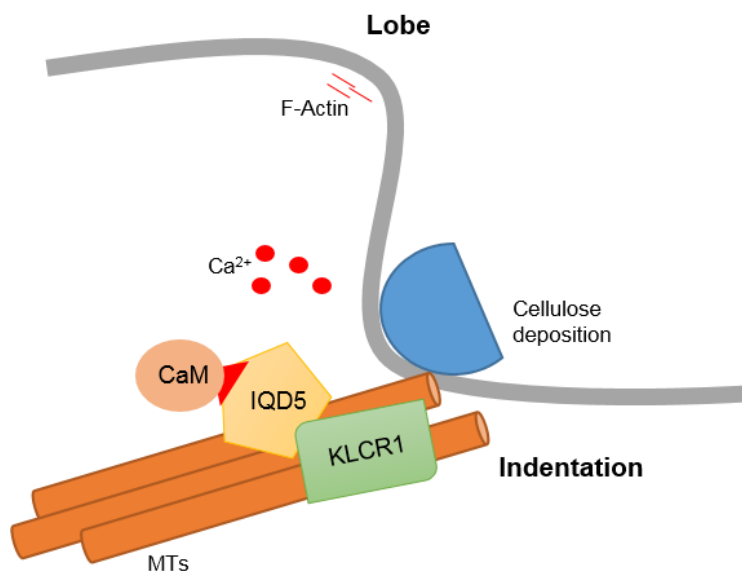


**Fig 39: Model shows the hypothetical role of IQD5-KLCR1 module in PC shape formation**

IQDs in general might function with KLCRs between  $\text{Ca}^{2+}$  signaling and plant PC shape by integrating CaM-dependent signals and by stabilizing MTs at PC indentation/neck region.

PC regulators have shown any elicitation in  $\text{Ca}^{2+}$  signals. Several studies implicated that  $\text{Ca}^{2+}$ -CaM has been shown to depolymerize MTs *in vitro* (Marcum et al. 1978; Hepler 2016).

Despite these indirect indications for functions of  $\text{Ca}^{2+}$  in the regulation of MTs, precise molecular mechanisms are largely unknown. This project thus offers for the first time a framework to elucidate functions IQDs in cell shape, growth and plant development. Together, we believe that the research on IQD5 will significantly broaden our understanding

of  $\text{Ca}^{2+}$  mediated regulation of MTs, and possibly provides a link between hormone and  $\text{Ca}^{2+}$  signaling. IQDs in general might function between  $\text{Ca}^{2+}$  signaling and plant growth by integrating CaM-dependent signals at multiple subcellular sites. Together our data elucidates the emerging function of IQD5:KLCR1 CaM modules, with respect to the  $\text{Ca}^{2+}$  CaM-dependent regulation of MT organization and dynamics in PC cell shape formation (Fig 40).

Altogether, understanding the molecular mechanism regulating PC growth and development is an important aspect of plant biology since leaves which consists of PCs in general forms the basis for crop yield, biomass production, and agronomics. Leaves and their growth and morphogenesis are major features in plant development because leaves are essential not only for photosynthesis and gas exchange but also it is an important parameter in plant biomass productivity (Hectors et al. 2010, Weraduwege et al. 2015). Leaf morphogenesis requires coordination of three fundamental processes at the cellular level: cell division, cell expansion, and cell differentiation. Plant cytoskeleton is one of the major factors responsible for these processes and various environmental and endogenous factors might affect their orientation thus affecting the leaf shape and growth (Chen et al. 2016). IQD5 might be one of the novel regulators of PC shape and possibly might act as a hub for coordination of  $\text{Ca}^{2+}$  signaling, MT organization, and cell wall formation. Our work thus provides a framework to understand the cellular processes guiding PC shape complexity in more detail.

## 8 Materials and Methods

### 8.1 Materials

#### 8.1.1 Chemicals

Unless specified differently, chemicals were obtained from Carl Roth (Karlsruhe, Germany), SIGMA Aldrich (St. Louis, USA), Merck KGaA (Darmstadt, Germany), Applichem GmbH (Darmstadt, Germany). Plant medium was ordered from Duchefa (Haarlem, Netherlands). Enzymes were acquired from Thermo Fisher Scientific (Waltham, USA), Serva (Heidelberg, Germany). Primers were obtained from MWG (Ebersberg, Germany). Primer synthesis, as well as sequencing, was performed by MWG Eurofins Genomics.

#### 8.1.2 Media and Buffers

- ***Arabidopsis thaliana* Salts (ATS) media**

In about 800 millilitres (ml) of ddH<sub>2</sub>O, the following ingredients were added first before bringing up to the final volume to 1 liter (l).

2.5 ml of 20 milli Molar (mM) Fe-EDTA, 5 ml of 1 M KNO<sub>3</sub> (Molecular weight MW 101.1), 2 ml of 1 M Ca (NO<sub>3</sub>)<sub>2</sub>·4 H<sub>2</sub>O (MW 236), 2.5 ml of 1 M KPO<sub>4</sub>, 2 ml of 1 M MgSO<sub>4</sub> (anhydrous, MW 120) and 1 ml of Micronutrients (70 mM H<sub>3</sub>BO<sub>3</sub>, 14 mM MnCl<sub>2</sub>·4H<sub>2</sub>O, 0.5 mM CuSO<sub>4</sub>, 1 mM ZnSO<sub>4</sub>·7H<sub>2</sub>O, 0.2 mM Na<sub>2</sub>MoO<sub>4</sub>·2H<sub>2</sub>O, 10mM NaCl, 0.01 mM COCl<sub>2</sub>·6H<sub>2</sub>O).

The solution was poured into a 2 l flask, and 5 gram (g) of agar was added. It was autoclaved, cooled, and poured about 25 ml per 100x100x15 millimeter (mm) plate (preferably in a laminar flow hood) to make about 40 plates per liter of solution.

- **Luria Bertani (LB ) broth (1 l) (pH 7.5)**

10 g of Bacto-tryptone, 5 g of Yeast extract, 10 g of NaCl were added in 1 l of ddH<sub>2</sub>O. The pH was adjusted to 7.5.

Bacterial glycerol stock was prepared using LB medium and 30% (w/v) Glycerol.

10 g (optional) of Agar was used when LB plates were made.

- **Super Optimal Broth (SOC ) medium (1 l)**

10 g of Tryptone, 2.5 g of Yeast extract, 5 ml of 1M NaCl, 1.2 µl 1M KCl, 5 ml of 1M MgCl<sub>2</sub>, 5 ml of 1M MgSO<sub>4</sub>, 10 ml of 1M Glucose.

pH was adjusted to 7 with NaOH. After autoclaving at 121°C, 0.95 g/l MgCl<sub>2</sub> and 3.6 g/l glucose were added. The medium was subsequently sterile filtrated.

- **DNA electrophoresis buffers and solutions**

Buffer	Composition
i) 1X TAE DNA running buffer (1 l- pH 8.0)	<u>4.84 g</u> of Tris base, <u>1.14 ml</u> of Acetic acid, <u>0.37 g</u> of EDTA
ii) 6X Orange-G DNA loading buffer (10 ml)	<u>10 mM</u> of Tris-HCl, <u>0.15%</u> (w/v) of Orange-G, <u>60%</u> (v/v) of Glycerol and <u>60 mM</u> of EDTA.

- **RNA extraction buffer**

TRI-Reagent, Isopropanol, 800 mM Sodium acetate + 1.2 M NaCl (High salt solution), Chloroform, 70% (v/v) Ethanol (absolute) and Tissue lyser and steel beads (5 mm).

- **Protein electrophoresis buffers**

Buffer	Composition
i) 4X SDS loading buffer	<u>3 ml</u> of 1M Tris-HCl (pH 6.8), <u>1.2 g</u> of SDS, <u>600 µl</u> of 10% (w/v) Bromophenol-Blue, <u>7.5 ml</u> of Glycerol and <u>20%</u> (v/v) β- Mercaptoethanol
ii) 10X SDS-PAGE running buffer	<u>250 mM</u> Tris (pH 8.3), <u>1.92 M</u> Glycine and <u>1%</u> (w/v) SDS
iii) Coomassie staining solution	<u>40%</u> (v/v) Ethanol, <u>10%</u> (v/v) Acetic acid and <u>0.1%</u> (w/v) Coomassie Brilliant- Blue R250
iv) Coomassie destaining solution	<u>40%</u> (v/v) Ethanol and <u>10%</u> (v/v) Acetic acid

v) SDS-PAGE gel (non-denaturing)	<u>6 ml</u> of 10X TAE, <u>21 ml</u> of Acrylamide:bisacrylamide, <u>90 µl</u> of TEMED, <u>900 µl</u> of 10% (v/v) APS
----------------------------------	---

- **Western blotting buffers**

Buffer	Composition
i) 10X PBS buffer (pH 7.4)	<u>1.39 M</u> NaCl, <u>27 mM</u> KCl, <u>125 mM</u> Na <sub>2</sub> HPO <sub>4</sub> ·2H <sub>2</sub> O, <u>18 mM</u> KH <sub>2</sub> PO <sub>4</sub> . For PBST <u>0.5%</u> (v/v) of Tween 20 was added.
ii) 10X TBS buffer (pH 7.8)	<u>500 mM</u> Tris-HCl, <u>1.5 M</u> NaCl, <u>10 mM</u> MgCl <sub>2</sub> ·6H <sub>2</sub> O. For TBST <u>0.5%</u> (v/v) of Tween 20 was added.
iii) Blocking Solution	<u>2%</u> (w/v) BSA and <u>2%</u> (w/v) Milk powder in 1X TBST
iv) Towbin buffer	<u>25 mM</u> Tris, <u>192 mM</u> Glycine, <u>20%</u> (v/v) Methanol and <u>1.3 mM</u> SDS
v) Protein Extraction Buffer	For 10 ml buffer, <u>1 ml</u> of 50 mM HEPES – KOH (pH 8), <u>100 µl</u> of 1 mM EDTA, <u>60 µl</u> of 5 mM DTT, 1 ml of <u>10%</u> Glycerin (v/v), <u>2.5 ml</u> of 125 mM Tris HCl (pH 6.8), <u>4 ml</u> of 4% SDS (w/v), <u>2 ml</u> of 20% Glycerol (v/v), <u>1 ml</u> of 10% β-Mercapto-ethanol (w/v), <u>0.01%</u> Bromophenol blue (w/v), <u>0.5 ml</u> of H <sub>2</sub> O and 1x Protease Inhibitor Cocktail.

- **GUS solution**

For 10 ml of solution: 1 ml of 50mM K<sub>3</sub>Fe(CN)<sub>6</sub> (50ml) (MW=329.25), 1 ml of K<sub>4</sub>Fe(CN)<sub>6</sub> 3H<sub>2</sub>O (50ml) (MW=422.1), 20 µl of 0.5M Na·EDTA·2H<sub>2</sub>O (100ml, MW=372.2) pH 8.0, 5 ml of solution from a stock mixture of 32 mL of 0.2M Monobasic NaH<sub>2</sub>PO<sub>4</sub> (1L, MW=120) and 68 ml of 0.2M Dibasic Na<sub>2</sub>HPO<sub>4</sub> (1l, MW=142) (pH 7), 1 ml of 10% Triton X-100 Reaction.

X-Gluc (5-Bromo-4-Chloro-3-Indoyl-Beta-D-Glucuronide) in N, N- Dimethylformamide at a concentration of 25mg/ml was added. The reaction solution was mixed with X-Gluc at a ratio of 352 µl of reaction mix to 48 µl of X-Gluc.

## 8.2 Methods

### 8.2.1 Molecular biology techniques

- **Designing primers**

i) **Primers for cloning** - The gene of interest usually has to be amplified from genomic or cDNA by PCR before it can be cloned into an expression vector. For the amplification, primers were designed by entering the target sequence (genomic /Coding sequence CDS) to the PCR template in the NCBI Primer-BLAST tool and then the required product size was entered. The organism was set as *Arabidopsis thaliana* (taxid: 3702). The obtained primer pairs were checked for specificity using the same tool.

ii) **Primers for SDM:** For a nucleic acid sequence that encodes the amino acid to be changed, the fewest number of nucleotides were converted to get the desired codon. The variable region was then flanked with 10-12 nucleotides on both sides. The guanine-cytosine (G-C) base was always tried to be kept even at each end and have the non-complementary region in the center.

iii) **Primers for sequencing:** Since sequencing results from MWG Eurofins gave us the quality sequenced data only for 1,100 bps, for longer target sequences, F.P and R.P. were designed for every 800-900 base pairs (bps).

- **Primer dilution**

To prepare the primers for PCR reactions, the master mix was diluted in a sterile microcentrifuge tube with molecular grade distilled MilliQ water in a 1:10 ratio. Thus the final working stock concentration used for the PCR reactions is 10  $\mu$ M.

- **PCR reaction**

DNA was amplified in a PCR Thermocycler that fitted 96 well plates. The annealing temperature ( $T_a$ ) was set at 5°C below the calculated melting temperature ( $T_m$ ) of the oligonucleotides. The average elongation time was calculated based on the size of the fragments to be amplified and the processivity of the DNA polymerase used in PCR reaction. Mostly for genotyping PCR, *Taq* polymerase was used with a processivity of 1000 bp per minute.



The PCR protocol used for 50 µl of reaction using *Taq* DNA polymerase is as follows:

10X PCR Buffer	5 µl
dNTPs (10 mM)	1.5 µl
F.P	1.5 µl
R.P	1.5 µl
DNA	2 µl
DNA polymerase	1 µl
dMilliQ water	37.5 µl

Thermocycling conditions:

Step	Temperature	Time	
Initial Denaturation			} 35 cycles
Denaturation	98°C	15-30 seconds	
Annealing	45-72°C	15-60 seconds	
Elongation/Extension	72°C	1 minute/kb	
Final Extension	72°C	5-10 minutes	
Final Hold	4°C		

For cloning mostly *Phusion* High fidelity DNA polymerase was used since is an ideal choice for cloning for long and difficult amplicons. It has an error rate > 50-fold lower than that of *Taq* DNA Polymerase and 6-fold lower than that of *Pyrococcus furiosus*. It is one of the most accurate thermostable polymerases available. *Phusion* DNA Polymerase possesses 5'→ 3' polymerase activity, 3'→ 5' exonuclease activity and generates blunt-ended products. *Phusion* polymerase has a polymerizing time of 500 bp/min.

The PCR protocol used for 50 µl of reaction using *Phusion* DNA polymerase is as follows:

5X *Phusion* HF Buffer                      10 µl

Each of these buffers contains MgCl<sub>2</sub> (1.5 mM at the final [1X] reaction concentration)

dNTPs (10 mM)                              1 µl

F.P (10 mM)	2.5 $\mu$ l
R.P (10 mM)	2.5 $\mu$ l
Template DNA	2 $\mu$ l
Phusion DNA polymerase	0.5 $\mu$ l
Nuclease-free water	22.5 $\mu$ l

Thermocycling conditions:

Step	Temperature	Time	
Initial Denaturation			} 35 cycles
Denaturation	98°C	15-30 seconds	
Annealing	45-72°C	15-60 seconds	
Elongation/Extension	72°C	1 minute/500bp	
Final Extension	72°C	5-10 minutes	
Final Hold	4°C		

- **Agarose gel electrophoresis**

Gel electrophoresis was used for the separation of DNA fragments, based on their size and charge. 1 g of Agarose powder was added to 100 ml of 1X TBE, Tris/Borate/EDTA buffer to obtain 1% (w/v) of Agarose gel. The total gel volume varied depending on the size of the casting tray. 2  $\mu$ l volume of loading buffer was added to 20  $\mu$ l of PCR samples. 20  $\mu$ l of samples were loaded into the wells. The first well was loaded with 5  $\mu$ l of diluted DNA ladder. Electrophoresis was conducted at 60 volts (V) for 30 min for good separation of bands and after that, the gel was viewed under Gel imager.

- **Purification of PCR products**

The agarose band was cut at the proper size and the excess agarose gel was trimmed. DNA fragments were purified using the GeneJET Gel extraction kit (Thermo Scientific). 200 mg was cut and taken in a sterile 2  $\mu$ l Eppendorf tube, binding buffer was added so that the DNA is not degraded and the gel was melted at 55°C for 10-15 minutes. The solution mixture was transferred to a column provided with the kit and centrifuged for 1 min, followed by washing with 70% Ethanol (v/v) twice. The flow-through was removed and collected.

PCR amplified DNA was eluted with 40  $\mu$ l sterile Milli Q water after transferring the column to a new reaction tube and stored at 4°C for long-term storage at -20°C.

- **Gateway Cloning**

Gateway cloning involves preparation of a Gateway Entry clone in one of the gateway pENTR or pDONR vectors. The pENTR/D-TOPO vector allows rapid, directional TOPO cloning of blunt-end PCR products for entry into the Gateway system without any ligase or restriction enzyme. 10-15 ng/ $\mu$ l of purified PCR product was incubated with 15 ng/ $\mu$ l pENTR/D-TOPO vector and salt solution provided in the kit at room temperature (RT) for 30 minutes. In this system, the PCR product is directionally inserted by adding four bases to the gene-specific F.P (CACC). The reaction mixture was transformed into One Shot TOP10 chemically competent *E.coli* cells.

- **Gateway BP Reaction**

Generation of ENTR plasmids was alternatively done by BP reaction. For generation of Gateway entry clones from an attB-flanked PCR product the following procedure was followed:

In a 1.5 ml tube at RT, the attB-PCR product (15–150 ng) 1–7  $\mu$ l, Donor vector (150 ng/ $\mu$ l) 1  $\mu$ l and TE buffer, pH 8.0 to 8  $\mu$ l were added and mixed. BP Clonase™ II enzyme mix was thawed on ice for about 2 minutes and then it was vortexed briefly to mix 2  $\mu$ l of BP Clonase™ II enzyme mix was added to the reaction and mixed well by vortexing briefly twice. The reaction was incubated at RT for 1 hour. 1  $\mu$ l of the Proteinase K solution was added to the mixture and samples were then incubated at 37°C for 10 minutes to terminate the reaction. Samples were subsequently transformed in TOP10 cells.

- **Gateway LR Reaction**

The gene cassette in the Gateway Entry clone can be efficiently transferred into any Gateway Destination vector using the proprietary enzyme mix provided in the kit. LR recombination was performed using Gateway LR Clonase II Enzyme mix (Life Technologies) by incubating 2  $\mu$ l of 150 ng/ $\mu$ l of Entry clone with 2  $\mu$ l of 150 ng/ $\mu$ l of DEST vector along with 4  $\mu$ l of LR Clonase II Enzyme mix for 10  $\mu$ l of total reaction volume at room temperature (RT, 25°C) for 1 hour. This is followed by transformation of 5  $\mu$ l of LR reaction mix into 50  $\mu$ l of chemically competent *E.coli* TOP10 cells.

- **Bacterial growth conditions**

Bacterial cells were cultured overnight at 37°C and 170 rpm; *A.tumefaciens* cells were cultured for 48 hours at 28°C at 160 rpm. After transformation, bacterial cells were plated on agar plates and incubated overnight at 37°C for *E.coli* and 48 hours for *A.tumefaciens*. All cells were grown in LB medium with respective antibiotics, depending on the vector and strain used. Table 10.1 in the attachments summarizes antibiotic resistances of vectors and concentrations of antibiotics used.

- **Transformation**

For the heat shock transformation of TOP10 *E.coli* cells, the transformation was done by adding 5 µl of plasmid to 50 µl of TOP10 chemically competent *E.coli* TOP10 cells and the mixture was incubated in ice for 30 minutes, followed by heat shock at 42°C for 30 seconds. Subsequently, cells were plated on LB plates with selective antibiotics and incubated overnight at 37°C.

For the cold shock transformation of competent *Agrobacterium tumefaciens* cells- transformation of *A.tumefaciens* was done using GV101pk cells 5 µl of the purified plasmid with a concentration of 200-500 ng/µl was added to 50 µl of competent GV101pK cells, then was incubated on ice or 30 minutes, frozen in liquid nitrogen for 5 minutes and incubated at 37°C for 5 minutes. 250 µl of SOC medium was added and the cells were incubated at 28°C and 140 rpm for 2-4 hours. Finally, 200 µl of the cells were plated on LB agar plates and incubated at 28°C for 48 hours.

- **Plasmid isolation**

Plasmids were isolated using the GeneJET Plasmid Miniprep Kit according to the manufacturer's protocol. Single colonies of *E.coli* were inoculated in 5 ml of liquid LB media containing selective antibiotics and incubated overnight. Cells were harvested by centrifugation at 13,200 rpm for 5 minutes at room temperature, followed by washing and removing of the remaining ethanol. The flow-through was removed and collected for autoclaving. Purified plasmids were eluted with 30-50 µl MilliQ water after transferring the column to a new reaction tube. The DNA was stored at 4°C or for long-term storage at -20°C.

- **Quantification of nucleic acids**

The concentration of the plasmid DNA was measured using NanoQuant (TECAN, Infinite M200). It is a Quad-4 monochromators system that detects DNA concentration as low as 1 ng/μl. It possesses a UV Silicon photodiode detector and measures the absorbance at two different wavelengths, 260 nm, and 280 nm. It possesses automated Z-focusing with background correction for automatic optimization of signal to noise ratio that provides purity factor.

- **DNA Sequencing**

The concentration of plasmid DNA was adjusted to 50-100 ng/μl for sequencing at Eurofins MWG. Sequencing was carried out using universal primers, M13 Fwd and M13 Rev to sequence and check the fidelity of insert. For long constructs more than 1.5 Kbp, primers sequencing flanking middle regions were given as a template along with the universal primers. The results were evaluated with the program Clone Manager Professional 9.

- **SDM**

SDM was carried out to remove the stop codons and thus to generate a construct with C-terminal tag. And also SDM was used to mutate or delete bases in case of generating the apo/holo CaM deleted IQD5 variant mutant. This was performed using AccuPrime Pfx DNA Polymerase (Invitrogen). Template DNA with a concentration of 10 pg-200 ng concentration was mixed with specific primers designed for mutation. AccuPrime Pfx reaction mix, and 1 unit (0.4 μl) of Accuprime Pfx DNA polymerase for 50 μl of total reaction volume. The control reaction was prepared without AccuPrime Pfx polymerase. Reaction tubes were placed into PCR cycler, with a number of cycles ranging from 12-18, depending upon the type of mutation. PCR products of reaction and control samples were digested with 1 μl of *DpnI* (Thermo Scientific) restriction enzyme and 5.6 μl of buffer Tango (Thermo Scientific) overnight at 37°C. DNA plasmid isolated from most of the *E.coli* strain is methylated by the *dam*. The *DpnI* endonuclease specifically digests the methylated parental DNA template and allows the selection of mutated DNA synthesized by PCR. 5 μl of digested PCR products were transformed to 50 μl of chemically competent *E.coli* TOP10 cells.

- **Reverse transcription polymerase chain reaction (RT-PCR)**

To extract Ribonucleic acid (RNA) two steel beads were put to each 2 ml tube and pre-cooled. The (50-100 mg) plant material was harvested and froze immediately in liquid

nitrogen. The tissue lyser was used to homogenize plant material: The steel beads were removed from the tube and add 500 µl of TRI reagent was added and vortexed until we got a homogeneous liquid. The mixture was incubated for 5 minutes. After 5 min incubation at RT 100 µl, Chloroform was added and the tube was inverted slowly for 12 s and incubated for 10 minutes. After that, the mixture was centrifuged for 15 min at 15000 g and 4°C.

250 µl of the aqueous phase was transferred to a new 1.5 ml tube and was precipitated with 125 µl Isopropanol and 125 µl high salt solution. This step mostly helps to increase the RNA yield. This step was followed by a small vortex and then the mixture was incubated for 10 min at RT and centrifuged 10 min at 15000 g and 4°C. The supernatant was discarded and the pellet was washed. The pellet was washed with 500 µl of 70% Ethanol and centrifuged at 7500 g and 4°C for 5 min.

The excess Ethanol was removed and was let dry under the hood for approx. 10-15 min. When dried 40 µl RNAase free water was added and the pellet was dissolved by vortexing for 10 min at 65°C. The samples were stored at 4°C. The concentration was measured using NanoDrop and the stability of RNA extracted was checked using a control gel: 1% Agarose gel by loading 1 µg RNA/10 µl.

For the complementary DNA (cDNA) synthesis following master mixture was prepared:

Total volume: 20 µl

RNA	1 - 5 µg
dNTPs, 10 mM each	1 µl
Oligo-dT-Primer, 0,5 µg/µl	0.5 - 1 µl
H <sub>2</sub> O	added to 15 µl

The mixture was incubated for 5 min at 65°C to open the secondary structure and the chilled for 1 minute on the ice and the remaining components were added.

+ 5x reactions buffer	4 µl
+ RNase Inhibitor (40 U/µl)	0.5 µl
+ Revert Aid MuLV-Reverse Transcriptase (200 U/µl)	0.5 µl

The transcription was done at 42°C for 1 h. The reaction was stopped at 70° for 15 minutes. And the cDNA was stored at -20°C and used for the RT-PCR using *Actin2* as a control.

- **Western blotting**

- **Protein Extraction**

Western blot detection for fusion proteins from transient transformed *Nicotiana benthamiana* was done to check if the complete construct is present or not. The plant material of 3-days old after the transformation of the construct was harvested in using liquid nitrogen. The plant material was already checked for fluorescence in a confocal microscope. The plant material was taken and was put immediately to a pre-cooled mortar and it was homogenized. From the homogenized material, approximately 200 mg was taken and transfer to precool sterile 2 ml Eppendorf tube. 1 ml extraction buffer was added to the sample and it was vortexed to mix it well. Then the mixture was incubated 30 min on a rotating shaker at 4°C. A pre-centrifugation was performed to remove most of the cell debris. It was centrifuged 5 min at 500g / 4°C. 700-800 µl was transferred to a fresh sterile 1.5 ml Eppendorf tube and was centrifuged for 20 min at 21.000g and 4°C. 100 µl was collected from supernatant for loading SDS page. The pellet was resuspended in 200 µl extraction buffer. Laemmli buffer was added to all collected fractions and it was boiled for 10 min at 95°C.

- **SDS PAGE**

For the preparation of separating gel, 4 ml of a mixture of 30% (v/v) Acrylamide; 0.8% (v/v) Bis-Acrylamide, 5 ml of dMilliQ, 3 ml of 1.5 M Tris-HCl pH8.8 / 0.3% SDS (w/v) into 50 ml falcon tube. 100 µl of 10% APS(v/v) (Ammonium persulfate) and 10 µl TEMED were added. The falcon was inverted to mix all the solutions well and were filled in the gel chamber. Water was poured over it to get a plain edge. After the gel gets dried, the water was removed and the stacking gel was prepared. For the stacking gel, 0.75 ml of a mixture of 30% (v/v) Acrylamide; 0.8% (v/v) Bis-Acrylamide, 3 ml of water, 1.25 ml 0.5 M Tris-HCl, 50 µl APS and 5 µl TEMED were added to 50 ml falcon tube and mixed well. The comb is inserted and was kept until the gel got dry. 20 µl sample was loaded and 5 µl pre-stained protein marker was loaded in the first well. For each gel, 100 V and 25 mA was used.

- **Blotting**

Separated proteins were transferred to a nitrocellulose membrane using semi-dry blotting a sandwich layer of 6 Whatman (filter) paper and 1 membrane (6 x 8.5 cm) for one gel was made. The gel was removed from the chamber. All three components in Towbin buffer for few minutes. The blotter was run for 1h at 20 V, 150 W and 250 mA for one gel (for more gels = +10 mA per gel). After the blotting step was done, membranes were stained with Ponceau stain for 2 min and rinsed with water and were scanned for loading control image.

- **Blocking and Antibody incubation**

The blot was incubated for 1hour in 1x TBS (Tris-buffered saline) with 2% (w/v) milk powder and 2% (w/v) BSA (Bovine serum albumin). The membrane was washed for 10 min with 1xTBS. It was incubated with primary antibody (10 ml) overnight at 4°C. It was washed for 10 min with 1xTBS. Then the membrane was incubated with secondary antibody for 1hour at room temperature. It was rinsed twice with 1x TBS. Then it is washed for 1h with TBST (1xTBS + 0.5% (v/v) Tween20). The last step, the membrane was rinsed 2x with 1xTBS.

Antibody dilutions used so far for GFP\_IQD fusions: 1:500 anti-GFP (Santa Cruz)

1:3000 anti-rabbit (Thermo)

Antibody dilutions for RFP-fused proteins:

1:750 anti-RFP (GeneTex)

1:3000 anti-rabbit

- **Detection**

1000 µl of each solution from SuperSignal™ West Pico Chemiluminescent was added in a 2 ml Eppendorf tube. The substrate solution was added to the blot. It was mixed via slowly shaking per hand. A small waste bag was cut on 2 sides and the membrane was put in foil. The blot was developed with a FluorChem system by Alpha Innotech and image was captured.

- ***In vitro* pull down assay**

The GST-polypeptides were attached to glutathione agarose beads in GST-binding buffer, i.e PBS at pH 7.4, 8 mM DTT, and 0.1% (v/v) Triton X-100. After overnight incubation at 4 °C, the beads were washed 5 times in the same GST-binding buffer and incubated with



CaM beads in PBS at pH 7.4. CaM was incubated with the GST-polypeptides with EGTA, 2 mM, or with high Ca<sup>2+</sup>, 2.0 mM. Following 2 hours incubation at 4°C, beads were washed, and proteins were eluted with 1 mL of 10 mM reduced glutathione in 50 mM Tris-HCl at pH 8.0 (Edrington et al. 2007). Samples were analyzed on 10% SDS-PAGE gel and by Western blotting. The blot was developed with a FluorChem system by Alpha Innotech and image was captured.

## **8.2.2 Plants biology techniques**

- **Plant growth conditions**

Seeds were surface sterilized with chlorine gas, stratified for 2 days at 4°C on *Arabidopsis thaliana* Salts (ATS) medium (x ATS salts, 0.5 % (w/v) agar gel, x % (w/v) sucrose) (Lincoln et al. 1990), and grown at 21°C under long-day conditions (16 hrs light, 8 hrs dark). Macroscopic growth parameters were analyzed in the 5-day-old seedling.

- **Floral dip method**

Floral dip method was used to transform *Arabidopsis thaliana*. Plants were infiltrated or dipped when most secondary inflorescences were about 1–10 cm tall and plants were about 5-6 weeks old. For the infiltration, *Agrobacterium tumefaciens* strain GV3101 carrying the binary plasmid were grown to stationary phase in Spec Rifampicin plate at 28 C for 48 hours until there was a mat of colonies formation. For each of the construct, two plates were made. The mat of cells was harvested and to liquid LB medium without any antibiotic. And then resuspended in infiltration medium to a final OD600 of approximately 0.80 prior to use. The revised floral dip inoculation medium contained 5 % (w/v) sucrose and 0.05% (v/v) Silwet L-77. For floral dip method, the inoculum was added to a tray, plants with inflorescence were inverted into this suspension tray such that all above-ground tissues were submerged, and plants were then removed after 12 secs of gentle shaking. Plants were placed in plastic greenhouse trays and were covered with a cellophane plastic to maintain humidity and were kept covered for 2 days in the greenhouse. Plants were grown for a further 5-6 weeks until siliques were brown and dry and T<sub>0</sub> seeds were harvested.

- **Selection of putative transformants using Basta**

T<sub>0</sub> seeds were spread on soil and were grown for one week. Since the most of the destination vectors encode the *Bar* gene conferring resistance to the herbicide Basta, T<sub>0</sub>

plants were sprayed with Basta herbicide and the resistant seedlings that produced green leaves and well-established roots after spraying them with the selective medium were identified as transformed plants. The plants resistant to the selective media are the  $T_1$  plants.

- **Establishment of  $T_3$  homozygous mutants**

The  $T_2$  seeds were harvested and were surface sterilized by vapor-phase methods. For vapor-phase sterilization, seeds in open containers were placed into a 10 l desiccator jar, placed in a fume hood. Just prior to sealing the desiccator, a 250 ml beaker containing 100 ml NaOHCl was added and 3 ml concentrated HCl was carefully added into the NaOHCl. The desiccator with chlorine fumes remained sealed for 45 minutes and then the vacuum pump was switched on to remove all the chlorine gas. The seeds were then transferred to the hood and were kept for 2 hours with an open lid before they were plated on Basta resistant plate with *k1cr1-1* as a positive control and WT Col-0 as negative controls. After two weeks the ratio of living: nonliving plants were calculated and lines with 3:1 i-e with 1 insertion were selected. The lines were grown on the soil to obtain the  $T_3$  generation. The Basta screening was repeated with the  $T_3$  seeds and the homozygous lines were selected for our phenotyping and GUS experiments.

- **Establishment of GUS lines and histochemical assays**

The plant material was fixed for 30 minutes in ice-cold fixative 90% (v/v) Acetone, shaking occasionally. Then it was washed for 30-60 minutes in several changes of ice cold GUS solution without X-Gluc. After that GUS solution with X-gluc was added and was vacuum infiltrated for easy absorption. The set up was then incubated in darkness at 37 C several overnights or until distinct blue staining appeared (no longer than 24h). The material was rinsed in the distilled increasing concentration of Ethanol and incubated in 70% (v/v) ethanol until the chlorophyll is removed, then transfer to distilled water again. Plant materials were cleared in chloral hydrate, and roots and seeds were imaged 204 with a Zeiss axioplan 2 microscope using a DIC objective. Imaging of whole seedlings, leaves, 205 flowers, and siliques was performed with a Nikon SMZ 1270 stereo microscope.

- **Transient transformation in *N.benthamiana***

*A.tumefaciens* colonies harboring respective plasmids and *A.tumefaciens* P19 cells were grown in selective liquid LB media at 30 degrees C for 48 hours. Cells were harvested by

centrifugation at 10,000 rpm for 5 minutes, washed twice with infiltration (IF) buffer and finally re-suspended in IF buffer. Optical density (O.D) was measured at 600 nm and it was adjusted to 0.5-0.8 with IF buffer. The prepared *A.tumefaciens* cell suspension was mixed with silencing suppressor P19 in 1:1 ration. The mixture was incubated at 20 C for 1 hour and infiltrated in the abaxial surface of the *N.benthamiana* leaf. Subcellular localization of GFP/YFP- fusion proteins was analyzed three days after infiltration by the CLSM. The P19 protein is encoded by tomato bushy stunt virus (TBSV), involved in suppression of posttranslational gene silencing.

### **8.2.3 Cell biology assays**

- **CLSM**

Cell biological assays were performed with infiltrated tobacco leaves 3 days after infiltration. A leaf disc was placed on a glass slide with water and covered with a glass coverslip. Imaging was performed by capturing single optic sections with LSM700 inverted microscope (Carl Zeiss) using a 40X water immersion objective. GFP and YFP fluorescence were detected with an excitation at 488nm and emission were detected between 485 nm and 560 nm. RFP fluorescence was detected with an excitation at 555 nm and emission was detected between 580nm and 700nm (Borkowski et al. 2017).

- **Whole seedling phenotyping**

Seeds were surface sterilized with chlorine gas, stratified for 2 days at 4°C on *Arabidopsis thaliana* Salts (ATS) medium (x ATS salts, 0.5 % (w/v) agar gel, x % (w/v) sucrose) (Lincoln et al. 1990), and grown at 21°C under long-day conditions (16 hours light, 8 hours dark). Macroscopic growth parameters were analyzed in the 5-day-old seedling.

- **Trichome patterning**

Trichome patterning on *Arabidopsis* rosette leaves serves as a model to study how cells are specified in a regular spacing pattern from initially equivalent cells. The trichome patterning analysis was done using images of 4 weeks old plants grown in a greenhouse. The images were taken in with a Zeiss axioplan 2 microscope using bright field mode and manually quantified for the preliminary results.

- **PC shape**

For visualization of cell contours, cell outlines were visualized by FM4-64 as described in Bürstenbinder et al. (2017b) and imaged with a 20x objective (3-10 DAG). FM4-64 was excited with a 555 nm laser, and emission was detected between 560 and 620 nm. Segmentation, feature quantification, and graphical visualizations of PC shapes were conducted with the ImageJ plugin PaCeQuant and the associated R script (Möller et al. 2017).

- **Hormone treatments**

To examine the effect of exogenous Auxin and Cytokinin on the degree of PC interdigitation, Naphtalic Acetic Acid (NAA) and Kinetin (Sigma) was dissolved in dimethyl sulfoxide (DMSO) and prepared as a stock solution of 100  $\mu\text{m}$ , which was added into one-half-strength ATS media to obtain a final concentration of 20 nM NAA to 100 nM IAA and 20 nM to 100 nM Kinetin for seedling treatments. I had used different concentrations and also I had grown the plants in liquid ATS and in ATS plates to check which concentration and which condition effect the leaves the most. 50 nM Kinetin and 100 nM NAA worked best for me when added in liquid media, where 3 day-old seedlings were grown in liquid ATS media under constant shaking in 16 hours light and 8 hours dark conditions with control. After two days, the cotyledons were cut were stained with 10  $\mu\text{m}$  propidium iodide (PI) stain (Sigma) for 15 min and imaged using a confocal microscopy and the PC shape was analyzed using the Fiji (Image J) plugin.

- **Cellulose staining**

For histochemical cellulose staining in cell walls, 5-day-old seedlings were incubated for 4-5 hours in 0.4 % (v/v) Calcofluor-white M2R dissolved in Milli Q To stain callose and the cuticle, seedlings were incubated for 4-5 hours and 5 min in 0.1% (v/v) Aniline blue in 100 mM  $\text{Na}_2\text{PO}_4$  buffer (pH 7.2) in 50 mM Tris HCl buffer (pH 7.2). Seedlings were then co-stained with 0.5 % (w/v) PI stain for minimum 10 minutes to visualize cell outline. The cotyledons were then imaged with a Zeiss LSM 700 inverted microscope, using a 40x water immersion objective. Calcofluor-white and Aniline blue were excited with a 405 nm laser, and emission was detected with a 490 nm short pass filter.

## 9 References

- Akhmanova, A.; Hammer, J. A. (2010): Linking molecular motors to membrane cargo. In *Current opinion in cell biology* 22 (4), pp. 479–487. DOI: 10.1016/j.ceb.2010.04.008.
- Berridge, M. J. (2011): Calcium signalling and Alzheimer's disease. In *Neurochemical research* 36 (7), pp. 1149–1156. DOI: 10.1007/s11064-010-0371-4.
- Boyle, J. (2008): Molecular biology of the cell, 5th edition by B. Alberts, A. Johnson, J. Lewis, M. Raff, K. Roberts, and P. Walter. In *Biochem. mol. biol. educ.* 36 (4), pp. 317–318. DOI: 10.1002/bmb.20192.
- Borkowski O.; Bricio C.; Murgiano M.; Stan G. B. and Ellis T. (2017). Cell-free prediction of protein expression costs for growing cells. In *BioRxiv preprint* <https://dx.doi.org/10.1101/172627>.
- Brill, S.; Li, S.; Lyman, C. W.; Church, D. M.; Wasmuth, J. J.; Weissbach, L. et al. (1996): The Ras GTPase-activating-protein-related human protein IQGAP2 harbors a potential actin binding domain and interacts with calmodulin and Rho family GTPases. In *Molecular and cellular biology* 16 (9), pp. 4869–4878.
- Bringmann, M.; Li, E.; Sampathkumar, A.; Kocabek, T.; Hauser, M.T.; Persson, S. (2012): POM-POM2/cellulose synthase interacting1 is essential for the functional association of cellulose synthase and microtubules in Arabidopsis. In *The plant cell* 24 (1), pp. 163–177. DOI: 10.1105/tpc.111.093575.
- Brown, M. D.; Sacks, D. B. (2006): IQGAP1 in cellular signaling. Bridging the GAP. In *Trends in cell biology* 16 (5), pp. 242–249. DOI: 10.1016/j.tcb.2006.03.002.
- Brown, M. D.; Sacks, D. B. (2009): Protein scaffolds in MAP kinase signalling. In *Cellular signalling* 21 (4), pp. 462–469. DOI: 10.1016/j.cellsig.2008.11.013.
- Bürstenbinder, K.; Mitra, D.; Quegwer, J. (2017a): Functions of IQD proteins as hubs in cellular calcium and auxin signaling. A toolbox for shape formation and tissue-specification in plants? In *Plant signaling & behavior* 12 (6), e1331198. DOI: 10.1080/15592324.2017.1331198.
- Bürstenbinder, K.; Moller, B.; Plotner, R.; Stamm, G.; Hause, G.; Mitra, D.; Abel, S. (2017b): The IQD family of calmodulin-binding proteins links calcium signaling to microtubules, membrane subdomains, and the nucleus. In *Plant physiology* 173 (3), pp. 1692–1708. DOI: 10.1104/pp.16.01743.

- Bürstenbinder, K.; Savchenko, T.; Muller, J.; Adamson, A. W.; Stamm, G.; Kwong, R. et al. (2013): Arabidopsis calmodulin-binding protein IQ67-domain 1 localizes to microtubules and interacts with kinesin light chain-related protein-1. In *The Journal of biological chemistry* 288 (3), pp. 1871–1882. DOI: 10.1074/jbc.M112.396200.
- Caillard O., Moreno H., Schwaller B., Llano I., Marco R. C., and Marty A. (2000). Role of the calcium-binding protein parvalbumin in short-term synaptic plasticity. In *PNAS* 97 (24) 13372-13377.
- Day, I. S.; Reddy, V. S.; Shad A., G.; Reddy, A. S.N. (2002): Analysis of EF-hand-containing proteins in Arabidopsis. In *Genome biology* 3 (10), research0056.1-research0056.24.
- Deavours, B. E.; Reddy, A. S.; Walker, R. A. (1998): Ca<sup>2+</sup>/calmodulin regulation of the Arabidopsis kinesin-like calmodulin-binding protein. In *Cell motility and the cytoskeleton* 40 (4), pp. 408–416. DOI: 10.1002/(sici)1097-0169(1998)40:4<408::aid-cm8>3.0.co;2-6.
- Duan P; Xu J; Zhang B, Geng M, Zhang G, Huang K, Huang L; Xu R; Ge S; Quan Q; Li Y. (2017). Natural variation in the promoter of GSE5 contributes to grain size diversity in rice. In *Molecular plant* 10(5):685-694. doi: 10.1016/j.molp.2017.03.009.
- Edrington T.C.; Yeagle P.L.;Gretzula C. L.; and Boesze-Battaglia K (2007). Calcium-dependent association of calmodulin with the C-terminal domain of the Tetraspanin protein peripherin/rds. In *Biochemistry*, 46(12):3862-3871.
- González-Aguilera K. ; Saad C.F. ; Chávez Montes R. ; Alves-Ferreira M. and Folter S. (2016). Selection of reference genes for quantitative Real-Time RT-PCR studies in tomato fruit of the genotype MT-Rg1. In *Frontiers of plant sciences*. doi: 10.3389/fpls.2016.01386.
- Gu, Y.; Kaplinsky, N.; Bringmann, M.; Cobb, A.; Carroll, A.; Sampathkumar, A. et al. (2010): Identification of a cellulose synthase-associated protein required for cellulose biosynthesis. In *Proceedings of the national academy of sciences of the United States of America* 107 (29), pp. 12866–12871. DOI: 10.1073/pnas.1007092107.
- Hedman, A. C.; Smith, J. M.; Sacks, D. B. (2015): The biology of IQGAP proteins. Beyond the cytoskeleton. In *EMBO reports* 16 (4), pp. 427–446. DOI: 10.15252/embr.201439834.

- Kabachinski G and Schwartz (2015): The nuclear pore complex – structure and function at a glance. In *Journal of cell science* (128): 423-429; doi: 10.1242/jcs.083246.
- Kudla, J.; Becker, D.; Grill, E.; Hedrich, R.; Hippler, M.; Kummer, U. et al. (2018): Advances and current challenges in calcium signaling. In *The New phytologist* 218 (2), pp. 414–431. DOI: 10.1111/nph.14966.
- Levy, M.; Wang, Q.; Kaspi, R.; Parrella, M. P.; Abel, S. (2005): Arabidopsis IQD1, a novel calmodulin-binding nuclear protein, stimulates glucosinolate accumulation and plant defense. In *The Plant journal for cell and molecular biology* 43 (1), pp. 79–96. DOI: 10.1111/j.1365-313X.2005.02435.x.
- Li, S.; Lei, S.; Chris R.; Gu, Y. (2012): Cellulose synthase interactive protein 1 (CSI1) links microtubules and cellulose synthase complexes. In *Proceedings of the national academy of sciences of the United States of America* 109 (1), pp.185–190. DOI: 10.1073/pnas.1118560109.
- Li R.; Zhang J.; Wei J.; Wang H.; Ma R. (2009). Functions and mechanisms of the CBL–CIPK signaling system in plant response to abiotic stress. In *Progress in natural sciences* 9 667–676.
- Li Z. and Sacks D. B. (2003): Elucidation of the Interaction of Calmodulin with the IQ Motifs of IQGAP1. In *The Journal of biological chemistry* (278): 4347–4352.
- Liang H.; Zhang Y.; Martinez P.; Rasmussen C.G.; Xu T.; Yang Z.(2018). The Microtubule-Associated Protein IQ67 DOMAIN5 Modulates Microtubule Dynamics and Pavement Cell Shape. In *Plant Physiology* DOI: <https://doi.org/10.1104/pp.18.00558>.
- Liu, Z.; Schneider, R.; Kesten, C.; Zhang, Y.; Somssich, M.; Zhang, Y. et al. (2016): Cellulose-microtubule uncoupling proteins prevent lateral displacement of microtubules during cellulose synthesis in Arabidopsis. In *Developmental cell* 38 (3), pp.305–315. DOI: 10.1016/j.devcel.2016.06.032.
- Ma W.; Smigel A.; Verma R.; Berkowitz G. A. (2009). Cyclic nucleotide gated channels and related signaling components in plant innate immunity. In *Plant signal behaviour* 4(4): 277–282.
- McAinsh, M. R.; Pittman, J. K. (2009): Shaping the calcium signature. In *The New phytologist* 181 (2), pp. 275–294. DOI: 10.1111/j.1469-8137.2008.02682.x.

- McFarlane, H. E.; Doring, A.; Persson, S. (2014): The cell biology of cellulose synthesis. In *Annual review of plant biology* 65, pp. 69–94. DOI: 10.1146/annurev-arplant-050213-040240.
- Mitra D.; Klemm S.; Kumari P.; Quegwer J.; Möller B.; Poeschl Y.; Pflug P.; Stamm G., Abel S.; Bürstenbinder K.(2019). Microtubule-associated protein IQ67 DOMAIN5 regulates morphogenesis of leaf pavement cells in *Arabidopsis thaliana*. In *Journal of exp. botany* 70(2): 529–543..
- Mruk K.; Farley B. M, Ritacco A. W and William R. K., William R (2014): Calmodulation meta-analysis: Predicting calmodulin binding via canonical motif clustering. In *Journal of general physiology* (1)144:105–114.
- Mukhtar, M. S.; Carvunis, A.-R.; Dreze, M.; Epple, P.; Steinbrenner, J.; Moore, J. et al. (2011): Independently evolved virulence effectors converge onto hubs in a plant immune system network. In *Science (New York, N.Y.)* 333 (6042), pp. 596–601. DOI: 10.1126/science.1203659.
- Narasimhulu, S. B.; Reddy, A. S. (1998): Characterization of microtubule binding domains in the *Arabidopsis* kinesin-like calmodulin binding protein. In *The Plant cell* 10 (6), pp. 957–965.
- Nelson, M. R.; Chazin, W. J. (1998): An interaction-based analysis of calcium-induced conformational changes in Ca<sup>2+</sup> sensor proteins. In *Protein science: a publication of the Protein Society* 7 (2), pp. 270–282. DOI: 10.1002/pro.5560070206.
- Nelson, M. R.; Chazin, W. J. (1998): Structures of EF-hand Ca<sup>2+</sup>-binding proteins: diversity in the organization, packing and response to Ca<sup>2+</sup> binding. In *Biometals*: 11(4):297-318.
- Nogales, E. (2001): Structural insight into microtubule function. In *Annual review of biophysics and biomolecular structure* 30, pp. 397–420. DOI: 10.1146/annurev.biophys.30.1.397.
- O'Neil K.T; DeGrado W.F. (1990). How calmodulin binds its targets: sequence independent recognition of amphiphilic alpha-helices. In *Trends biochem science* 15(2):59-64.
- O'Neil KT; DeGrado WF. (1998). An interaction-based analysis of calcium-induced conformational changes in Ca<sup>2+</sup> sensor proteins. In *Protein Science* 7(2):270-82.



- Pathmanathan, S.; Hamilton, E.; Atcheson, E.; Timson, D. J. (2011): The interaction of IQGAPs with calmodulin-like proteins. In *Biochemical society transactions* 39 (2), pp. 694–699. DOI: 10.1042/BST0390694.
- Prebil D. S, Slapsak U.; Puz .; Pavsik, G. I.; Puz V.; Euripedes deA. R., Anrather D., Hartl M., Backman L., Janez P. B. L. & Djinović-Carugo K. (2016) Structure and calcium-binding studies of calmodulin-like domain of human non-muscle  $\alpha$ -actinin-1. In *Scientific Reports*. 6:27383, DOI: 10.1038. srep27383.
- Ranty B; Aldon D; Galaud J.P. (2006) Plant calmodulins and calmodulin-related proteins. In *Plant signal behaviour* 1(3): 96–104.
- Ryu S.-Y.; Beutner G.; Dirksen R. T; Kinnally K. W.; Sheu S.-S.. (2010). Mitochondrial ryanodine receptors and other mitochondrial  $\text{Ca}^{2+}$  permeable channels. In *FEBS letter*, 584(10): 1948–1955. doi:10.1016/j.febslet.2010.01.032.
- Schmidt H. (2012). Three functional facets of calbindin D-28k. In *Front. mol. neurosci.*. doi.org/10.3389/fnmol.2012.00025.
- Schnapp, B. J. (2003): Trafficking of signaling modules by kinesin motors. In the *Journal of cell science* 116 (11), p. 2125. DOI: 10.1242/jcs.00488.
- Somerville, C.; Bauer, S.; Brininstool, G.; Facette, M.; Hamann, T.; Milne, J. (2004): Toward a systems approach to understanding plant cell walls. In *Science (New York, N.Y.)* 306 (5705), pp. 2206–2211. DOI: 10.1126/science.1102765.
- Sugiyama Y.; Wakazaki M.; Toyooka K.; Fukuda H. and Oda Y.(2017). A Novel PlasmaMembrane-Anchored Protein Regulates Xylem Cell-Wall Deposition through MicrotubuleDependent Lateral Inhibition of Rho GTPase Domains. In *Current Biology* 27, 2522–2528.
- Wang, S.; Watanabe, T.; Noritake, J.; Fukata, M.; Yoshimura, T.; Itoh, N. et al. (2007): IQGAP3, a novel effector of Rac1 and Cdc42, regulates neurite outgrowth. In the *Journal of cell science* 120 (4), p. 567. DOI: 10.1242/jcs.03356.
- Wang X.; Zhu L.; Liu B.; Wang C.; Jin L.; Zhao Q. and Yuana M. (2007). Arabidopsis Microtubule-associated protein18 functions in directional cell growth by destabilizing cortical microtubules. In *The plant cell* (19): 877–88.

- Wasteneys, G. O.; Galway, M. E. (2003): Remodeling the cytoskeleton for growth and form. An overview with some new views. In *Annual review of plant biology* 54, pp. 691–722. DOI: 10.1146/annurev.arplant.54.031902.134818.
- Weissbach, L.; Settleman, J.; Kalady, M. F.; Snijders, A. J.; Murthy, A. E.; Yan, Y. X.; Bernards, A. (1994): Identification of a human rasGAP-related protein containing calmodulin-binding motifs. In *The Journal of biological chemistry* 269 (32), pp. 20517–20521.
- Wendrich J.R.; Möller B. K.; Li S., Saiga S.; Sozzani R.; Benfey P. N.; Rybel B. D. , and Weijers D.(2017) Framework for gradual progression of cell ontogeny in the *Arabidopsis* root meristem. In *PNAS* 114 (42) E8922-E8929.
- Zaichick, S. V.; McGrath, K. M.; Caraveo, G. (2017): The role of Ca<sup>2+</sup> signaling in Parkinson's disease. In *Disease models & mechanisms* 10 (5), pp. 519–535. DOI: 10.1242/dmm.028738.
- Zhang, L.; Du, L., Poovaiah, B. W. (2014): Calcium signaling and biotic defense responses in plants. In *Plant signaling & behavior* 9 (11), e973818. DOI: 10.4161/15592324.2014.973818.
- Zheng W; Wang P; Zhang H. X. and Zhou D. (2011). Photosynthetic characteristics of the cotyledon and first true leaf of castor (*Ricinus communis* L.). In *Australian journal for crop sciences* 5(6):702 -708.

## 10 Supplementary data

### 10.1 Bacterial Strains and constructs

Strain	Source
<i>E. coli</i> One-shot TOP10®	Invitrogen DE
<i>E. coli</i> DH5α	Promega, USA
<i>E. coli</i> M15	Qiagen, DE
GV3101	
GV3101pK	
EHA101	

Construct	Antibiotic resistance	Source
pDONR221	Spec	Invitrogen™
pENTR/D-TOPO	Kan	Thermo Fischer
pDONR207	Gent	Invitrogen
pDEST15	Carb	Thermo Fischer
pDEST-N110	Amp	(Dyson, Shadbolt, Vincent, Perera, & McCafferty, 2004)
pB7WGF2	Spec	(Karimi, Inze, & Depicker, 2002)
pB7WGY2	Spec	(Karimi, Inze, & Depicker, 2002)
pGWB455	Spec	(Nakagawa et al., 2007)
pG7WG,0	Spec	-
pBGWFS7	Spec	-
pB7WG2	Spec	-
pB7FWG2	Spec	-
pVYCE	Kan	(Gehl, Waadt, Kudla, Mendel, & Hansch, 2009)
pVYNE	Kan	(Gehl, Waadt, Kudla, Mendel, & Hansch, 2009)

## 10.2 DNA and Protein markers

marker	size	source
1 kb GeneRuler™ DNA ladder	250-10,000 bp	Thermo Scientific, DE
100 bp GeneRuler™ DNA ladder	100-1500 bp	Thermo Scientific, DE
100 bp plus GeneRuler™ DNA ladder	100-3000 bp	Thermo Scientific, DE
PageRuler™ prestained protein ladder	10-180 kDa	Thermo Scientific DE

## 10.3 Instruments and Kits

Instrument/ Kits	manufacturer
Benchtop centrifuge	Eppendorf
DNA gel chamber	Biotech Fischer, DE
DNA Gel Doc Bioimaging System	Syngene Gene Genius, DE
Gel rocker Duomax 2030	Heidolph, DE
Incubator shakers	New Brunswick, DE
NanoQuant™ Photometer M200	Tecan, DE
pH meter	inoLab, DE
Protein gel imager FluorChem® Q	AlphaInnotech, DE
Heat block	Eppendorf, DE
Ultrapure MilliQ	Millipore, TKA, DE
GeneJET Plasmid Miniprep Kit	Thermo Scientific
LR Clonase II Enzyme mix	Life Technologies

## 10.4 List of Server/Softwares

Server/Software	purpose
CloneManager9	Cloning, sequence analysis
TAIR	Gene sequences, promoter activity
Image J	Image analysis
Fiji	Pavement cell shape quantification
Adobe Photoshop	Image processing
Zeiss software	Processing of confocal microscope images
NEB Tm Calculation	Calculation of melting temperature

## 10.5 List of Primers

Name	locus	sequence	Tm	information
Primers for IQD subclade IIIa:				
Genotyping				
IQD5 F	At3g22190	ATGGGAGCTTCAGGGAGATG	60	GABI_288E09 PRODUCT_SIZE 599
IQD5R	At3g22190	GCGTTACAGCAGCTTGTTTTTC	60.07	BP+RP_PRODUCT_SIZ E 374-574
IQD5F	At3g22190	CACCATGGGAGCTTCAGGGAG ATG	61.53	Ox - Directional TOPO cloning
IQD5R	At3g22190	CTATGCAAGCCTCTGTTTTATTG G	61.27	Ox - Directional TOPO cloning
IQD6F	At2g26180	CACCATGGGTGCTTCAGGGAAA T	59.35	Ox - Directional TOPO cloning
IQD6R	At2g26180	TTAACCTCTCGGCTTCTCGA	60.09	Ox - Directional TOPO cloning
IQD7F	At1g17480	CACCATGGGTGGGTCAGGAAAT T	59.05	Ox - Directional TOPO cloning
IQD7R	At1g17480	TTAGCTTCGCTGGCTCTTG	59.45	Ox - Directional TOPO cloning
IQD8F	At1g72670	CACCATGGGTGGCTCTGAAAT T	59.35	Ox - Directional TOPO cloning
IQD8R	At1g72670	TTAGCCTCTCTGGCTCTTGC	61.14	Ox - Directional TOPO cloning
Promoter GUS constructs				
IQD5F	At3g22190	CACCTCTATATATGGTTCACAAT CGAGACAC	59.73	P::GUS
IQD5R	At3g22190	TCTATCTCAATTCCAACGATCAG	58.34	P::GUS

IQD6F	At2g26180	CACCTTCATCTTTTTCTCTGTC TGATTAAT	58.15	P::GUS
IQD6R	At2g26180	AGATTA AAAAGTTTCGATCTTTT TGG	59.54	P::GUS
IQD7F	At1g17480	CACCGTAACAGCGTCAACAATG GCT	60.19	P::GUS
IQD7R	At1g17480	TTCTCAAATCGAGACCTTGTT	60.11	P::GUS
IQD8F	At1g72670	CACCATGTTGCTCAAAGGAAGG AATAAT	59.45	P::GUS
IQD8R	At1g72670	TTGCTCAAATTTGAAACCTTT	59.98	P::GUS
IQD5F	At3g22190	CACCATAAATCACATCACTGTTT TTGGGT	59.94	pro:GUS 2.2 kb fragment
IQD6F	At2g26180	CACCTCGAGTATGATTCTTAATT TGAATTAA	56.95	pro:GUS 2.2 kb fragment
IQD7F	At1g17480	CACCACAAGCCATCAAAGTTG AAACT	59.23	pro:GUS 2.2 kb fragment
IQD7F	At1g17480	AGATGCGAGATCTCATCGGT		sequencing of long promoter construct
IQD7R	At1g17480	TCATCACTTATTAATTTGTC		sequencing of long promoter construct
IQD5F	At3g22190	ATAGCAGCCATACCATAAAA		sequencing of long promoter construct
IQD5R	At3g22190	ATCTTTTTTAATCTAAATTA		sequencing of long promoter construct
IQD6F	At2g26180	GGTGGATTA AATTGTGTAA		sequencing of long promoter construct
IQD6R	At2g26180	ATGACAAGGTTTTCTTTCTA		sequencing of long promoter construct
CDS without stop codon and also for cloning				
IQD5F	At3g22190	AATAAAACAGAGGCTTGCAAAG GGTGGGCGCGCCGA	>75	SDM-stop deletion
IQD5R	At3g22190	TCGGCGCGCCACCCTTTGCAA GCCTCTGTTTTATT	>75	SDM-stop deletion
eGFP		ACGTAAACGGCCACAAGTTC	60.06	detection of GFP in pB7WGF2 (2615)
eGFP		AAGTCGTGCTGCTTCATGTG	60.04	detection of GFP in pB7WGF2 (2430)
IQD5R	At3g22190	TCACTATGCAAGCCTCTGTTTTA TTGG	61.9	second stop codon, von primer 117
IQD5R	At3g22190	GGGCTATGCAAGCCTCTGTTTT ATTGG	65	
IQD5F	At3g22190	GGGG ACAAGTTTGTACAAAAA GCAGGCTTCATGGGAGCTTCAG GGAGATG	>75	cloning into pDONR21
IQD5R	At3g22190	GGGGACCACTTTGTACAAGAAA GCTGGGTCCTATGCAAGCCTCT GTTTTATTGG	>75	cloning into pDONR21
IQD5R	At3g22190	AAATGCAAGCCTCTGTTTTATTG G	57.6	cloning of genomic IQD5
IQD6R	At2g26180	AAAACCTCTCGGCTTCTCGAAT CG	62.7	cloning of genomic IQD6
IQD7R	At1g17480	AAAGCTTCGCTGGCTCTTGCC CA	66.1	cloning of genomic IQD7
IQD8R	At1g73670	AAAGCCTCTCTGGCTCTTGCC CACA	66.4	cloning of genomic IQD8

IQD8F	At1g17480	GGAATCAGCTGCACCATTACT	57.9	sequencing of promoter construct
IQD8R	At1g17480	GCGAGCATTCTCATACCTGTC	59.8	sequencing of promoter construct
For cloning of KLCR1 interactors				
TLSP1F	AT1G5589 0.1	GGGGACAAGTTTGTACAAAAA GCAGGCTTCATGTCGTCTCTAT CTCGCGTTC	>70	cloning into pDONR221
TLSP1R	AT1G5589 0.1	GGGGACCACTTTGTACAAGAAA GCTGGGTCTTACTCTTCCTGGG ACGGC	>70	cloning into pDONR221
TLSP2F	AT3G0562 5.1	GGGGACAAGTTTGTACAAAAA GCAGGCTTCATGTCACTAACC AGATCGTGA	>70	cloning into pDONR221
TLSP2R	AT3G0562 5.1	GGGGACCACTTTGTACAAGAAA GCTGGGTCTCAAAGAATACCGG AGCTCC	>70	cloning into pDONR221
PPR596 F	AT1G8027 0.1	GGGGACAAGTTTGTACAAAAA GCAGGCTTCATGTTGCTCTTT CCAAGGT	>70	cloning into pDONR221
PPR596 R	AT1G8027 0.1	GGGGACCACTTTGTACAAGAAA GCTGGGTCTCAATCCAGAATAT CAGAGATAGCTG	>70	cloning into pDONR221
TLSP3F	AT3G1316 0.1	GGGGACAAGTTTGTACAAAAA GCAGGCTTCATGTCGTCTCTCT CTCGCTTTC	>70	cloning into pDONR221
TLSP3R	AT3G1316 0.1	GGGGACCACTTTGTACAAGAAA GCTGGGTCTTACTCTTTGGGAA AGAGACGAAG	>70	cloning into pDONR221
TLSP4F	AT3G5356 0.1	GGGGACAAGTTTGTACAAAAA GCAGGCTTCATGGAGTCTCTGG GGAAGCT	>70	cloning into pDONR221
TLSP4R	AT3G5356 0.1	GGGGACCACTTTGTACAAGAAA GCTGGGTCTCAACTAGTTGATC CAGCCATCT	>70	cloning into pDONR221
For cloning of IQD2 interactors				
TTL1F(I QD2 int)	At1G53300 .1	GGGGACAAGTTTGTACAAAAA GCAGGCTTCATGCCAAGTCAG TTAAACCC	>70	cloning into pDONR221
TTL1R(I QD2 int)	At1G53300 .1	GGGGACCACTTTGTACAAGAAA GCTGGGTCTTAACCGCTATAGT GTCTACCG	>70	cloning into pDONR221
TTL2F(I QD2 int)	At3G14950 .1	GGGGACAAGTTTGTACAAAAA GCAGGCTTCATGTCTGAAGCTCA AGAAACCTATACT	>70	cloning into pDONR221
TTL2R(I QD2 int)	At3G14950 .1	GGGGACCACTTTGTACAAGAAA GCTGGGTCTTAAAGGCCATAGT GCCTCACT	>70	cloning into pDONR221
TTL3F(I QD2 int)	At2G42580 .1	GGGGACAAGTTTGTACAAAAA GCAGGCTTCATGTCTCATTCTA GAAGACTTTCGTTG	>70	cloning into pDONR221
TTL3R(I QD2 int)	At2G42580 .1	GGGGACCACTTTGTACAAGAAA GCTGGGTCTCATAAGAGGAAAT GCTTATAGAGTC	>70	cloning into pDONR221

TTL4F(I QD2 int)	At3G58620 .1	GGGGACAAGTTTGTACAAAAA GCAGGCTTCATGTCACATTATA GAAGACATTCGCT	>70	cloning into pDONR221
TTL4R(I QD2 int)	At3G58620 .1	GGGGACCACTTTGTACAAGAAA GCTGGGTCTTATAAGAGGAAAT GCGTAACAGAGTC	>70	cloning into pDONR221
For cloning of IQD8 interactors				
TPLS(IQ D8 int)	AT3G5128 0.1	GGGGACAAGTTTGTACAAAAA GCAGGCTTCATGATGAGAGATG TTTTCAGGC	>70	cloning into pDONR221
TPLS(IQ D8 int)	AT3G5128 0.1	GGGGACCACTTTGTACAAGAAA GCTGGGTCTTAGAGACTCTGAT TGAGACACAAAGT	>70	cloning into pDONR221
Cysteine /Histidin e-rich C1 domain family protein	AT1G5570 0.1	GGGGACAAGTTTGTACAAAAA GCAGGCTTCATGGAAGAAATCA CATTGAA		cloning into pDONR221
Cysteine /Histidin e-rich C1 domain family protein	AT1G5570 0.1	GGGGACCACTTTGTACAAGAAA GCTGGGTCTTATATAATTTTAAG TACTCTATCCCA		cloning into pDONR221
Kinesin-related protein	AT5G5552 0.1	GGGGACAAGTTTGTACAAAAA GCAGGCTTCATGAAAACGATGA AGTCACCAG		cloning into pDONR221
Kinesin-related protein	AT5G5552 0.1	GGGGACCACTTTGTACAAGAAA GCTGGGTCTCAGTAGTGATGGT CATGGTCTT		cloning into pDONR221
Kinesin-related protein	AT5G5552 0.1	GGGGACCACTTTGTACAAGAAA GCTGGGTCTCAGTAAGGTAACCCA ACAG		cloning into pDONR221
Rho GTPase activatin g protein	AT4G0310 0.1	GGGGACAAGTTTGTACAAAAA GCAGGCTTCATGACGGGGCTA GTGATGA		cloning into pDONR221
Rho GTPase activatin g protein	AT4G0310 0.1	GGGGACCACTTTGTACAAGAAA GCTGGGTCTTAGTCGCTAGTGC TTGAGCTC		cloning into pDONR221
KIP1-NET3C	At2g47920 .1	GGGGACAAGTTTGTACAAAAA GCAGGCTTCATGGTTAGAGAAG AGGAGAAATCG		cloning into pDONR221
KIP1-NET3C	At2g47920 .1	GGGGACCACTTTGTACAAGAAA GCTGGGTCTTAAAGGACCTTGT TGCCATC		cloning into pDONR221
For Complementation line of IQD8				
IQD8F	At1g17480	AGGGTTTCAAATTTGAGCAAAT GGTGAGCAAGGGCGAGGA		Cloning genomic construct by overlap PCR(pIQD8: GFP-IQD8)



IQD8R	At1g17480	TCCTCGCCCTTGCTCACCATTT GCTCAAATTTGAAACCCT		Cloning genomic construct by overlap PCR(pIQD8: GFP-IQD8)
ProlQD8 :glQD8		GGGGACAAGTTTGTACAAAAA GCAGGCTTCATGTTGCTCAAAG GAAGGAATAAT	73.9	glQD8 under native promoter (short promoter)
ProlQD8 :glQD8		GGGGACCACTTTGTACAAGAAA GCTGGGTCGCCTCTCTGGCTCT TTGC	>75	glQD8 under native promoter (short promoter)
glQD8 premix1		TATATATATGTACCTAACTC		position 951
glQD8 premix1		CCGATGAAGTCCTCCATAGTT		position1750
glQD8 premix2		ACTGATTCTATTGTTTTTGCA		position1703
glQD8 premix2		CAAAACATATACATTTAGTCT		position2504
glQD8 premix3		ATATGGATTTTGGGATAGAATG		position2471
glQD8 premix3		GAGCTGGTGGGTATAGATCAGT		position3270
glQD8 premix4		AGTCAATGTCTTACAACGGAG		position3199
glQD8 premix4		GCAACCGGCGCAGGAACACT		position3971
For sequencing				
USERF		GTTAGTTAGTTACTTAAGCT		sequencing USER- constructs
USERL		CGGGCCAGAGCTGCAGCTGG		sequencing USER- constructs
pBGWF S7		TCGACCTGCAGGCGGCCGCA		sequencing of stable transformed IQD promotor constructs
pBGWF S7		ACCTGCAGGCATGCAAGCTCTC CC		sequencing of stable transformed IQD promotor constructs
For Complementation line of IQD5				
ProlQD5 S:glQD5 w/-stop		GGGGACAAGTTTGTACAAAAA GCAGGCTTCTCTATATATGGTT CACAATCGAGACAC		cloning genomic IQD5 under native promotor via BP
ProlQD5 S:glQD5 w/-stop		GGGGACCACTTTGTACAAGAAA GCTGGGTCGCAAGCCTCTGTT TTATTGGGTCGG		cloning genomic IQD5 under native promotor via BP
ProlQD5 S:glQD5 w/-stop		ATTTAGTTGCTAAATTGGC		premix sequencing (1805 - 2611)
ProlQD5 S:glQD5 w/-stop		CTCGAACTCGGGCTTCATCT		premix sequencing (1805 - 2611)
ProlQD5 S:glQD5 w/-stop		GCAGATGAAGCCCGAGTTCG		premix sequencing (2590-3408)
ProlQD5 S:glQD5 w/-stop		TGAAGTGTGGCATCTTA		premix sequencing (2590-3408)
IQD5 apoCaM binding deleted variant				

IQD5		AGCCAAACGGCTTATCAGGGAT TTCTGGCTCAGAGGGCTTTACG AGCGTTG		position 295 CGG<CAG (SDM1 R<Q);position 310 AGG<CAG
IQD5		CAACGCTCGTAAAGCCCTCTGA GCCAGAAATCCCTGATAAGCCG TTTGGCT		position 295 CGG<CAG (SDM1 R<Q);position 310 AGG<CAG
IQD5		AGAAGCCAAGCCCTTGTTCAAG GACATGCTGTGCAAAAACAAGC TGCTGTA		position 361 AGA<CAA (SDM3R<Q);position 376 AGA<CAA
IQD5		TACAGCAGCTTGTTTTGCACA GCATGTCCTTGAACAAGGGCTT GGCTTCT		position 361 AGA<CAA (SDM3R<Q);position 376 AGA<CAA
IQD5		AGAAGCCAGGCTCGTGTACAG GCAAGACGTGTTGAGCTCGCCT TGGAATTG		position439CGC<CAG(S DM5R<Q);position 454CGT<CAG
IQD5		CAATTCCAAGGCGAGCTGAACA CGTCTTGCTGTACACGAGCCT GGCTTCT		position439CGC<CAG(S DM5R<Q);position 454CGT<CAG
IQD5 Ca <sup>2+</sup> CaM binding deleted variant				
IQD5		GCTGCAACGCGTGACCAAACG GCTGACCGGGGATTTCTGGACA GGAGGGC		position 280(ATC- GAC);position 292(TAT- GAC);position 307(GCT- GAC)
IQD5		GCCCTCCTGTCCAGAAATCCCC GGTCAGCCGTTTGGTCACGCGT TGCAGC		position 280(ATC- GAC);position 292(TAT- GAC);position 307(GCT- GAC)
IQD5		TTGGTTAGAGACCAAGCCCTTG ACAGAGGACATGCTGACAAACA AGCTGC		position 346(CTT- GAC);position 358(GTT- GAC);position 373 (GTG- GAC)
IQD5		GCAGCTTGTTTGTGTCAGCATGTC CTCTGTCAAGGGCTTGGTCTCT AACCAA		position 346(CTT- GAC);position 358(GTT- GAC);position 373 (GTG- GAC)
IQD5		TTGTAAGAGACCAGGCTCGTG ACCGCGCAAGACGTGACCGTC TCGCCTT		position 421(GTT- GAC);position 433(GTA- GAC);position 448(GTT- GAC)
IQD5		AAGGCGAGACGGTCACGTCTT GCGCGGTCACGAGCCTGGTCT CTTACCAA		position 421(GTT- GAC);position 433(GTA- GAC);position 448(GTT- GAC)
Primers used for KLCRs				
KLCR1F	At4g10840	CACCGAGAAATACCATGGATAG CTTGG		pro:GUS 2.2 kb fragment
KLCR1R	At4g10840	GAATGTGTCTCTCTGTGGGAAG T		pro:GUS 2.2 kb fragment
KLCR2	At3g27960	CACCGGGATTCGAGCGGCGAA A		pro:GUS 2.2 kb fragment
KLCR2	At3g27960	GGCCTCCAAAACCTCACAACCTCA		pro:GUS 2.2 kb fragment
KLCR3	At1g27500	CACCTTGATTTGGACTCAGAAT GTTTTT		pro:GUS 2.2 kb fragment

KLCR3	At1g27500	TTTCTTTATTTCTGAATAAACAGC TATC		pro:GUS 2.2 kb fragment
KLCR3	At1g27500	TCAGCTCTTCGTAAGGGTGGGC GCGCCGA		site directed mutagenesis - stop
KLCR3	At1g27500	TCGGCGCGCCACCCTTACGA AGAGCTGA		site directed mutagenesis - stop
KLCR1	At4g10840	GCGACTTCTCACTCGAGGA		sequencing of promoter construct
KLCR1	At4g10840	CTAAGAGGTGAGCAGTATTAT		sequencing of promoter construct
KLCR3	At1g27500	CCAGAAGTTGTTTACATAT		sequencing of promoter construct
KLCR3	At1g27500	GAACTGATTTTTAGTT		sequencing of promoter construct
KLCR3 w/o stop codon	R.P	ACGAAGAGCTGAAGAAGAAGTG	58.4	klcr1-2 SAIL_584_A06 PRODUCT_SIZE 863
KLCR1		TCACGTAGAACAACATTCACG	56.5	klcr1-2 SAIL_584_A06 PRODUCT_SIZE 863
KLCR1		TACACAGTGGGGAGGTACGAG	61.8	BP+RP_PRODUCT_SIZ E 443-743
pKLCR2 new		GGGGACAAGTTTGTACAAAAA GCAGGCTTCgattcacgaacgaatgat tttacg	>75	amplification of promoter region of KLCR2
pKLCR2 new		GGGGACCACTTTGTACAAGAAA GCTGGGTcggcctccaaaactcacaac tcaat	>75	amplification of promoter region of KLCR2
For Complementation line of KLCR1				
gKLCR1		GGGGACAAGTTTGTACAAAAA GCAGGCTTCGAGAAATACCATG GATAGCTTGG		genomic KLCR1 promotor 2.2kb
gKLCR1		GGGGACCACTTTGTACAAGAAA GCTGGGTCAACTTGAACCGA GGC		genomic KLCR1 without stop codon for cloning into pDONR221
pKLCR2 short		GGGGACAAGTTTGTACAAAAA GCAGGCTTCacatctggaccataaac cagg		cloning short promoter (1607bps)
pKLCR3 short		GGGGACAAGTTTGTACAAAAA GCAGGCTTCGAAAAATCGCTGA CTTTGGG		cloning short promoter (1540bps)
pKLCR3 short		GGGGACCACTTTGTACAAGAAA GCTGGGTCTTTCTTTATTTTCGAA TAAACAGCTATC		cloning short promoter (1540bps)
pKLCR2		CGTTTTTTCACAATAAAATTGAC TCA	55.5	promoter sequencing
pKLCR2		AGAAGATGACTTCTTCCCTACTT GC	61.3	promoter sequencing
gKLCR1 premix1		GCTTGCGGGTTTAGATG	52.8	position 903
gKLCR1 premix1		GACTTCTGCTTCAGTTTGT	52.4	90osition 1701
gKLCR1 premix2		AGGGTTGTGACACAAACTG	54.5	position 1690
gKLCR1 premix2		TGAACTCACAAATTTAGAT	45.9	position 2489

gKLCR1 premix3		AACTTAGATTGCATTAC	43.1	position 2439
gKLCR1 premix3		CGGAGCAACGGCGGCGCA	65.1	position 3228
gKLCR1 premix4		AGCAACTAAGTCCTTTGAG	52.4	position 3203
gKLCR1 premix4		CGTCGGATGAGTCTCTCCTT	59.4	position 3999
gKLCR1 premix5		ATATTTACATGTGCTGTG	50.2	position 3921
gKLCR1 premix5		CAAACGCGTTTCTTGCGTC	56.7	position 4714
For genotyping				
KLCR1	klcr1_3_LP	GCGAGTGGACAAGAATCTGAG	59.8	SALKseq_043957.2;PRODUCT_SIZE 1093
KLCR1	klcr1-3_RP	GGACTTTACCTTCCCATAGCG	59.8	SALKseq_043957.2;BP+RP_PRODUCT_SIZE 580-880
KLCR3	klcr3-1_LP (fwd)	CGTCCATATATCACCATTGGC	57.9	SALKseq_119893.1 ;PRODUCT_SIZE 1004
KLCR3	klcr3-1_RP (rev)	CTCTCCCAAAGCAAGATGTTG	57.9	SALKseq_119893.1 ;BP+RP_PRODUCT_SIZE 458-758
KLCR3	klcr3-2_LP (rev)	AGCTTCTTTCAAGAGTTGGGC	57.9	SAIL_1148_A07 ;PRODUCT_SIZE 1130
KLCR3	klcr3-2_RP (fwd)	TGACCCAAGAGTTGGTGA AAC	57.9	SAIL_1148_A07 ;BP+RP_PRODUCT_SIZE 473-773

## 11 Supplementary Figures

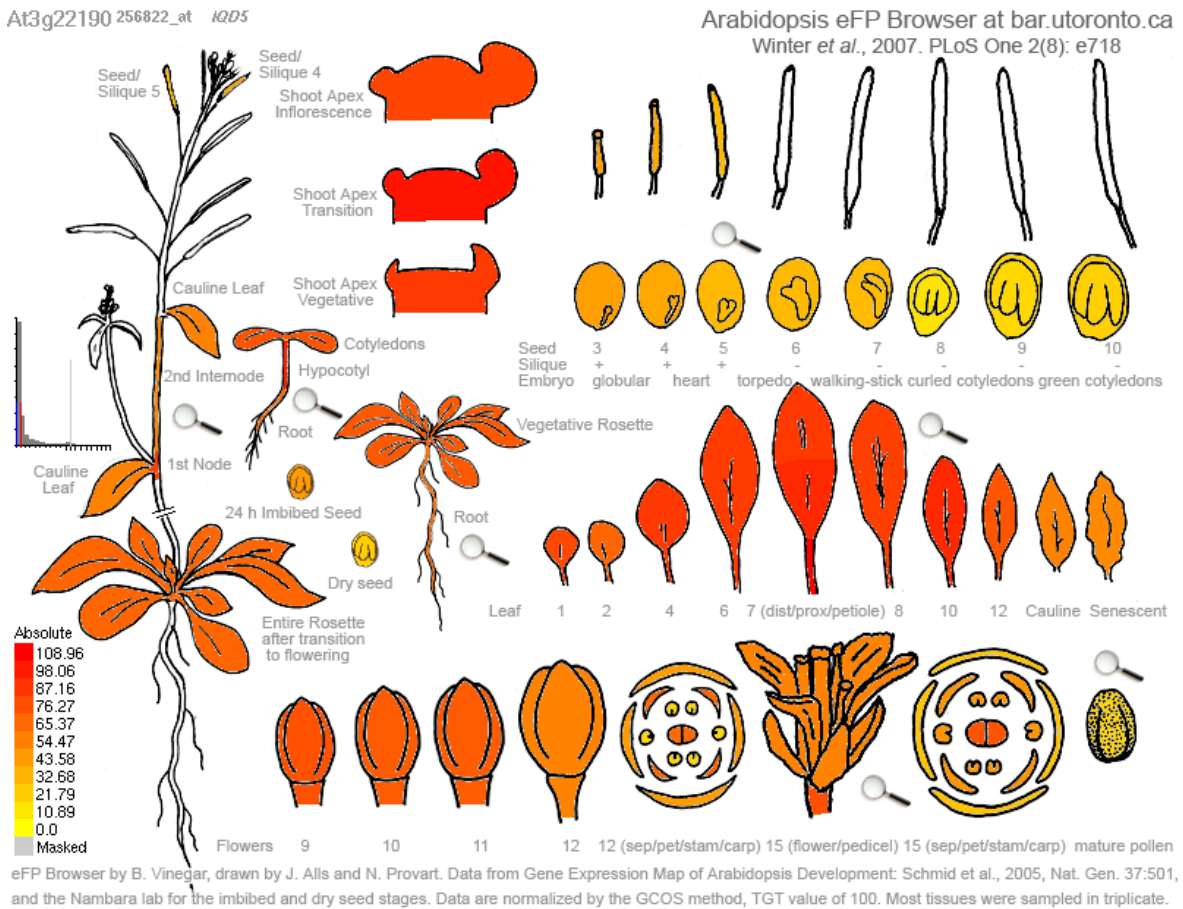
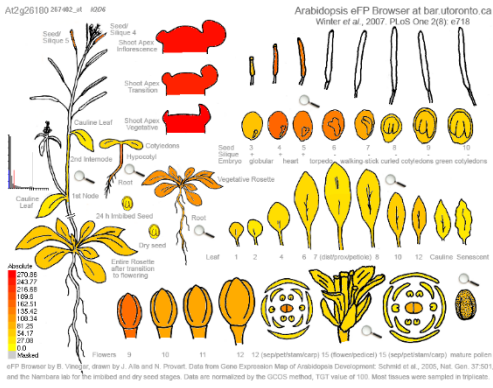
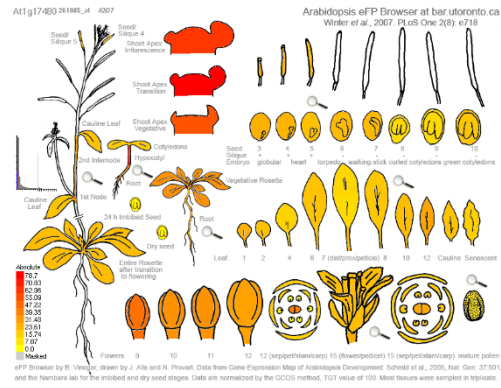


**Fig S1: *in silico* data on *IQD5* expression pattern** *in silico* expression of *IQD5* data obtained from eFP browser.

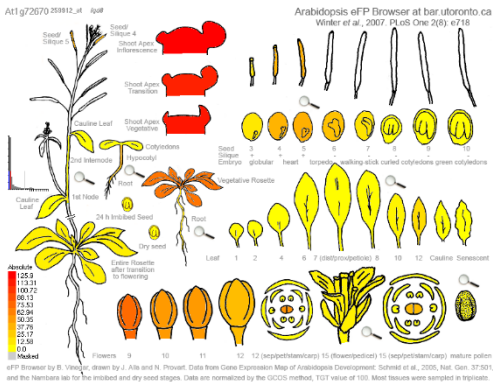
**IQD6**



**IQD7**



**IQD8**



**KLCR1**

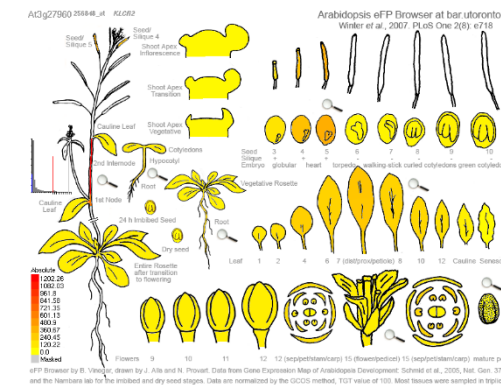


**Fig S2: *in silico* data on IQD6-IQD8 and KLCR1-KLCR2 expression pattern. There is no *in silico* data available for KLCR3 in *in silico* expression of IQD6-IQD8 and KLCR1-KLCR3 obtained from eFP browser.**

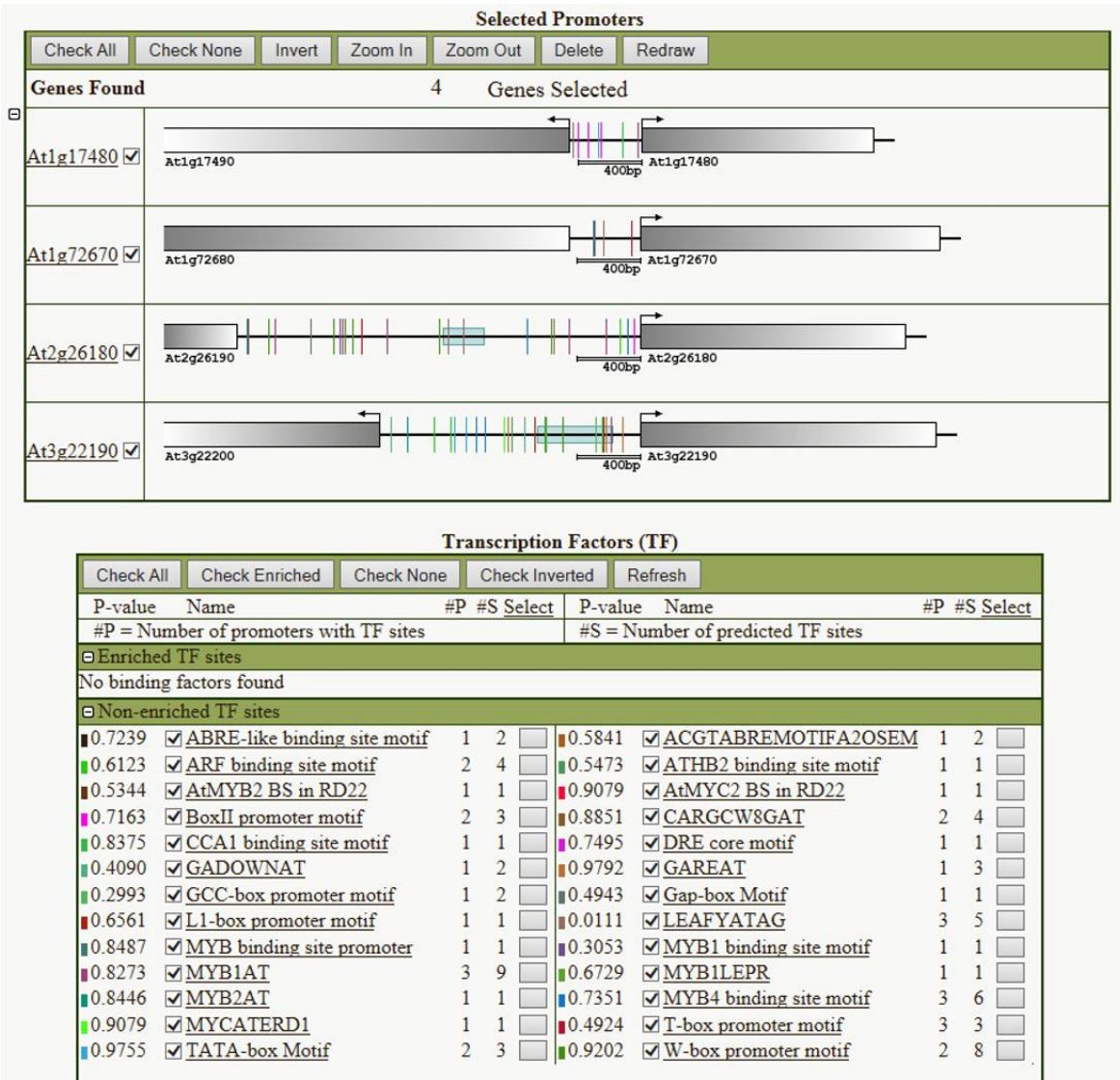


**Fig S3: *in silico* data on IQD5 cis factors shows Auxin binding motifs** *in silico* data obtained from auxin binding motifs tool for IQD5 promoter region.

A.

TABLE 1  
Canonical CaM-binding motifs

Motif	Sequence
Ca <sup>2+</sup> dependent	
1-10	[FILVW]xxxxxxxx[FILVW]
1-5-10	[FILVW]xxx[FAILVW]xxxx[FILVW]
Basic 1-5-10	[RK][RK][RK][FAILVW]xxx[FILVW]xxxx[FILVW]
1-12	[FILVW]xxxxxxxx[FILVW]
1-14	[FILVW]xxxxxxxxxx[FILVW]
1-8-14	[FILVW]xxxxx[FAILVW]xxxx[FILVW]
1-5-8-14	[FILVW]xxx[FAILVW]xx[FAILVW]xxxx[FILVW]
Basic 1-8-14	[RK][RK][RK][FILVW]xxxxx[FAILVW]xxxx[FILVW]
1-16	[FILVW]xxxxxxxxxxxx[FILVW]
Ca <sup>2+</sup> independent	
IQ	[FILV]Qxxx[RK]Gxxx[RK]xx[FILVWY]
IQ-like <sup>a</sup>	[FILV]Qxxx[RK]xxxxxxxx
IQ-2A	[IVL]QxxxRxxxx[VL][KR]xW
IQ-2B	[IL]QxxCxxxxKxRxW
IQ unconventional	[IVL]QxxxRxxxx[RK]xx[FILVWY]

Numbers for the Ca<sup>2+</sup>-dependent motifs indicate the positions that require a hydrophobic residue. Residues in the brackets can substitute for each other; x indicates any amino acid residue.

<sup>a</sup>Some IQ-like motifs require Ca<sup>2+</sup> for CaM binding.

B.

Protein

>IQD5

MGASGRWIKALVGF<sup>T</sup>TKSDKSRSSK<sup>K</sup>DENVKVATKSRFGRKNSVDFDFEKFQDGFEDSNTR  
SMVD<sup>T</sup>GVST<sup>S</sup>TSLQSYGGVAYDEQSRENRAATR<sup>T</sup>QTAR<sup>R</sup>GFLARR<sup>L</sup>RAL<sup>R</sup>KGLV<sup>R</sup>LOALV<sup>L</sup>  
<sup>R</sup>GHA<sup>V</sup>R<sup>K</sup>QAAVT<sup>L</sup>RCMQAL<sup>V</sup>R<sup>V</sup>QAR<sup>V</sup>RARR<sup>V</sup>RLALELESETSQQT<sup>L</sup>QQQLADEARVREIE  
EGWCDSIGSVEQIQAKLLKRQEAAAKRERAMAYAL<sup>T</sup>HQWQAGTRLLSAHSGFQPDKNNWG  
WNL<sup>R</sup>WMAVRP<sup>W</sup>ENRFLDSNLRDDAKLGENGMEQSENVPKTQIKSVSKMPNTSNLVSGV  
SSQMTGPCQSDGDS<sup>S</sup>SPGI<sup>S</sup>SSIPV<sup>V</sup>SKAKSKPAKDDLAVEVNSRPGAGPRSHSNPKERS  
REP<sup>N</sup>RSSKERLSLPNSGKSLGSQSTKANRAGKLT<sup>P</sup>ASQKVVEEKSAQNQRRRNSDPIKQR  
LA

**Fig S4: *in silico* CaM binding motifs in IQD5.** (A) CaM binding motifs and their sequences (Table from Mruk *et al.* 2014) (B) CaM binding motifs for IQD5.



## 12 Appendix

### 12.1 Curriculum Vitae

**Name:** Dipannita Mitra  
**Date of Birth:** 29.09.1987  
**Place of Birth:** Burdwan (West Bengal), India  
**Nationality:** Indian

#### Educational Qualifications:

2018 – present	<b>Quality Management</b> CynTEGRITY Germany GmbH Frankfurt, Germany
2013 – 2017	<b>Ph.D. student</b> , (DAAD Scholar) Leibniz Institute of Plant Biochemistry Martin-Luther University, Halle, Germany Ph.D. Defense on: 11.09.2020
2010 – 2012	<b>Master of Technology (M.Tech.)</b> , Biotechnology National Institute of Technology, Durgapur, India Score - 9.2/10 CGPA
2006 – 2010	<b>Bachelor of Technology (B.Tech.)</b> , Biotechnology SRM University, India Score – 9.4/10 CGPA
2003 – 2005	<b>Senior Secondary Education</b> Kendriya Vidyalaya Ballygunje, Kolkata, India Score - 80.41 %
1993 – 2003	<b>Secondary School</b> Kendriya Vidyalaya Ballygunje, Kolkata, India Score – 86.67%

## 12.2 List of Publications

- **Mitra D**, Klemm S, Kumari P, Quegwer J, , Möller B, Poeschl Y, Pflug P, Stamm G, Abel S, Bürstenbinder K  
*Microtubule-associated protein IQ67 DOMAIN5 regulates morphogenesis of leaf pavement cells in Arabidopsis thaliana.*  
**Journal of Experimental Botany, Jan 2019.**
- Bürstenbinder K, **Mitra D**, Quegwer J  
*Functions of IQD proteins as hubs in cellular calcium and auxin signaling: a toolbox for shape formation and tissue specification in plants?*  
**Plant Signaling & Behavior, June 2017**
- Ghosh S, **Mitra D**  
*Elimination of Chromium (VI) from wastewater using various biosorbents.*  
**Springer book on Water Science and Technology Library, March 2018**
- Bürstenbinder K, Möller B, Plötner R, Stamm G, Hause G, **Mitra D**, Abel S  
*The IQD Family of Calmodulin-Binding Proteins Links Calmodulin Signaling to Microtubules, Membrane, Microdomains, and the Nucleus.*  
**Plant Physiology, March 2017**

### **12.3 Acknowledgments**

I am exceptionally thankful to my Head of the Department Prof. Dr. Steffen Abel for giving me an opportunity to become a member of this prestigious institution. I am thankful to supervisor/mentor, Dr. Katharina Bürstenbinder for helping me to learn and understand science and positively guiding me through my Ph.D. work. Under her supervision, I was genuinely encouraged and supported by my experimental planning and research framework. She provided me with an equipped laboratory and a very conducive working environment. She has guided me immensely, in my scholarship and review paper writing and explained to me how to formulate a scientific idea and apply it. Dr. Bürstenbinder has been extremely considerate in understanding my scientific potential and henceforth positively asking me to mend the gaps in terms of learning new techniques, reading and updating new scientific literature and also promoting extracurricular activities. Prof. Abel and Dr. Bürstenbinder have helped me throughout 1 year of my illness, always motivating me with positive inputs to finish my thesis successfully.

I am extremely thankful to my lab members, Paul Pflug and Pratibha Kumari for genuinely helping me with all my problems, both scientific and personal. I am also thankful to Jakob Quegwer and Gina Stamm who have been immensely supportive and understanding during my Ph.D. labwork. I am grateful to Romina Plötner and Sandra Klemm for their help during my Ph.D. work. My special thanks to Anshu, Dinesh, Romel Ahmed, Kalidoss, Tamilrasan, Ranju, Shiv, Heena for their great support during my Ph.D. I extend my thanks to Prof. Bettina Hause, Hagen Stellmach, and Dr. Luz Irina for always motivating me during my Ph.D. and helping me with scientific problems.

My special thanks to my husband Rajeev and my parents, who has been the most supportive people I have known and have always encouraged me to do things I like and is the main motivating power behind the completion of my thesis during my illness. I am very blessed and thankful to the Almighty that I met such wonderful people and everybody has played a significant part in my life.

### 13 **Declaration**

I hereby declare that I have completed this dissertation titled “Characterization of IQD67-domain protein family and their interacting Kinesin light chain-related proteins” by my own without the unauthorized help from a second party and only with the assistance acknowledged therein. I have duly acknowledged and referenced all text passages that are derived literally from or are based on the content of published or unpublished work of others, and all information that relates to verbal communications. I have abided by the principles of good scientific practice and conduct laid down in the charter of the Leibniz Institute for Plant Biochemistry (Halle) and Martin Luther University, Halle (Saale) in carrying out the investigations described in the dissertation.

---

Place, Date, Signature

## 14 Ehrenwörtliche Erklärung

Ich erkläre ehrenwörtlich, dass ich die dem Fachbereich Biologie Halle zur Promotionsprüfung eingereichte Arbeit mit dem Titel " Characterization of IQD67-domain protein family and their interacting kinesin light chain-related proteins " im Institut für Leibniz Institut für Pflanzenbiochemie(IPB) unter Leitung von Dr Katharina Bürstenbinder ohne sonstige Hilfe selbst durchgeführt und bei der Abfassung der Arbeit keine anderen als die in der Dissertation aufgeführten Hilfsmittel benutzt habe. Ich habe bisher an keinem in- oder ausländischen Biologie Fachbereich ein Gesuch um Zulassung zur Promotion eingereicht, noch die vorliegende oder eine andere Arbeit als Dissertation vorgelegt.

---

Ort, Datum, Unterschrift